Generation of tunable single/multiwavelength fiber laser based on balloon like shape Mach-Zehnder interferometer

A Thesis Submitted to the Institute of Laser for Postgraduate Studies, University of Baghdad in Partial Fulfillment of the Requirements for the Degree of Master of Science in Laser / Electronic and Communication Engineering

By
Haneen Qassim Merza

B.Sc. Laser and optoelectronic Engineering – 2009

Supervisor
Prof. Dr. Abdul Hadi Al-Janabi

2021 AD   **1443 AH**

ABSTRACT

Fiber optic filter is a potentially brilliant method for tunable full waveband and adjustable multi-wavelength spacing in a continuous-wave (CW) Erbium-doped fiber laser (EDFL) and Ytterbium doped fiber laser (YDFL). Owing to their plentiful benefits, the simplicity, lightweight, low-cost fabrication, reliability, wide range, and repeatability are highly desirable features in fiber optic filters. In the present, an innovative all-fiber filter based on Mach-Zehnder interferometer (MZI) is planned and experimentally proved. The wavelength selection, channel spacing, and switching techniques are based on the whispering gallery mode (WGM) effect in a Mach-Zehnder interferometric comb-filter formed by bending a standard single-mode fiber (SMF) into a balloon-like shape.

By incorporating the proposed comb-filter into the laser ring cavity and adjusting the SMF's bending diameter to control the spectral cavity losses, the single-wavelength lasing was tuned from 1065.26 to 1048.6 nm with a tuning range of 16.76 nm for YDFL. Furthermore, by appropriately rotating the polarization controller (PC) cascaded with the filter, the laser can be switched between the dual- and triple-wavelength lasing operations. Two sets of switchable triple-wavelength lasing operations around 1045 nm were obtained with a side-mode suppression ratio (SMSR) of 26.9 dB and 22.4 dB, respectively. Also, when the launched diode pump power in the fiber laser set up was increased from 110 to over 210 mW, the YDFL cavity lased at a dual- and triple-wavelength. The dual-wavelength laser was achieved at 1048.6 nm and 1046.38 nm with a channel spacing of 2.22 nm.

The tunable full waveband EDFL operation with a wide wavelength-tunable range of 11.9 nm was realized by gradually varying the bent diameter of the interferometric filter structure. Also, when the launched diode pump power was increased from 110 to 195 mW, the central wavelength of the EDFL was shifted from 1562.9 nm to 1559.5 nm with channel spacing 2.4 nm. Moreover, by adjusting

the polarization state inside the cavity, the wavelength operation was switched from a single to multi-wavelength operation. Dual-, triple-, and quadruple- wavelength emissions were achieved.

To the best of our knowledge, this is the first time that a bending SMF into a balloon-like MZI has been employed as an all-fiber filter to manipulate the spectral output characteristic of YDFL and EDFL. The proposed YDFL and EDFL output characteristics of tunable single / multi-wavelength can provide great potential in diverse photonics and communication applications.

LIST OF CONTENTS

Chapter one

Introduction and Basic Concept

CHAPTER THREE

Results and Discussions

LIST OF TABLES

Table	**Title**	**Page**
Table 1-1	Rare-Earth Ions with their Absorption and Emission Wavelengths	18
Table 1-2	Summary of the Published Works in OFCF.	35
Table 3-1	The insertion losses of the proposed balloon-like filter at the various bending diameter.	60
Table 3-2	Summary of the proposed balloon-like filter with various bending diameter.	76
Table 3-3	Summary of the proposed balloon-like filter with increasing power.	77
Table 3-4	Summary of the proposed balloon-like filter at rotate PC.	77

LIST OF FIGURES

LIST OF SYMBOLS

λ_{dip}	interference dip at specific wavelengths
φ_{in}	initial phase
Δn_{eff}	effective refractive index difference between the core and coating mode
$\Delta\varphi$	phase difference between core & cladding mode
Θ_i	angle of incidence
Θ_c	Critical angle
Λ	signal wavelength
V	normalized frequency
a	core radius
m	positive integer No.
r	curvature radius of the balloon region
v	Poisson ratio
x	perpendicular to the bending axis
ρ	radius of the fiber
I_c	Core modes intensity
I_{cl}	Clad modes intensity
L_{eff}	effective length of the bending region
P_{11} & P_{12}	components of the photo-elastic tensor
$n'(x)$	refractive index of the straight SMF
$n(x)$	refractive index of the bent SMF
r_{eff}	equivalent bending radius

d	SMF's bending diameter
Er^{3+}	Erbium ions
L	total length of SMF
N	number density
n_2	refractive index of the clad
Nd^{3+}	Neodymium ions
Pr^{3+}	Praseodymium ions
R^2	linear tendency
RIs	effective refractive indices
Th^{3+}	Thulium ions
Yb^{3+}	Ytterbium ions
n_1	refractive index of the core
n_o	refractive index of the medium outside

LIST OF ABBREVIATONS

AM	active medium
ASE	amplified spontaneous emission
C-band	Conventional Band
CW	Continues wave
DFL	doped fiber laser
EDFL	Erbium doped fiber laser
FBGs	fiber Braggs
FPI	Fabry–Perot interferometers
FSR	free spectral range
GIF	graded index fiber
IR	Infrared wavelength
ISO	Optical Isolator
LD	Laser diode
LPG	long-period grating
MFDs	mode field diameters
MMF	Multi-modes fiber
MZI	Mach-Zehnder interferometers
NA	numerical aperture
OCs	Output Couplers
OPD	optical phase difference
OSA	optical spectrum analysis
PC	Polarization controller

PHB	polarization hole burning
PMF	polarization maintaining fiber
PPM	Part per million
SHB	spectral hole burning
SI	Sagnac interferometers
SIF	step index fiber
SMF	Single mode fiber
SMS	Single mode-Multimode-Single mode
SMSR	side-mode suppression ratio
SM-NLPCF-SM	Single mode-Nonlinear photonic crystal fiber-Single mode
SNR	signal to noise ratio
TIR	total internal reflection
UV	Ultraviolet wavelength
WDM	wavelength division multiplexing
WGM	Whispering gallery mode
YDFL	Ytterbium doped fiber laser

CHAPTER ONE

1.1 General introduction and motivation

Optical fiber communication system components have been developed extensively due to the increasing demand for an effective technology for high-speed information transmission medium in both the long haul systems and the local networks. In recent years, spectral manipulation of fiber laser is an important issue, and efforts have been devoted to achieving a versatile performance such as tunability, switching, or spacing-tunable multi-wavelength lasers due to their wide broad range of applications such as in fiber communication systems, fiber optic sensors, etc. [1,2].

Tunable wavelength fiber lasers have been under intensive study in recent years due to their growing optical spectroscopy applications, optical sensors, and wavelength division multiplexing (WDM) [3,4]. In certain applications, such as fabrication of light source for the wavelength routers of WDM network and photonics systems' characterization, switching the fiber laser's operation from one single lasing line to another is preferable [5]. On the other hand, in some applications, such as (WDM) optical networks, signal processing, generation of soliton pulses, and multi-parameter measurement, a multi-wavelength operation is ideal [6,7].

Moreover, in a practical view, a multi-wavelength fiber laser has more potential than a fixed wavelength fiber laser since the variable wavelength output with adjustable spacing may satisfy various applications such as in high-resolution spectroscopy, optical frequency metrology, microwave/Terahertz generation, optical sensing, and in fiber communications where the current WDM systems require various channels spacing depend on their specific applications [2,8]. However, most

of the multi-wavelength fiber lasers reported to date are not tunable or are only discretely tunable in spacing [2] . In addition, their advantages, like low operating costs, compactness, long operational lifetimes, and a high signal-to-noise ratio, are all benefits from these multi-wavelength fiber lasers [7,9,10]

The basic principle behind a tunable and multi-line output characteristic of a fiber laser at room temperature requires an optical filter to alleviate the mode competition of the gain medium [11-13]. However, two main concerns need to be carefully handled to achieve a stable operation of tunable and multi-wavelength fiber lasers. The strong homogeneous line broadening and the cross-grain saturation induced in the doped fiber gain medium [14]. These limitations are still challenging to obtain stably tunable-, and multi-wavelength fiber laser outputs [15,16]. In some practical applications, it is also desirable to be able to enhance the functionality and the flexibility of a multi-wavelength fiber laser. Therefore, the tunability of the channel-spacing and the number of channels should be investigated [17].

Up to now, there are several methods have been proposed to achieve channel spacing tunable operation of optical fiber comb filters [18]. Optical fiber comb filters are one form of these optical filters [19]. Various techniques to realize all-fiber comb filters have been reported, including the usage of tapered fibers [20,21], fiber Braggs (FBGs) in combination with tapers [22-24], Sagnac interferometers (SI) [25-27], and Fabry–Perot interferometers (FPI) [27,28] have been proposed to towards tunable and multi-wavelength doped fiber lasers generation. Therefore, high-performance optical filters with low cost, ease of handling, and fabrication to implement these types of Erbium-doped fiber laser (EDFL) and Yttrium doped fiber laser (YDFL) output characteristics are of great interest [14].

Mach–Zehnder interferometers (MZI) have many advantages over other types of interferometers, such as high reliability and environmental change insensitivity [29]. In this regard, many structures have been investigated in the literature for the construction of all-fiber MZI-based filters, such as single-mode multimode single-mode (SMS) fiber structure [30], tapered fibers [31], microfibers [32], and photonic crystal fiber [33]. Temperature, electrical, and mechanical approaches are used to manipulate and tune the spectral response of these MZI comb filters [34]. However, the manufacturing of such MZI structures can be complicated and expensive [26,35,36].

Recently, MZI featuring ease of fabrication, simplicity, and cost-effectiveness based on bending a single-mode fiber (SMF) into a balloon-like structure has gained a lot of interest in sensing applications [36-39]. On the other hand, very recently, He et al. reported the possibility to generate individually tunable adjacent single wavelength, dual-wavelength, triple-wavelength, quadruple-wavelength, and quintuple-wavelength operation by appropriate adjustment of the polarization controllers (PC) in the laser cavity [40]. Some researchers have proposed and demonstrated optically tunable comb filters whose characteristics can be adjusted by pump light strength [41,42].

In this work, a tunable full waveband and spacing adjustable multi-wavelength doped fiber laser based on balloon-like bent SMF structure act as MZI based filter is experimentally demonstrated. First, the proposed filter's attenuation bands are reshaped by changing a traditional SMF's bending diameter d, achieving a tunable full waveband lasing operation. Second, the effect of enhancing the pump power on the wavelength tunability was investigated. The laser emission was tuned/switched for the smallest wavelength with the blue shift as the pump power was increased gradually from (110–210) mW. Finally, the multi-wavelength generation

with spacing tunability was achieved by adjusting the state of polarization inside the ring cavity.

1.2 Fiber Lasers

Fiber lasers are a special kind of solid-state lasers in which the active medium (AM) is the core of an optical fiber doped with a rare-earth element. These types of lasers show high gain with high pump efficiency, good beam quality, high reliability, and compactness. Thus, they are found in potential applications for communications, remote sensing, and medicine. YDFL emitting near 1.0 µm allows the production of a cost-effective and robust alternative device for several applications in biomedical, material processing, science, and high power laser operation [43].

On other hand, EDFL has many excellences such as narrow bandwidth and long-range tunability. It can be used in many potential applications such as sensing and communication because it radiates at 1.55 µm lying in the third window of low loss in fiber-optic communications [44]. Fiber lasers were developed in the early days of laser demonstration, but they have become of great practical interest only in recent years because of the advent of techniques for fabricating doped single-mode silica fibers as well as the suitable diode lasers allowing efficient pumping [45].

Intense absorption bands are constructed by the rare earth ion, whereas the low loss wave guiding features of the fiber are preserved at the emission wavelength of the rare earth ion. This rare-earth is optically active, therefore it can absorb light at one wavelength and emit light at another. The fiber core can be doped with ions of rare-earth elements, then it can be used as AM of a fiber laser. Such rare-earth ions are erbium (Er^{3+}), neodymium (Nd^{3+}), ytterbium (Yb^{3+}), thulium (Th^{3+}) or praseodymium (Pr^{3+}). These ions have different absorption and emission spectra associated with transitions between states of energy. The suitable wavelength for

pumping and the wavelength of the emitted signal depends on the energy levels of each rare-earth element, the output of the fiber lasers can show several temporal operation regimes.

In addition to the amplifying gain medium, there is a difference in passive fiber optics elements that are utilized in optical fiber laser systems to implement precise jobs. These passive elements split, redirect or combine the light signals. the integrated cavities and all-fiber designs have become possible with the most popular passive fiber optics elements that are commonly utilized are WDM, isolator, fiber filters, polarization controller, and coupler, complemented by the ability of direct pumping by semiconductor lasers diodes [46]. Therefore, silica glass represents the main glass host for fiber lasers which allows fiber lasers to take advantages of its unique properties of excellent optical transmission from ultraviolet (UV) to near-infrared wavelengths, excellent refractive index homogeneity with a low nonlinear refractive index, a very low coefficient of thermal expansion, small strain birefringence, very high thermal stability, high mechanical strength, and resistance to radiation [47].

Another inherent feature of fiber lasers is usually pumped by low-cost laser diodes that emit light with low-quality output mode. The wavelength of the diode laser should be compatible with the excitation of the selected dopant ions of the active medium. Fiber lasers are now competitive with solid-state and semiconductor sources in several domains, over which they have proved the advantage of excellent mode quality, high brightness, efficient coupling into an SMF, far superior wavelength stability with temperature, and enhanced heat dissipation because of the larger surface to volume ratio of the AM [48].

1.3 Principle of Fiber Lasers Operation

Absorption, spontaneous emission, and stimulated emission are the operation processes to generate photons in the gain medium of fiber lasers. The fiber laser system consists of a pump source used to pumps light into the active fiber which is placed between two reflectors such as mirrors or FBGs. When light is pumped into the cavity, the light is absorbed by the ions of the doped fiber. These ions will travel from the ground energy level to the higher one. At the higher energy state, the ions will emit the absorbed light as photons. This process is called spontaneous emission.

The mirrors reflect some of the emitted photons back and forth within the amplifier. One mirror is closest to the pump source, which is transparent to the pump wavelength and has 100% reflectivity at the lasing wavelength. The other, placed at the end of the amplifier with 80-99% reflectivity at the lasing wavelength. The reflected photons by mirrors will stimulate the ions in the higher energy level to emit more photons in a process called stimulated emission shown in Fig. 1.1 [49]. Fiber lasers can be classified according to the cavity configuration into two major types: fiber laser with ring cavity [50,51] and fiber laser with linear cavity [45,52]. The next sub-sections will describe both cavities.
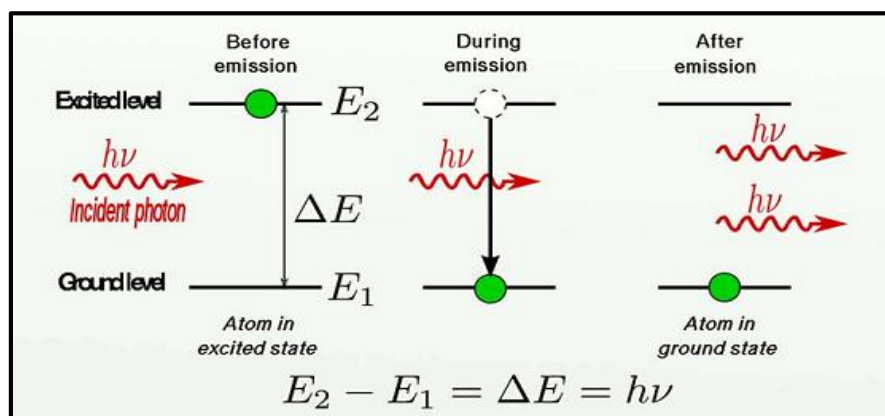
Fig. 1.1: Illustration of stimulated emission process [49].

1.3.1. Fiber Laser with Linear Cavity

Typically, Fig. 1.2 shows the most common type of fiber laser with a linear cavity which is known as the Fabry-Perot cavity. It can be designed by placing the active medium between two highly reflecting mirrors. Mirrors are often butt coupled to the fiber ends to minimize diffraction losses. To avoid passing the pump light through dielectric mirrors, many alternatives can be used. For example, one can take advantage of fiber couplers so that most of the input pump power comes out of the port that is a part of the laser cavity. Such couplers are called (WDM) couplers. Another solution is to use fiber gratings as mirrors. FBGs can behave like a high reflective mirror for the laser wavelength while being transparent to the pump wavelength.

Generally, the two counter-propagating signal waves in the fiber laser linear cavities interfere and produce a standing wave. Owing to the roundtrip character of the light path within the laser cavity, the interference generated by the minimum amplitudes of the standing wave is responsible for the spatial hole-burning influence that is generated inside the laser cavity. this type of fiber design with a somewhat lengthy cavity and great gain-bandwidth will experience prompt mode hopping influence resulted from the spatial hole burning [53]. As well the light travels twice per roundtrip cycle via the gain medium, and then the laser gain/loss is considered twice per cycle, In this case, the peak power alternative is quite small [54].
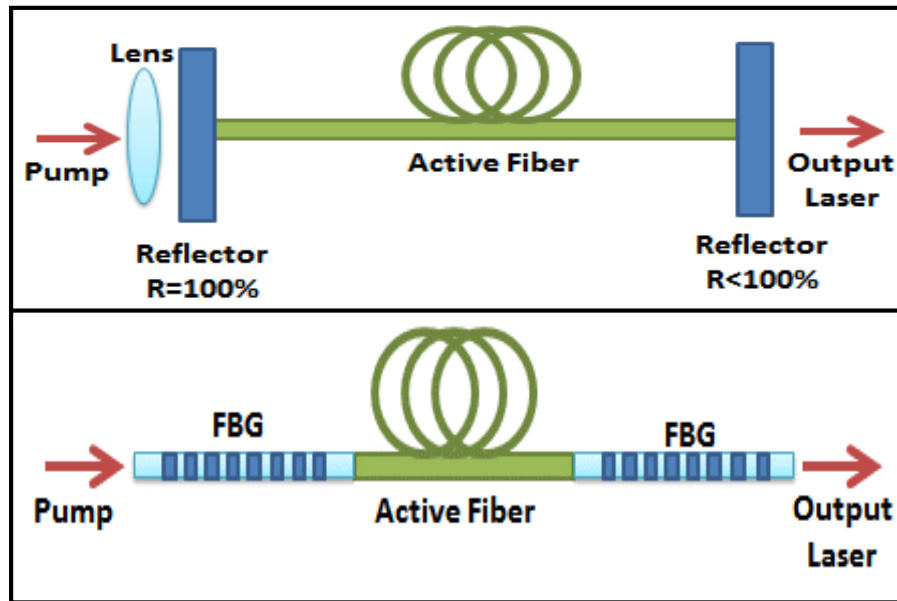
Fig. 1.2: Fiber laser linear cavity configuration based on (a) two dielectric mirrors [53], (b) FBG [45].

1.3.2 Fiber Laser with Ring Cavity

Ring cavities are usually used to allow the unidirectional operation of laser output. In the case of fiber lasers, there is another advantage which is a ring cavity can be designed without using mirrors which results in an all-fiber cavity. In the simplest form, a WDM coupler is used to form a ring cavity containing the active medium as illustrated in Fig. 1.3. Because such a ring cavity resonates in both directions and, therefore, has a bidirectional output, its conversion efficiency is only half as high as that of a Fabry-Perot linear cavity.

This problem is solved by introducing an optical isolator (ISO) in the laser cavity, which forces unidirectional operation and prevents the AM from any possible spatial hole burning to the AM [55]. A PC is required for conventional doped fiber that does not preserve polarization. It controls the state of polarization inside the cavity against the physical movement and bending.
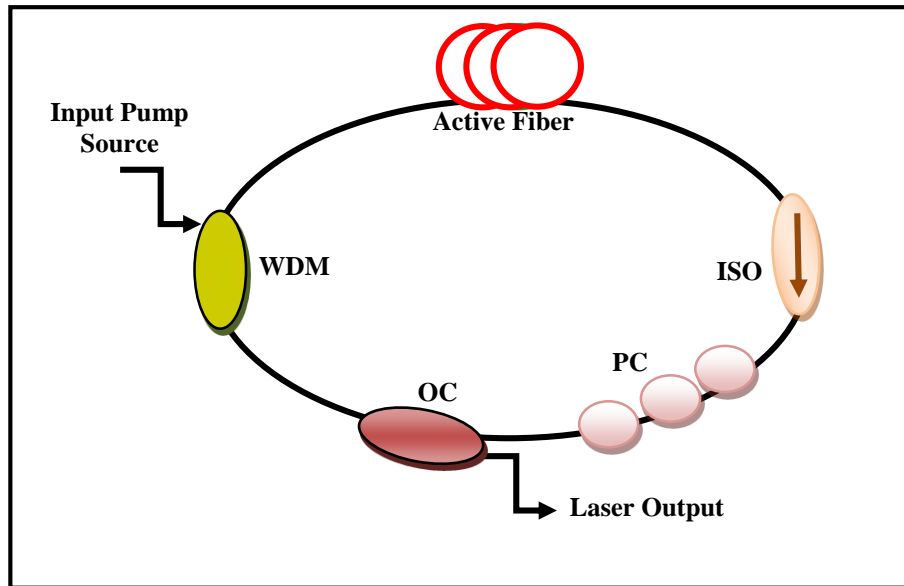
Fig. 1.3: Fiber Laser with Ring Cavity [55].

The stability of laser output power is affected by several factors, such as the length of the active medium (the doped fiber), the coupling ratio on the output, and the total cavity length. It can be improved by the appropriate selection of laser parameters [56]. A standard ring cavity fiber laser includes doped fiber as an active gain medium and various related fiber-coupled devices. These devices include WDM, fiber coupler, optical isolator, polarization controller, and pump source. The following sections review the basic principles of these optical components. The major passive optical components of the fiber laser ring cavity are overviewed in the next subsections.

1.3.2.1 Fiber Output Couplers (OCs)

Fiber OCs are commonly used for light coupling between different fibers. They are directional couplers, having one or more input fiber ports and one or more output fiber ports. Light injected into an input fiber port will appear at one or several output fiber ports, but not at other input fiber ports. The most forms 2x2 or 1x2 ports couplers with various dividing are employed for the output of laser generations of

the fiber laser [57]. The simplest form of this device is a 1×2 coupler as depicted in Fig. 1.4 In general, those couplers are manufactured by twisting two SMFs together in which their cores become so close over a specific length of the fiber. As light guided in one fiber may then the evanescent fields leak over to the other one. The output ports can splitting the signal in different present [90:10], [80:20], [70:30], and [50:50]. This is a coherent approach that is greatly wavelength-dependent [45].
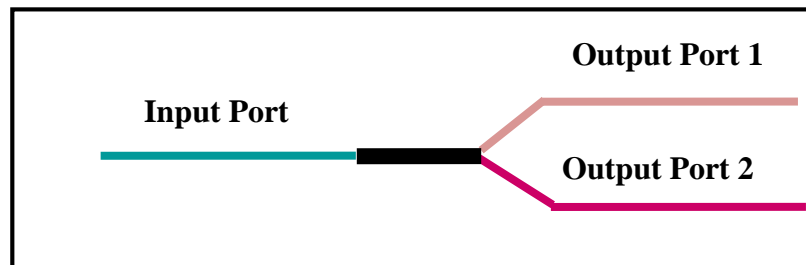
Fig. 1.4: Schematic Diagram of Fiber Output Coupler [45].

1.3.2.2 Wavelength Division Multiplexer (WDM)

In a fiber laser ring cavity, combining the pump and signal is achieved by an optical WDM. WDM elements are specified coupler kinds that permit light from two or more optical sources of various spectral wavelengths to be propagated in parallel into a single optical fiber. In a fiber laser, WDM is an ideal solution to combine signal and pump with little insertion attenuation, permitting the combined signal and pump to be traveled within the same gain fiber without interference [57].

For EDFL and YDFL, 980/1550 WDM is typically used and its chromatic dispersion distorts the optical signals propagating along with the output port of the WDM by making different wavelengths propagate with diverse groups velocities.

1.3.2.3 Optical Isolator (ISO)

When light propagates through fiber splices, connectors, and other optical elements there are several probabilities for back reflection. These reflections typically materialize after light propagates via an interface vertical to the direction of the light path. But, an ISO is utilized to save the signal and pump sources from back-reflections. Generally, the ISO is a two-port passive element that permits light (in a specific wavelength band) to travel through with little loss in one direction, although isolating (giving a high loss for) light traveling in the reverse direction [57, 58]. The operation principle of the ISO is illustrated in Fig. 1.5.

The Faraday effect is obtained when a magneto-optic material is positioned in a strong magnetic field [45]. Light propagating within this material has a polarization state which is rotated by an amount depending on both length and strength of the magnetic field. This is beneficial since this effect is asymmetric. So, the light traveling in one direction gets its polarization rotated by 45°, while the light traveling in the opposite direction gets rotated in the same direction by the same angle. As a result, light coming back into the input is perpendicular to the original signal.
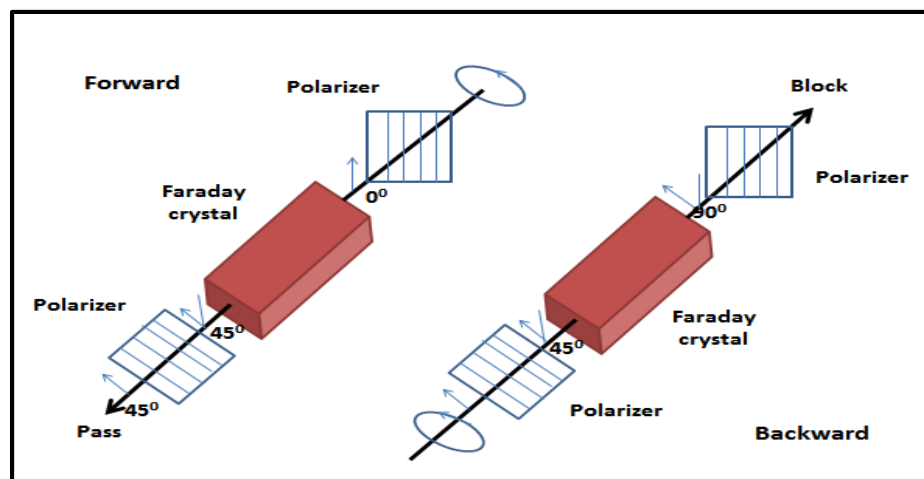
Fig. 1.5: A Polarization Independent Optical ISO [57].

1.3.2.4 Polarization Controller (PC)

Polarization controller (PC) is an optical device that permits controlling the state of polarization of light within the fiber. The fiber polarization controller invests the induced birefringence by bending a fiber [45]. The PC an in-line manual device (Thorlabs PLC-900) consists of a rotatable fiber squeezer and two fiber holding clamps were used.

The center portion of the fiber strand is sandwiched in the fiber squeezer. It creates stress-induced birefringence within SMF by mechanically compressing the fiber. This acts like a variable, rotatable wave plate. Both the angle and retardance of the wave plate can be continuously, independently adjusted, which permits any arbitrary input polarization state to be converted to any required output polarization state. Also, through the rotating of the fiber squeezer about the fiber, the induced birefringent axis can be changed as illustrated in Fig. 1.6 [59].
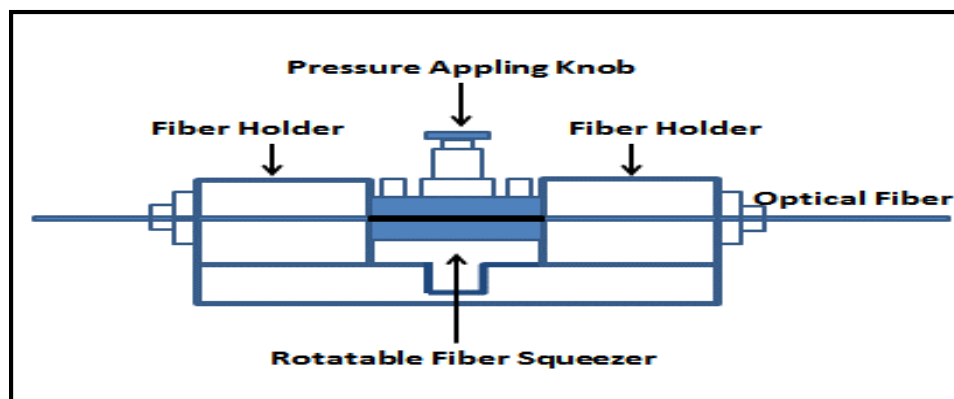
Fig. 1.6: In-line Polarization controller device [59].

1.4 Pumping Sources of Fiber Laser

Pumping of lasers can be achieved via electrical, chemical, and optical pumping. Fiber lasers are optically pumped by another diode laser with a suitable wavelength. The main advantage of diode pumping is the high opto-optical

efficiency because there is a very good matching between the emission spectrum of the diode laser and the absorption spectrum of the active gain medium [60]. Compared to other kinds of lasers, diode laser offers distinct advantages, namely its compact size, low cost, and wide operation wavelengths. There are different types of diode lasers used in fiber laser technology [61].

The most common semiconductors used in diode lasers are compounds based on gallium arsenide, indium gallium arsenide, phosphide, and gallium nitride. Different types of diode lasers can be used as a pumping source for fiber laser low and high power diode laser There are two main kinds of pumping: when the pumping radiation is coupled directly into the core of active fiber (doped fiber) it will be called core-pumped active fibers (which is good for a short active fiber length), and when pumping radiation is coupled into the cladding of active fiber so-called clad pumped active fibers(the main advantages include the ability to couple high-power pump radiation from low-brightness diode lasers) [53].

1.5 Whispering Gallery Mode (WGM)

Whispering gallery modes or waves are specific resonances (for instance, sound waves, electromagnetic waves, etc.) of a given resonator (a cavity) with smooth edges [62]. They correspond to waves that rotate around the cavity, supported by continuous total internal reflection off the cavity surface, that meet the resonance condition (after one roundtrip they return to the same point in the same phase ($2\pi n$, where n is an integer) and therefore interfere constructively with themselves, forming standing waves). These resonances depend dramatically on the resonator cavity geometry [63]. Consider a microsphere of radius a with refractive index n and a ray of light propagating inside, hitting the surface with an angle of incidence Θ_i, Fig. 1.7.

If $\Theta_i > \Theta_c = \arcsin(1/n)$, then total internal reflection occurs. Because of spherical symmetry, all subsequent angles of incidence are the same, and the ray is trapped. This simple geometric picture leads to the concept of resonances. For large microspheres ($a \gg \lambda$), the trapped ray propagates close to the surface and traverses a distance $\approx 2\pi a$ in a round trip. If one round trip exactly equals m wavelengths in the medium ($m = $ integer), then one expects a standing wave to occur. This condition translates into $2\pi a \approx m$ (λ/n) since λ/n is the wavelength in the medium.
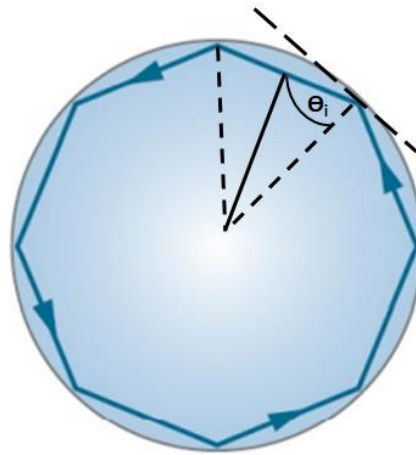
Fig. 1.7: Optical whispering gallery.

One of the most important quantities that describe the performance of any resonator is the quality factor or Q-factor, there are many reasons why Q factor is important, with increasing Q factor or quality factor, so the bandwidth of the tuned circuit filter is reduced. As losses decrease so the tuned circuit becomes sharper as energy is stored better in the circuit. Filters based on optical whispering gallery resonators are among the most developed applications of whispering gallery resonators. The intent is to use them for processing signals in optical communications, where ring resonators with Q-factors are adequate.

1.6 Wave-guiding Optical Fiber

Optical fibers can be defined as cylindrical dielectric waveguides that transport light. Each fiber consists of a core radius a and refractive index n_1 (has a diameter of about 5-100 μm), surrounded by a cladding of a slightly lower refractive index n_2 (most of the cladding has a diameter around 125-200 μm). The glass fiber structure is coated with a polymer layer to protect the glass surface and to prevent any unwanted light to propagate in the cladding layer. Fig. 1.8(a) shows the basic structure of the optical fiber. When an electromagnetic wave is injected into the core at an angle greater than the critical angle, it propagates through the core of the fiber via the principle of total internal reflection (TIR), as shown in Fig. 1.8(b).
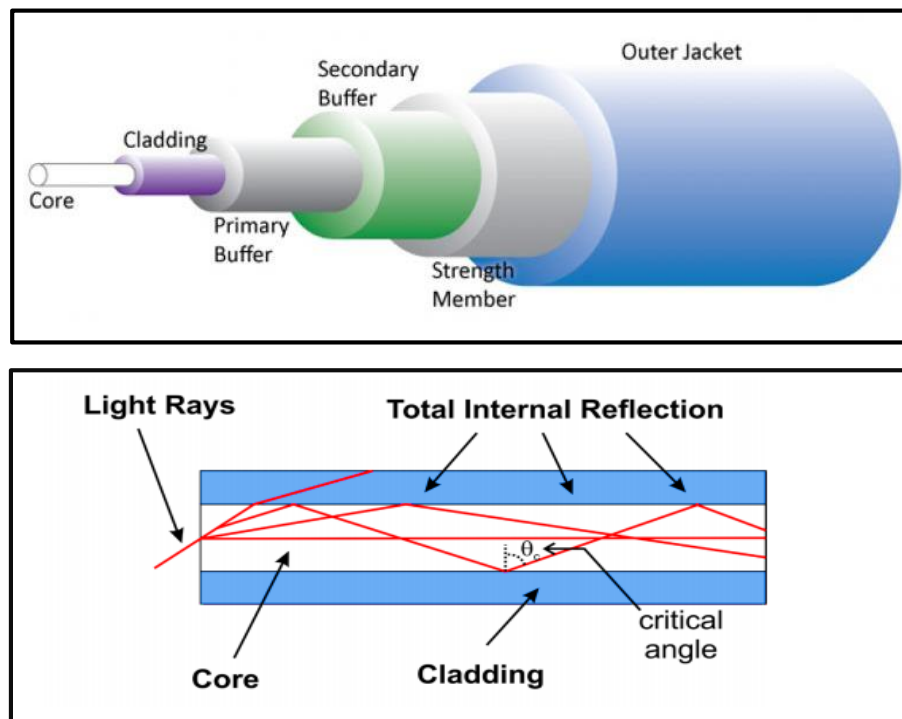
Fig. 1.8: (a) Basic structure of the optical fiber,

and (b)Confinement of light within fiber core by total internal reflection [64].

Depending on the fiber diameters of core and cladding, the fiber allows the propagation of a single transversal mode (SMF) or a multiple transversal modes

(MMF). The last one is classified depending on the fiber refractive index of core and cladding, step index fiber (SIF), or graded index (GIF) as showin in Fig. 1.9. When light incident on the fiber end face at a certain angle known as the acceptance angle, light will be confined into the fiber core. Cladding part prevents light propagation outside of the fiber.
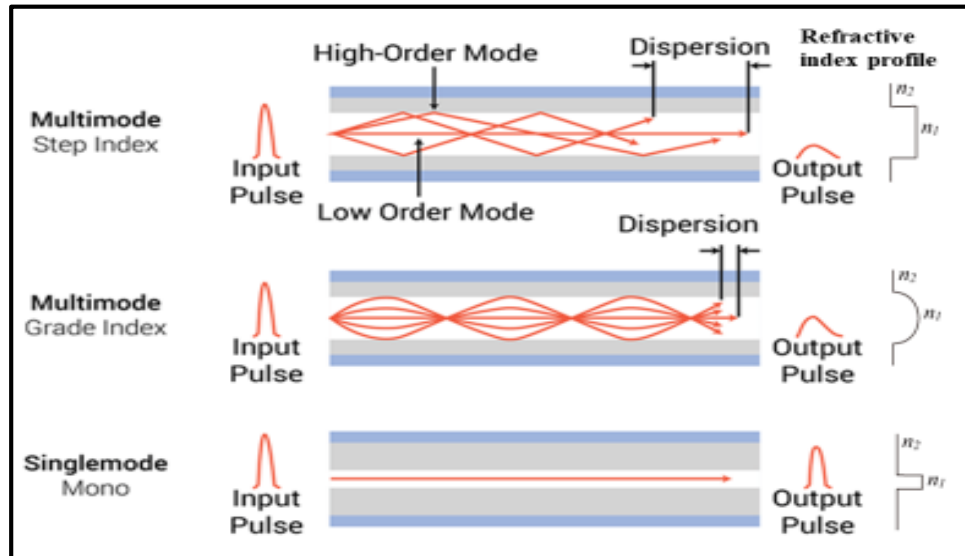
Fig. 1.9: types of optical fiber and light propagation.

The maximum angle of incidence (Θ_i) for coupling light into fiber core depends on the core and cladding refractive indices [64]:

$$n_o \sin\Theta_i = (n_1^2 - n_2^2)^{\frac{1}{2}} \qquad\qquad (1.1)$$

Where n_o is the refractive index of the medium outside the optical fiber and is usually 1 for air. The quantity $n_o\sin\Theta_i$ defines the capability of light confinement in a fiber which is known as the numerical aperture (NA). NA and normalized frequency (V) are important parameters of fiber to determine how many modes are supported by the waveguide at the signal wavelength (λ), V parameter can be defined as:

$$V = a \ (2\pi/\lambda_s) \ NA \hspace{4cm} (1.2)$$

A step-index fiber can only support a single mode if V < 2.405, which is known as the cut-off condition for single-mode fiber. For larger V parameters, the number of supported modes can be approximately calculated by $V^2/2$ [65]. A SMF operating at 1.55 µm has the lower attenuation and is free from intermodal dispersion making the optical signal to be maintained over a long distance. Therefore, optical fibers now hold a promising place as the backbone of communication systems and in fiber lasers that use rare-earth-doped fibers as a gain medium.

1.7 Rare-earth Ions and doping concentration (N)

Fiber lasers are based on glass fibers doped with rare-earth ions. An optical fiber becomes an active fiber when one or more rare-earth elements are incorporated into the fiber core during the fiber fabrication process. By incorporating different rare-earth ions, such as erbium, neodymium, and ytterbium, fiber lasers become capable to operate over a wide range of wavelength extended from 0.4 to 2.9 µm.

The dopant concentration of an active fiber is an important parameter of laser gain medium often specified in percentage of the dopant in molar parts per million (PPM) or by the number density (N) of the laser-active ions, i.e., the number of ions per cubic meter or cubic centimeter. The operation wavelength of fiber lasers is usually determined by the transitions between the energy levels of the doped rare-earth ions. Rare-earth ions have unique features that make them distinguished from other optically active ions. The emission and absorption transitions wavelength are independent of the doping concentration of the host material, they emit and absorb within narrow line-widths at wavelengths ranging from UV to IR, the lifetimes of metastable states are long, and the quantum efficiencies have a tendency to be high.

These properties are a result of their unique atomic structures which are very important for applications in lasers and amplifiers [64].

Table 1-1 shows the main rare-earth ions with their commonly used host glasses. Also, it contains their wavelength absorption and emission ranges [55]. The following sub-sections explain the spectroscopic properties of the greatest utilized rare-earth ions (Yb^{3+} and Er^{3+}).

Table 1-1: Rare-Earth Ions with their Absorption and Emission Wavelengths [55].

Ion	Common Host Glasses	Absorption Wavelength (nm)	Emission Wavelength (nm)
Neodymium (Nd^{3+})	Silicate and phosphate glasses	590, 807, 815	1030-1100
Ytterbium(Yb^{3+})	Silicate glass	850, 980, 1047	1000-1100
Erbium (Er^{3+})	Silicate, phosphate and fluoride glasses	800, 980, 1480	1550-1600
Thulium (Tm^{3+})	Silicate, germinate and fluoride glasses	790, 808, 1064, 1550	1700-2100
Praseody mium(Pr^{3+})	Silicate and fluoride glasses	888, 1048, 1080	1300, 634
Holmium (Ho^{3+})	Silicate, and fluorozirconate glasses	2040, 2076	2100, 2900

1.7.1 Ytterbium ion-doped Fiber (YDF)

Ytterbium ions are a versatile dopant of silica-based host medium. It gained several interests as a laser ion in the form of ytterbium-doped fiber lasers (YDFL). This can be attributed to certain defining features that appear from the simple structure of the energy level such as, longer upper-state lifetime and the ability to absorb pump photons over a wide spectral range. The simple electronic structure of Yb^{3+} is illustrated in Fig. 1.10 [53]. It is divided into two manifolds; $^2F_{7/2}$ is the ground level splits into four stark levels, and $^2F_{5/2}$ is the exciting level splits into three stark levels.

The main advantage of YDF comes from that, only one excited level manifold is concerned in the laser transition. The small energy gap between the ground and excited state of ytterbium ion results in low quantum defects. Thus high power efficiency is possible. In addition, YDF offers several advantages such absence of quenching, high gain-bandwidth which make it attractive for high power and ultra-short pulse applications [43].
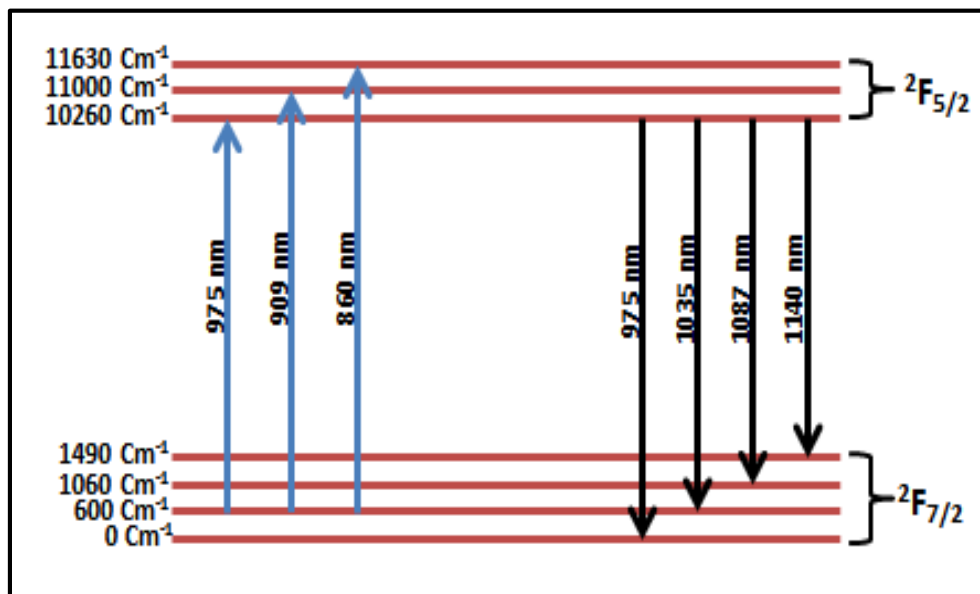
Fig. 1.10: Yb^{3+} energy level structure [53].

YDF has quasi-three-level or four-level behaviors based on the pump wavelengths. For emission wavelengths shorter than 1080 nm, the lower laser transition state is very close to the ground level similar to a quasi-three level system [43]. For wavelengths higher than 1080 nm, the laser transitions occur at energy levels higher than ground-level, therefore the system displays a four-level system behavior. The simple structure of the Yb^{3+} energy level leads to high absorption and emission cross-sections, which are also dependent on the host medium. The absorption and emission cross-section of Yb^{3+} is illustrated in Fig.1.11 [53].
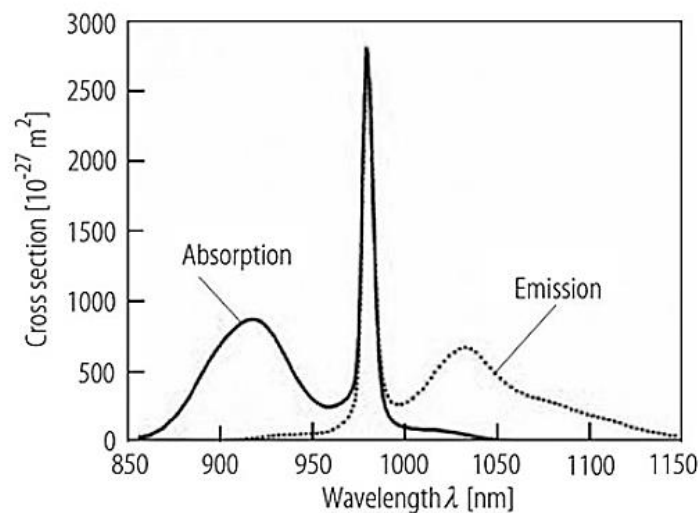
Fig. 1.11: Absorption and emission cross-sections of Yb^{3+} -doped glass [53].

1.7.2 Erbium ion-doped Fiber (EDF)

EDFLs operate in the important third communication window around 1550 nm which exhibits the minimum loss ~ 0.2 dB/km preferred in light wave communication systems. The performance of EDFLs was improved when they are pumped at the 0.98 or 1.48 µm wavelength because of the absence of excited-state absorption. This means that we can use a cheap diode laser as a pump source and we get very high quality and potentially high power beam out at 1550 nm [53]. Fig. 1.12 shows the energy level diagram of Er^{3+} with the optical transition of the 4f shell [66].

From this figure, one can observe that EDFLs have a three-level system since the lower laser level is the ground state.
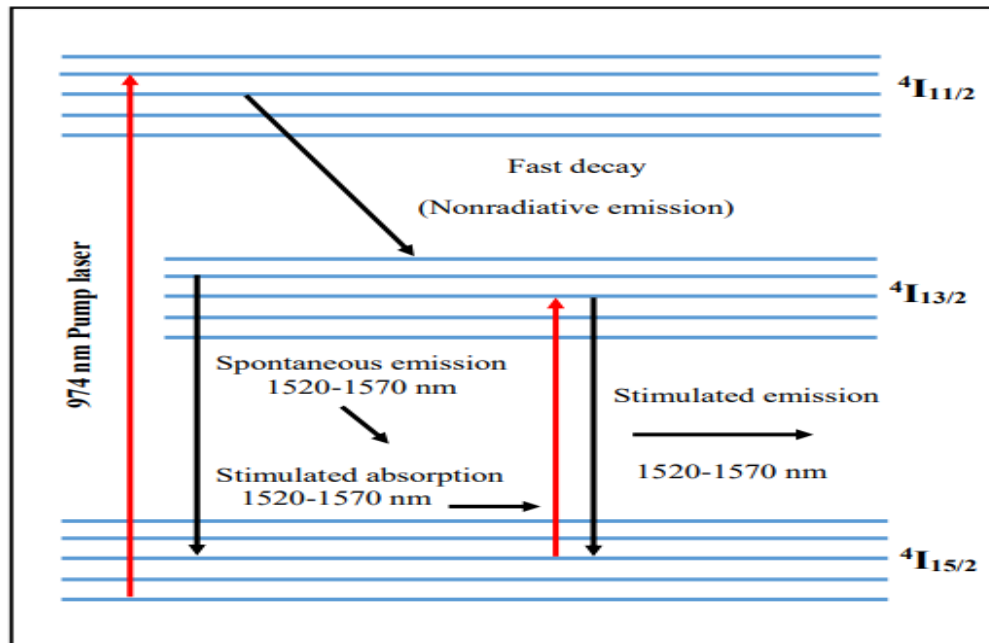
Fig. 1.12: Energy Level Scheme of Er^{3+} Transitions [66].

The energy level of Er^{3+} is split into multiple sub-levels due to stark effect. This splitting causes broad emission bandwidth. When the Er^{3+} doped fiber is pumped by 980 nm, Er^{3+} will be excited from the ground state $^4I_{15/2}$ to the higher level $^4I_{11/2}$. Then, the excited Er^{3+} at $^4I_{11/2}$ makes a fast decay to the lower energy level $^4I_{13/2}$ under non-radiative emission. The excited ions on $^4I_{13/2}$ finally return to the ground state $^4I_{15/2}$ through spontaneous emission [66].

The spontaneous emission will be amplified during its propagation through the fiber as a function of pump increasing. When the photon's energy equal to the energy difference between $^4I_{13/2}$ and $^4I_{15/2}$, amplified spontaneous emission (ASE) occurs. ASE extends over a wide wavelength range from 1520-1570 nm, thus it can be used as a broadband light source. If a laser signal with a wavelength between 1520 and 1570 nm, and a 974 nm pump laser is lunched into an erbium doped fiber.

Fig. 1.13 shows the absorption and the emission cross-sections measured at room temperature in the 1.5 μm spectral range. The absorption region between 1450 to 1550 nm gives the possibility to achieve high power efficiency. That is because of the closeness between the pump and signal wavelength. In erbium, the emission has a broad bandwidth of about 50 nm allowing the amplification to take place in the telecommunication window [53, 66].
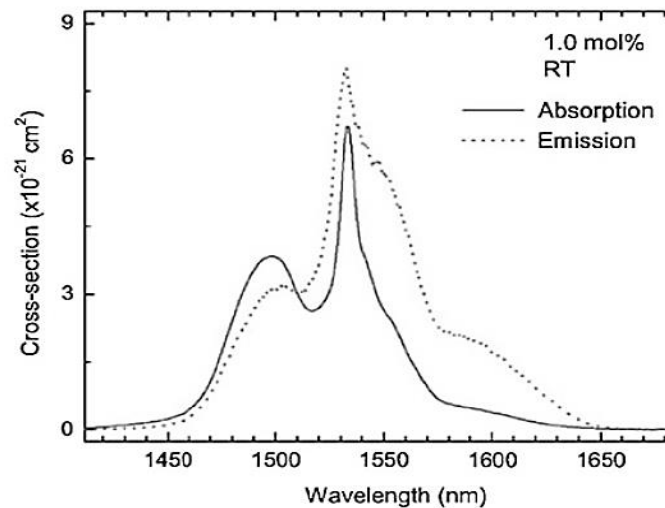
Fig. 1.13: Absorption and emission cross-sections of the Er^{3+} -doped , PKBAEr glass [8,53].

1.8 All Fiber comb-filter

Optical filters are utilized in widespread fields of application within optics and optical fiber systems. Optical filters are frequency domain systems that eclectically weaken or pass specific wavelengths. The common parameter in all-optical filters is their reliance on particular wavelength-sensitive influence. Generally, optical filters are dependent either on interference or diffraction phenomena [57]. Optical comb filters as essential components play a significant role in optical signal processing, isolating the unwanted neighboring channels causing cross-talks in WDM. This is due to their simple design, low insertion loss, low cost, ease of use, and good fiber compatibility with the communication system [30,67,68].

Besides, comb filters find potential applications to be used as selective elements in multi-wavelength laser generation, and it is possible to modulate their transmission spectra by the external physical perturbations, such as torsion, strain, and curvature. Furthermore, it can be implemented with various fiber structures and configurations [69]. In this sense variety of techniques have been proposed to realize all-fiber comb filter functions such as FPI filters [70], SI loop [26,71], birefringent material with the polarization-dependent loss [72], and MZI filter [69].

There is a huge variety of optical filter configurations. The next filters are the most familiar [58] : FPI filter, SI loop filter, MZI filter.

1.8.1 Fabry-Perot filter

A simple FPI (It is also called an etalon) comprises two reflecting surfaces placed in parallel separated with a certain distance [73]. In this configuration, the interference happens due to manifold superposition of both transmitted and reflected beams from the parallel surfaces [74]. In the optical fiber cases, the reflectors are built up inside or outside the fiber to achieve the FPI. FPI filters also could be split into two types: extrinsic and intrinsic. In the external cavity reflector used in FPI filters out of fiber the interference signal obtained with high finesse as shown in Fig. 1.14(a) [75].

Moreover, FPI based filter fabrication is simple and low cost. Nevertheless, these filters suffer from many drawbacks like packaging, alignment problems, and coupling efficiency [74]. Intrinsic FPI filter fabricated with reflection component inside the fiber itself adopts different techniques such as fiber Bragg grating, micromachining, thin-film deposition, and chemical etching As shown in Fig. 1.14(b) [73].
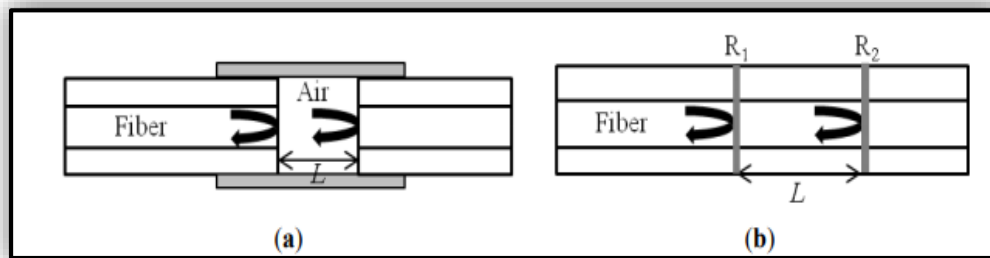
Fig. 1.14: FPI (a) extrinsic, (b) intrinsic [76].

1.8.2 Sagnac Loop Filter

Sagnac loop filter simply consists of a section of polarization maintaining fiber (PMF) and a 3 dB fiber coupler to form a loop. It resembles a ring cavity but performs differently because it has no feedback (single round trip) [77]. The operation principle of the loop filter is based on dividing the input light into two beams traveling with opposite arms. The two beams merge and create an interference

pattern at the output of the (50:50) coupler as shown in Fig. 1.15. Sagnac interferometer is incorporated inside the cavity from a Figure of eight configurations and acts as a comb filter.
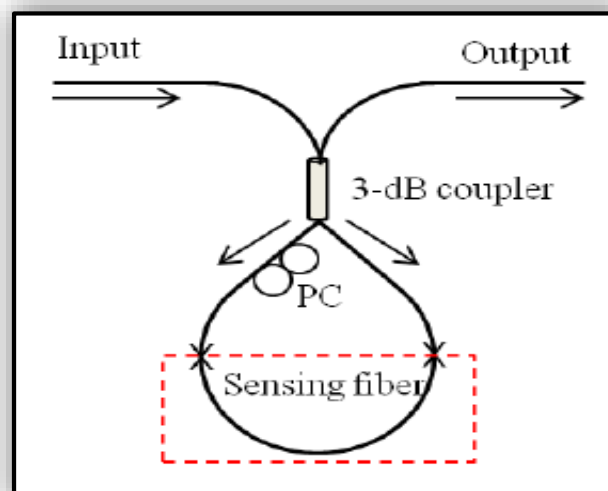
Fig. 1.15: Setup of Sagnac loop filter [77].

1.8.3 Mach-Zehnder filter

Fiber MZI has been considered as one of the oldest and most important optical fiber interferometers. These interferometers consist of two or more fiber beams (arms), which are split and combined by two optical couplers to measure the optical phase difference (OPD). Typically an incident light beam of an interferometer is split into two paths and then recombined together to create an interference pattern. The standard two beams fiber MZIs have been commonly used as optical filters [78], fiber modulators [MZM], and fiber sensors [79]. In general, these interferometers are constructed using two couplers.

The first 3-dB coupler divides the incident coherent beam equally between the two arms of the interferometer and recombines then at the output by the output coupler see Fig. 1.16. The OPD between the two arms is occurred either by changing the length of one of the arms or by changing the optical path length (like bending). This incident light beam will propagate along the same physical fiber length but with different optical path lengths due to modal dispersion; the core mode beam has a higher effective index than the cladding mode beam [80].
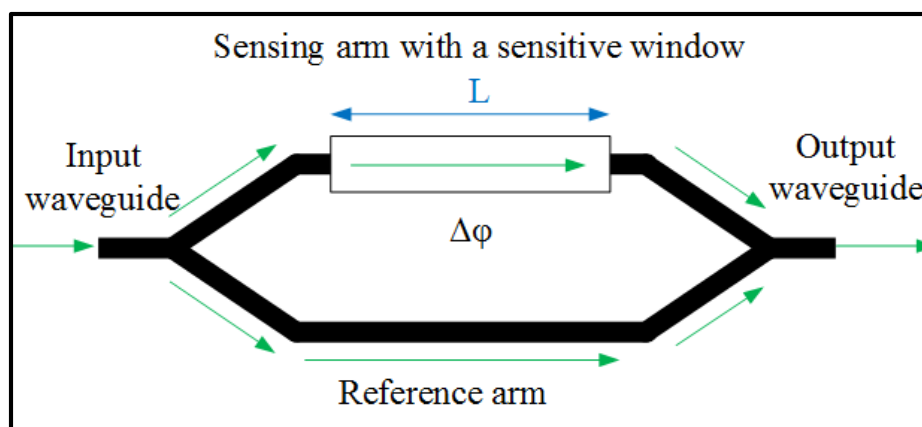
Fig. 1.16: The schematic diagram of MZI [78].

There are several configurations usually employed to form in-line fiber MZIs, i.e. taper, FBGs, core offset, mode mismatch, etc. The following subsections give brief descriptions of general types of in-line fiber MZIs.

1.8.3.1 Tapered Fiber MZI

Tapering is an effective way to convert a relatively large ratio of energy in the fundamental mode to the high-order cladding modes in optical fiber. As light travels along the tapered fiber region where the diameter of the tapered fiber can be only a few microns over a length of a few centimeters, thus, the energy loss from the fundamental mode would be coupled to the high order cladding modes. An effective tapered MZI can be constructed by tapering a fiber at two-point along with the fiber as shown in Fig. 1.17 [80].

This technique is cost, simple but weak mechanically essentially at the tapering region. This type of interferometer is widely used in sensing applications, especially in temperature and refractive index sensors since it has very sensitive to external disturbance [79].
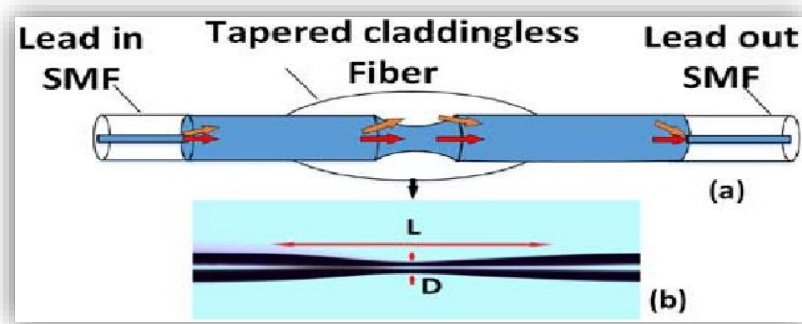
Fig. 1.17: A tapered fiber MZI configuration technique [80].

1.8.3.2 FBG based MZI

This type of fiber MZI has a pair of FBGs in which a part of the light beam guided as a fundamental mode within the core of the optical fiber is converted to cladding modes by the first FBG, now the core and the cladding modes are excited, and then recoupled again to the fundamental mode (core modes) by the second FBG [80]. In general, there are two categories of this interferometer, short period FBG with submicron period and long-period grating (LPG) with a period ranging 100 μm-1 mm.

The structure of an LPGMZI is depicted in Fig. 1.18. This interferometer is preferred in refractive index sensing applications. The main challenge of this interferometer is working in limited bands of wavelength because of the phase-matching phenomenon of fiber gratings and the LPG should be identical to have maximum performance.
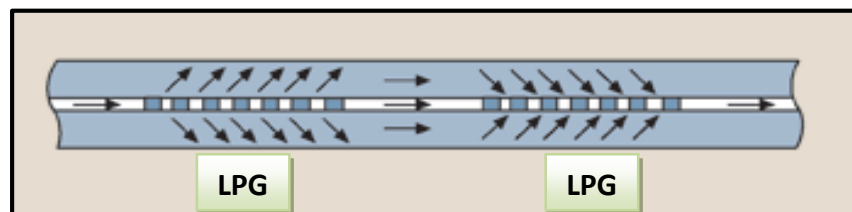
Fig. 1.18: A LPG MZI configuration technique [80].

1.8.3.3 Core-Offset Fiber MZI

Core-offset structure is formed by fusion splicing two segments of fibers with a pre-set offset value i.e. usually several micrometers. As shown in Fig. 1.19, a part of the beam guided into the lead-in fiber in form of core mode will be split into two parts. The first part represents the modes still guided within the core and the core mode give-up some of its energy to excite the cladding modes. Core-offset MZI has been used as an optical attenuator in optical communication systems [81].
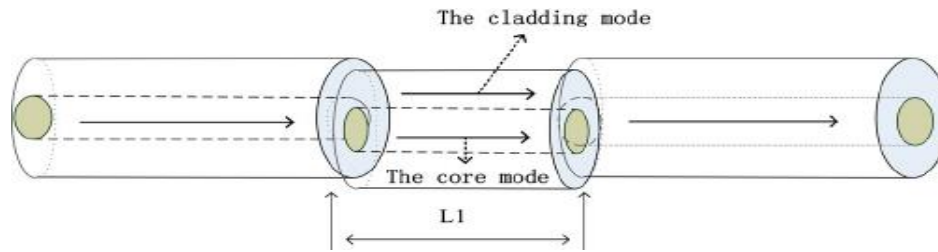
Fig. 1.19: A core offset fiber MZI configuration technique [81].

1.8.3.4 Core-mode mismatching based MZI

Core-mode misalignment between two fiber segments can also affect a portion of core mode light coupled into cladding modes. Through this technique, the beam inside the optical fiber is to utilize fibers having various core sizes or various mode field diameters (MFDs) as demonstrated in Fig. 1.20. In this design, the fabrication method is simply verified by splicing an MMF with two short sections of SMF (SMF-MMF-SMF MZI structure) [80].

The MMF has a greater core size besides standard SMFs. However, the variance in MFDs among the fundamental core mode of the SMF in addition to MMF leads to the splitter fraction of the fundamental core mode from SMF and excitation of the first limited modes supported in MMF. These modes will be joined again in the second spliced locations.
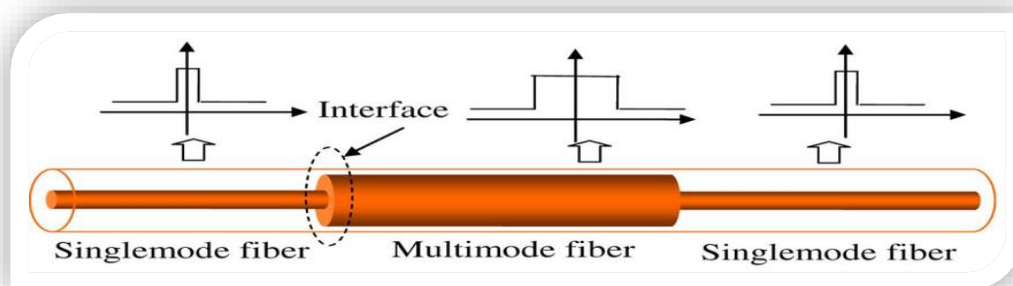
Fig. 1.20: core-mismatch MZI configuration [80].

1.8.3.5 Mach-Zehnder interferometer with Optical fiber bending loss

Optical fibers suffer radiation losses at curves on their paths. This is due to the energy in the Whispering Gallery Mode (WGM) field at the bend exceeding the velocity of light in the cladding. Bends are divided into two types: Macro bend loss which refers to losses generated in bends around mandrels of a specified diameter.

Microscopic bends with a radius of curvature approximating the fiber radius mustn't be produced in the fiber cabling process. These so-called micro bends loss denotes specified minimum scale "bends" in the fiber, often from pressure applied on the fiber itself [82].Recently, lots of configurations based on bent fibers are utilized as optical filtering configurations such as u-shaped, c-shaped, s-like, cascading multiple ring bent fibers [83], balloon-like bending optical fiber configuration.

Optical comb filters as essential components that play a significant role in optical signal processing, isolating the unwanted neighboring channels causing cross-talks in DWDM. That is owing to design the straightforward, minimum insertion loss, low cost, convenience of usage, that excellent fiber compatibility with the system of communication. All these specifications are highly desirable features in fiber optic filters.

Besides, comb filters find potential applications to be used as selective elements in multi-wavelength laser generation, channel spacing, and it is possible to modulate their transmission spectra by the external physical perturbations, such as torsion, strain, and curvature. Furthermore, it can be implemented with various fiber structures and configurations [69]. This structure can be fabricated by bending a section of optical fiber into the balloon-like shape utilizing a segment of a capillary

tube and adjusting the radius of curvature by several millimeters, by pulling the termination of the two ends of the fiber gradually to change the bending diameter.

When light reaches the bending section, a fraction of the light will be free from the core mode and penetrates the cladding as the light propagates within the structure bending segment. Then, the cladding modes will have recoupled back to the core mode called WGM, accordingly, an MZI modal interferometer can be efficiently formed between the cladding modes and the remaining core mode owing to the differences in effective refractive indices RIs of the core and cladding modes. As well as the optical path differences experienced through the light signals propagating in the core and the cladding modes [84].

In this thesis, MZI based on balloon-like fiber was proposed and constructed experimentally, the principle and operation of these MZIs interferometers will be clarified in detail in the next section.

1.9 Filtering Principles and Operation

The schematic structure of the proposed MZI based filter is shown in Fig. 1.21(a). Without being removed from the coating, the balloon-like interferometer with a bending diameter d and a total length L was implemented utilizing a conventional SMF (coring SMF-28) section. First, a 15 cm long SMF in its straight state was used to construct the balloon-like structure. A short section of a thin silica capillary tube with a length of 15 mm and a diameter of 800 μm was inserted into both ends of the straight SMF.

Then, the bending was performed with the aid of a thin silica capillary. This was performed by moving the capillary tube along the SMF and adjusting its location, different bending diameter of the balloon-like structure was easily adjusted. Then, to facilitate the incorporation of the filter inside the ring cavity, the automatic

mode of the commercial fusion splicer (Fujikura FSM-60S) was selected to splice the optical FC/PC connector with 0 dB losses at both ends of the bent SMF and to reduce the overall cavity losses as much as possible.

Finally, the constructed structure was adhered to a glass plate using UV glue around the capillary tube to prevent it from vibration or movement.
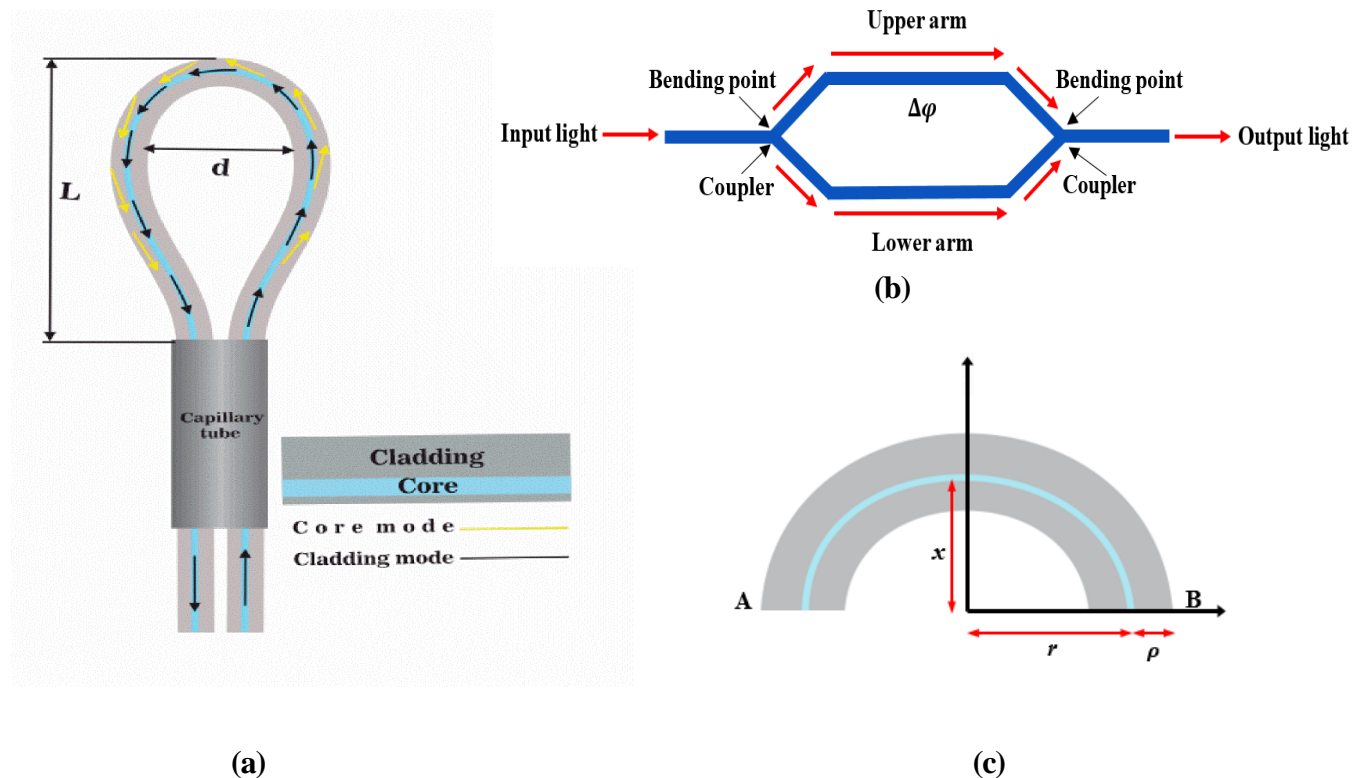
Fig. 1.21. (a) Balloon-like interferometer structure-based comb-filter, (b) schematic representation of the proposed MZI based comb, and (c) geometrical model of the macro bending structure.

The basic operational theory of the balloon-like MZI is based on the modal interference between the core mode and the cladding mode, which can be described as follows: when the light passes through the bent section, a part of the propagating light escapes from the constraint of the SMF core and penetrates the cladding at

which point it excites the cladding modes. As these excited cladding modes pass the balloon-shaped bending section it will then re-couple back into the SMF core at the waist of the bend and form the so-called whispering gallery mode phenomena (WGM), which then interact with the residual core mode.

Therefore, the optical path length difference in the cladding modes and core modes will establish the modal interference in the straight lead-out SMF [85]. Thus an MZI is formed due to the existence of differences in RIs of the core and cladding and the optical path differences experienced by the light signals propagating in the core mode and the cladding modes.

In this MZI the bending points act as fiber couplers while the core and cladding act as the interferometer arms as illustrated in Fig. 1.21(b). The balloon-shaped bending diameter would be modified as the capillary tube progressively goes up and down along the SMF. As a result, the impact of changing the bending diameter can be observed and measured via the resonance wavelength change of the transmitted spectrum. The transmitted light intensity passes through the balloon-like MZI can be represented as [37-40]:

$$I_o = I_c + I_{cl} + 2\sqrt{I_c I_{cl}} \cos{(\varphi_{in} + \Delta\varphi)} \qquad (1.3)$$

where I_c and I_{cl} represent the core and cladding modes intensities, respectively. φ_{in} is present the initial phase, and $\Delta\varphi$ defines the phase difference between the core and the cladding mode, which can be given by:

$$\Delta\varphi = \frac{2\pi\Delta n_{eff}L_{eff}}{\lambda} \qquad (1.4)$$

where λ is the light wavelength in free space, Δn_{eff} is the effective refractive index difference between the core and coating mode, and L_{eff} is the effective length of the bending region. When $\Delta\varphi = (2m + 1)\pi$, where m is a positive integer equal

to 0, 1, 2 …, an interference dip appears at specific wavelengths (λ_{dip}), which is given by:

$$\lambda_{dip} = \frac{2\Delta n_{eff} L_{eff}}{2m+1} \qquad (1.5)$$

the transmission spectrum of the balloon-like interferometer has a free spectral range (FSR) of which can be expressed by [86]:

$$\textbf{FSR} = \frac{\lambda_{dip}^2}{\Delta n_{eff} L_{eff}} \qquad (1.6)$$

As a consequence, a longerL_{eff} would result in a narrower FSR of the balloon-like MZI. In this work, L_{eff} is not just the length of the bent SMF segment but the effective length that enables the transmission of the exited cladding mode. In general, a smaller bending diameter allows the light to reach the cladding layer earlier and to obtain a greater transmitting length for the excited cladding mode. This implies that a longerL_{eff} can be accomplished with a smaller bending diameter.

Even as the bending diameter applied to the form of the balloon shape is different, the value of Δn_{eff} and L_{eff} can vary accordingly, resulting in a change in the FSR of the transmitting spectrum [86]. From the experiment work, it is obvious that the parameters L is directly proportional with d of our interferometer. The length of the silica tube was about 15 mm. The effective bending length L_{eff} is the effective bent length between point A and point B along the curved fiber as illustrated in Fig. 1.21(c).

The resonance wavelength of the bending section as a function of bending curvature radius can be expressed as:

$$\frac{d\lambda_{dip}}{dr} = \frac{\lambda_{dip}}{r} + \frac{\lambda_{dip}}{n_{eff}^{core}(r) - n_{eff}^{cladding}(r)} \times \left(\frac{dn_{eff}^{core}(r)}{dr} - \frac{dn_{eff}^{cladding}(r)}{dr} \right) \qquad (1.7)$$

Where r is the curvature radius of the balloon region. According to the elastic-optic effect, the outside layers' RI becomes higher than the inside layers for the bending region than the straight SMF. The equivalent RI model can be expressed as [87]:

$$n'(x) = n(x)(1 + \frac{x}{r_{eff}}) \qquad (1.8)$$

where $n'(x)$ and $n(x)$ describe the refractive index of the straight and the bent SMF, respectively. x is perpendicular to the bending axis, and r_{eff} is the equivalent bending radius that can be estimated as [88]:

$$r_{eff} = \frac{\rho}{1 - n(x)^2 \ /2[P_{12} - v(P_{11} + P_{12})]} \qquad (1.9)$$

where ρ is the radius of the fiber, P_{11} and P_{12} are components of the photoelastic tensor, and v is the Poisson ratio.

1.10 Literature Survey

Many research groups around the world have investigated different schemes that exploit the structure of the optical fiber comb filter (OFCF) technologies, so the macro-bending structure played an important role in recent years. A survey for the comb filter as MZI summarizes the most important published work related to the macro-bending sensor in Table 1-2.

Table 1-2: Summary of the Published Works in OFCF.

Year	Author	Type of structure	No. lasing line & range	Spacing adjusted & SNR	Ref.
2016	R E Nuñez-Gomez	two tapered SMF-28	Single tune from (1561.4-1530.41) nm Dual, triple /switch (1562.06 - 1528.43) nm	(15.81- 33.63) nm & OSNR= over 29 dB	[69]
2017	Mengmeng Han	2coupler 3dB with (PC) & a segment of tapered fiber in one arm.	Single tune	For FSR=0.8nm &SNR=17dB For FSR=0.4nm &SNR=11dB	[89]
2017	A.A. Jasim	Two SMF tapered with 9 micro-m	Dual switchable	Spacing (1.5, 3, 6)nm SMSR=55dB	[32]
2017	W A K haleel	SM-NLPCF-SM	Single(1549.7-1552.05)nm Dual (1549.3,1550.7)nm. Triple (1548.9, 1550.6 and 1552.2) nm	stable wavelength max spacing of 1.6 nm & SMSR= 48 dB.	[33]
2018	Guorui Zhou	SM-MM-MM mis-mach & gold coating	Multimode	SNR form (6 to 11.1) dB	[30]

2018	Anum Khattak	SMF/MMF/SMF	Single (1554.96 - 1564.25)nm Dual-V band 1557.936 nm L-band, 1565.582 nm	tuning range of 9.3 nm &SMSR= 45.1 dB largest spacing is 7.65 nm	[90]
2018	MENG MENG HAN	PC in 1st arm+ tapered in 2nd arm	Tune 16 lasing line	For Spacing 0.8nm SMSR= up to 35 dB For spacing 0.4nm SMSR= more than 30dB.	[31]
2019	Li Wei	two couplers + PC	Dual tune (1581.3-1581.5) nm & (1581.5-1581.8)nm	Spacing (0.2, 0.3)nm extinction ratio (40.9-27.3) dB	[91]
2019	Yanbiao Chang	SMF-few mode fiber (FMF) with two ellipsoidal structures and FMF-SMF with a core-offset splicing point	Switch dual-, triple- and quadruple wavelength	Spacing (1.6 -6.2)nm and SNR more than 30.68 dB	[92]
2020	Qi Zhao, Li Pei	two-segment Sagnac filter and Lyot filter with the assistance of nonlinear polarization rotation (NPR)	Group 1 tunable single-, dual-, triple-wavelength Group 2 tune quad-, quintuple-, sextuple- and septuple-wavelength	For group 1 spacing 18 nm and SNR 47dB For group 2 spacing not fixed and SNR more than 40 dB	[40]
2020	He Wei	SMF with two tapers.	Single, dual, triple switch (1557.92, 1563.2, and 1568.06) nm	For single(5.28& 4.86) nm SNR=24.7dB For dual(9.9, 6.6)nm, SNR=40.22, 41.43)dB For triple (5.7, 6.5) nm & SNR more(34.4, 33.7) dB	[20]
2020	J.D. Filoteo-Razo,	double-pass MZI & a Sagnac	Single tune	SNR(25, 30)dB	[93]

		interferometer (DP-MZI–SI)			
2020	He You	Cascaded MZI as filter (simulation design)	6 lasing line with flat top	-----------	[94]
2021	Pengfei Zheng	self-coupled microring assisted MZI	Single, dual / tune red shift	Spacing 0.3966 nm and 0.1983 nm extinction ratio is 35 dB for asymmetric MZI and 30 dB for symmetric MZI	[95]
2021	Fay F. Ridha	SM-NLPCF-SM	Single, dual, triple, quadruple (1030–1050) nm	For single SNR=45.13dB Dual spacing(0.77, 13.63)nm &SNR=30-40 dB Triple spacing(4.6, 9.5)nm& SNR more 34 dB Quadruple spacing(0.7, 12.44, 0.4)nm &SNR more 35.9dB	[96]

1.11 Aim of the Work

The main objective of this work is to demonstrate experimentally an adjustable channel spacing multi-wavelength fiber laser based on controlling cavity losses through macro-bending sensitive Mach-Zehnder interferometric as a comb filter. The simplicity and aspects like low-cost fabrication, reliability, and repeatability are highly desirable features in fiber optic filters. The results compare favorably in some aspects with other more complex filters and experimental setups.

CHAPTER TWO

Experimental Methodology

2.1 Introduction

Optical fiber filters have attracted special attention in abroad range of potential applications including WDM, optical signal processing, to be used as selective elements in multi-wavelength laser generation, and it is possible to modulate their transmission spectra by the external physical perturbations, such as torsion, strain, and curvature. Among several filter structures comprising the filter setup, all-fiber interferometers-based filters have been proposed and demonstrated to monitor various parameters. In this chapter, an optical filter is a good choice to achieve channel-spacing tuning range / switchable wavelength these filters based on macro-bending fiber structure have been designed and constructed.

The working principle of the macro-bending interferometer and the factors sensitive to change in lasing line from the fundamental to another lasing line has been elaborated. This filter configuration comprises a standard SMF that is bent with a specific bend diameter within obtains the assistance of a section of a capillary tube. The two ends of the SMF were spliced with an FC connector. The interference takes place between the core mode and cladding modes stimulated by the bent SMF. The experiments were carried out utilizing a small bending radius.

YDFL emitting near $1\mu m$ allows to produce a cost-effective and robust alternative device for several applications in biomedical, material processing, science, and high power laser operation [43]. On other hand, EDFL has many excellences such as narrow bandwidth and long-range tunability. It can be used in many potential applications such as sensing and communication because it radiates

at 1.55 μm lying in the third window of low loss in fiber-optic communications [44]. In this chapter, two-ring cavities of fiber lasers, YDFL and EDFL operating in continuous wave (CW) regimes were obtained with balloon shape-MZI structure as an optical filter.

2.2 Experimental Procedures

The experimental procedure of the doped fiber laser (DFL), all information of this system, methods, and fabrications will be described comprehensively follows many steps to fabricate the MZI-based balloon-like comb filter it will be explained in the following manner as illustrated in Fig. 2.1.

The first step of the experiment can be summarized in the following steps as illustrated in Fig. 2.2:

Experimental Procedures

↓

1st step build the setup of DFL Without proposed filter

↓

2nd step injected balloon shape like MZI as comb filter at different bending diameter

↓

3rd step, DFL with balloon shape like MZI as comb filter at minimum d and increasing pump power

↓

4th step, DFL with balloon shape like MZI as comb filter at minimum d, higher power and PC
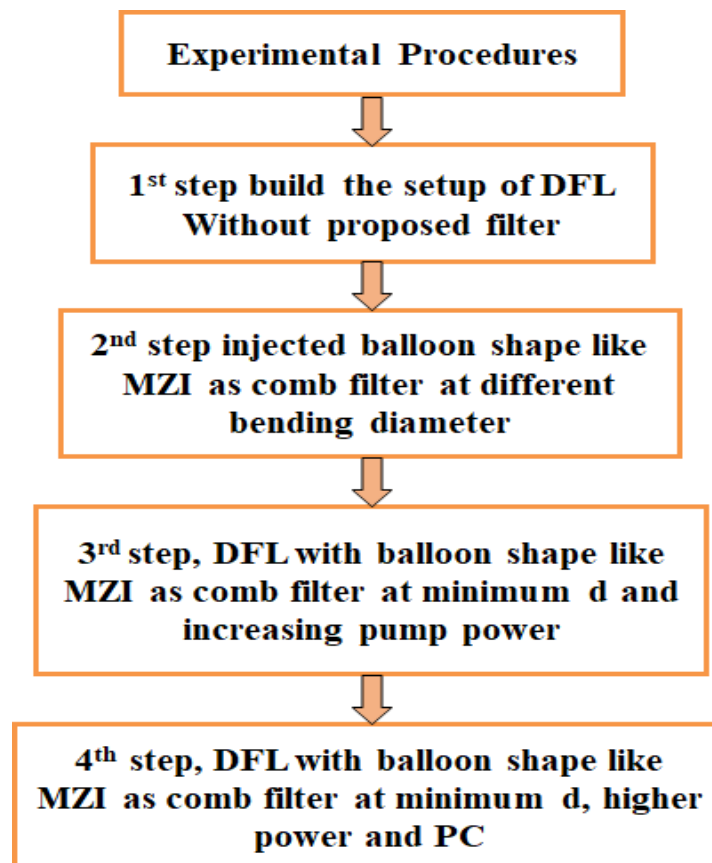
Fig. 2.1: The structure of chapter two.
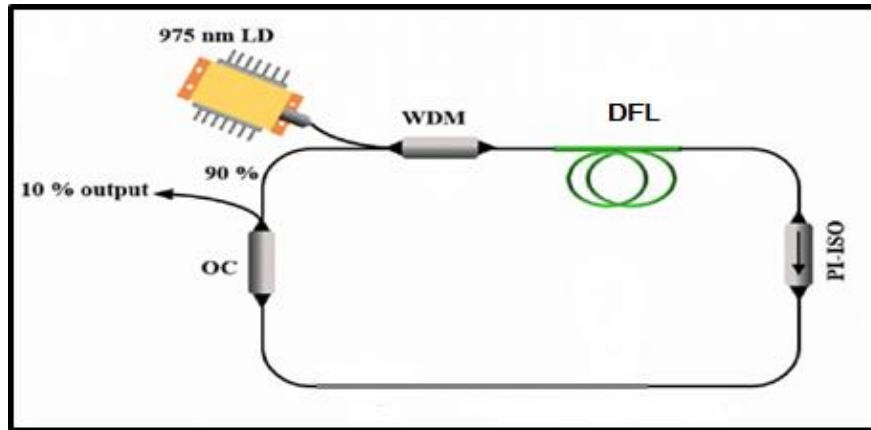
Fig. 2.2: Schematics diagram of doped fiber laser.

1. Connected the setups of DFL with 975 nm wavelength have been used for pumping the active fibers of both YDFL and EDFL. The pump source used in this experiment is a laser diode (LD) from Thorlabs (PL980P330J) which is a quantum well laser type chipped in a 14-pin butterfly package. It has a feature of high brightness and CW output which is coupled into an SMF pigtail. The compact design of this LD includes an integrated thermoelectric cooler, a monitor photodiode, and FBG to ensures very little shift in the output wavelength as the temperature and current are changed. The datasheet of the pump source is illustrated in appendix 1.

2. WDM consists of two inputs and one output as explained in appendix 2 for YDF and appendix 3 for EDFL. Where the first input connected to LD and the other input was connected to the terminal of OC (they combine the signal without interference with the two signals). While the output was connected to DFL.

3. Tow type of DFL was used in this experiment, YDFL, and EDFL (as illustrated in appendix 4 and 5 respectively) where the output port connects to the ISO.

4. In this step Connected to PI-ISO was a good choice to prevent feedback power and protect the DFL from damage (appendix 6, 7).

5. An optical coupler (appendix 8, 9) with 90:10, the 90% port returns to the cavity which is connected to WDM and the 10% port output of the CW-laser was connected to optical spectrum analysis (OSA) as demonstrated in appendix 8.

The second step of the setup was by inserted the proposed comb filter (SMF-28 corning appendix 10) based on balloon shape-like fiber structure inside the ring cavity of DFL. The position of the filter was connected between the ISO and OC with FC connector as showed in Fig. 2.3.

After completing the first step of the experiment, the studies amplify spontaneous emission (ASE) for YDFL and EDFL without the proposed filter, then measured the free spectral range (FSR) for the comb filter at different bending diameters.
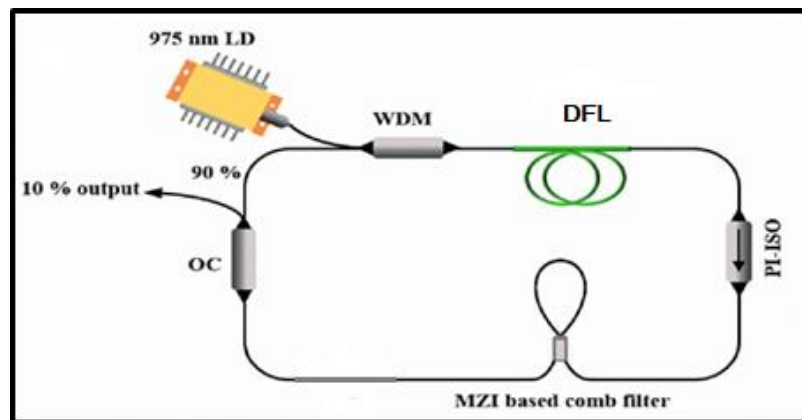
Fig. 2.3: Schematics diagram of comb filter based on balloon shape-like fiber structure.

In the third step, after fixed the bending diameter of the proposed filter to the lower limit, then started to increased the pumping power gradually to the higher limit of the pumping source.

Finally, when the setup was fixed the bending diameter and pumping power then cascaded the PC (appendix 11) with a balloon shape inside the ring cavity of DFL. The idea of PC was by squeezing to the last limit and then manually rotating the polarization state in a different direction as brief in Fig. 2.4.
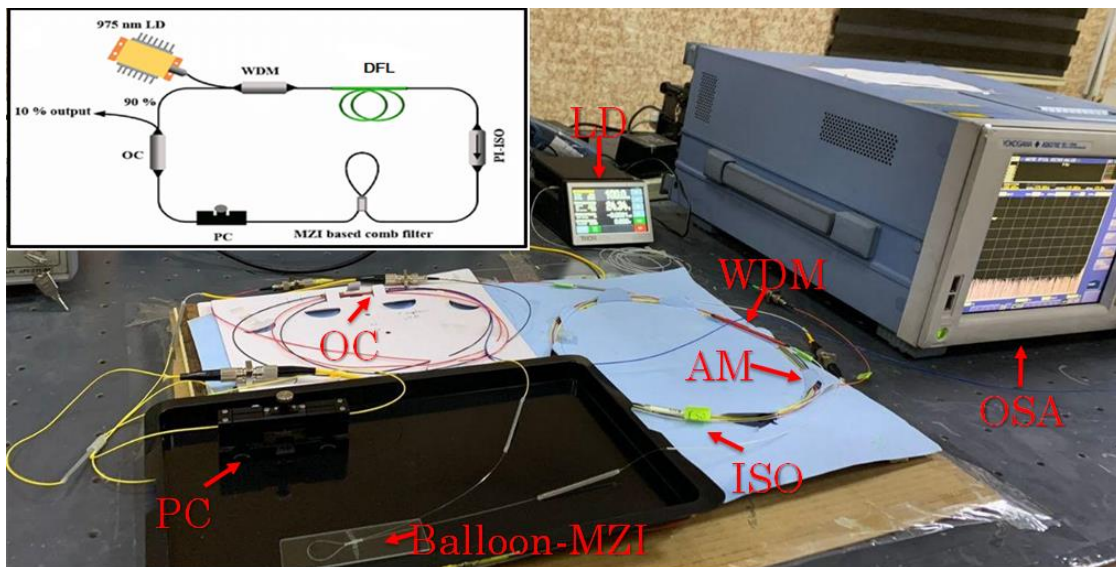
Fig. 2.4: Experimental setup of single- and multi-wavelength EDFL generation based on bent SMF structure.

2.3. The macro-bent balloon-like structure

The schematic structure of the proposed MZI based filter is shown in Fig. 2.5. Without being removed from the coating, the balloon-like interferometer with a bending diameter d and a total length L was implemented utilizing a conventional SMF (coring SMF-28) section. First, a 15 cm long SMF in its straight state was used to construct the balloon-like structure. A short section of a thin silica capillary tube with a length of 15 mm and a diameter of 800 μm was inserted into both ends of the

straight SMF.   The bending diameter and the overall length of the balloon-like structure section are termed as *d* and *L*, respectively.

One end of the bent structure was connected to the PC while the other part was connected to the PI- ISO. The two-terminal balloon shape is spliced with an Fc connector.
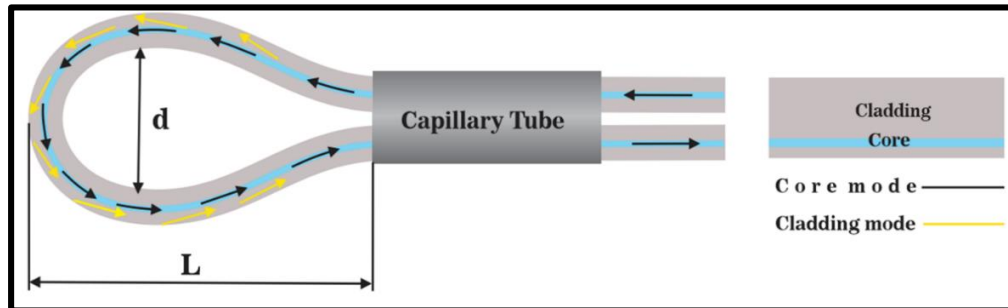
Fig. 2.5: Schematic of the balloon-like structure.

2.4 SMF cleaving and splicing

To prepare optical fiber for fusion splicing, the two fibers' ends should be cleaved at an accepted angle to minimize the splicing losses and to obtain good splicing. The first step for cleaving fibers was done by removing the polymer coating layer using mechanical stripping or alcohol. In these experiments, removing any protective coating such coatings can normally be mechanically removed with certain tools such as Optical Fiber Stripper (JIC – 375 Tri – Hole). The optical fiber stripper used for Stripping (by Fujikura Company).

The second step to prepare the fiber was done by fiber cleavers (cleaving machines) which allow to clamp the fiber into a well-defined position, to impose a suitable amount of tension, and to make the cleaving process by touching the fiber end with a sharp blade. The cleaving cuts the fiber at a 90° angle. The third step is cleaning the conventional single-mode fiber (SMF-28) with alcohol and tissue, Fig. 2.6 shows the photograph of optical fiber Cleaver (CT-30) (by Fujikura Company), which have been used in this experiment.

Splicer from Fujikura (FSM-60S) has been utilized in the experiments for splicing as shown in Fig. 2.7

Fig. 2.6: Optical fiber Cleaver (CT-30)   **Fig. 2.7:** photograph of (FSM-60S) fusion splicer.

2.5 Study the Influence of Varying the Bending diameter

In this study, the influence of various bend diameters has been investigated experimentally. After collecting information from the OSA, we obtained the small bending diameter. When the bending diameter is 4 cm or more, no resonance interference pattern occurs within the wavelength range since hardly any light is coupled into the SMF cladding and/or coating modes. As the bending radius decreases, more signals will leakage into the fiber cladding modes and recouples back to interfere with the residual core mode. From Fig. 3.12 and Fig. 3.1 (in the next chapter), it can be observed that as the bending diameter in a balloon shape structure decreases to values between 15 mm in EDFL and 5 mm for YDFL for no recognized interference dip was noticed again, which may be owing to the high loss caused by the variance in optical path lengths of the SMF core and cladding.

Furthermore, at 40-35 mm bend diameter, there is an obvious interference dip that was noticed. But then, if the bending diameter reduces further, an excess of light signals will escape into the cladding and also leak out of the fiber causing a weak

modal interference and substantial loss so the intensity of the output signal reduces significantly.

From the indicated figure, the optimum bending diameter of (15-5) mm for YDFL and EDFL respectively were selected to form the balloon-shaped structure due to its resonance fringe has a high depth and narrow bandwidth. Also, it can be noticed that without an original protective coating, the glass is easily broken.

Then, the bending was performed with the aid of a thin silica capillary. This was performed by moving the capillary tube along the SMF and adjusting its location, different bending diameter of the balloon-like structure was easily adjusted.

Then, to facilitate the incorporation of the filter inside the ring cavity, by splicing the Optical FC/PC connector with 0 dB losses at both ends of the bent SMF and to reduce the overall cavity losses as much as possible as shown in Fig. 2.7. Finally, the constructed structure was adhered to a glass plate using UV glue around the capillary tube to prevent it from vibration or movement.

2.6 Calculation of the insertion loss for the comb filter

To calculate the amount of the insertion losses inside the comb filter:

1. Inserted power through straight SMF with 15 cm length and measured output power through the power-meter device.

2. Making balloon-like MZI with bending diameter 40 mm, measured output power then calculate insertion loss in dB:

$$\text{Insertion loss (dB)} = 10 \log [P_{in} \text{ (watt)}/ P_{out} \text{ (watt)}].$$

3. Repeat previous steps (no. 2) for each bending diameter to calculate insertion loss in dB.

CHAPTER THREE

Results of MZI interferometer as a comb filter

3.1 Introduction

Novel fiber bent techniques were developed and produced as a highly sensitive comb filter for an adjustable wavelength spacing fiber laser. The properties and fabrication for balloon shape- MZI as comb filter probes are examined experimentally in this chapter, using EDF and YDF. In comparison to other MZI filters, this filter is a relatively simple and cost-effective option.

Two types of fiber lasers were used to characterize the suggested filters in terms of transmission spectra. the first one a 2 m long EDF with an absorption coefficient of 27 dB/m at 976 nm (Liekki ER-4/125) with a peak wavelength of 1550 nm and the second one is a section of 1.5 m length YDF with an absorption coefficient of 250 dB/m at 976 nm (Nufern SM-YSF-HI) with peak wavelength of 1064nm, as shown in the following sections.

The experiments were carried out under the 0.02 nm resolution of the optical spectrum analyzer (OSA, Yokogawa AQ6370). The balloon-like MZI was used as a tuning component, lasing line selector and tuning channel spacing combined with the polarization controller (PC). A PC was also utilized to diversify the polarization state, balance the gain and loss at a certain wavelength, and adjust the wavelength spacing of multi-lasing line regimes [97].

The measurements of tuning channel spacing / switchable multi-wavelength were demonstrated by elevating the mode computation that occurs for the transmitted spectrum. The response of comb filter with balloon shape was observed for different power and controlling in line PC was studied and recorded.

All the results are taken under scientific laboratory conditions (at stable room temperature and humidity). The employment of the safety requirements was committed during the experiments.

3.2 Characteristics and Fabrication of balloon-like MZI based Comb filter with YDFL

SMF with 15 cm was utilized in our experiment. Firstly, to characterize the transmission spectrum of the proposed MZI based comb-filter, amplified spontaneous emission (ASE) light from YDF was passed through the fabricated balloon-shaped structure to analyze the spectral response of the MZI. Fig. 3.1 shows the spectral response of the proposed balloon-like MZI with different bending diameters, where the ASE reference is the line with black color.

This figure shows that the transmission spectrum (FSR) has a comb-like shape using a broadband source (Thorlabs SLD1550S-A1) with a wavelength range of 1450-1650 nm. It is also evident that the interferometer periods of the transmission spectrum of the MZI with a bending diameter of 5 mm were improved from 39.5 to 16.4 nm.

Therefore, in this work, the bending diameter of 5 mm was adopted to construct a comb filter for the multi-wavelength fiber laser generation, due to the modal interferometer effect. Modal interferometer phenomena occurred due to the optical path difference, the modes of SMF core are spitted and then recoupled with cladding modes at the bending segment region.
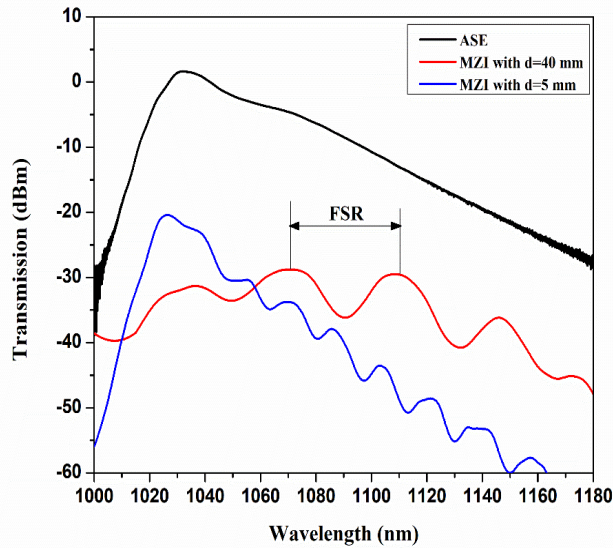
Fig. 3.1: Spectral response of the balloon-like shape based MZI at different bending diameters.
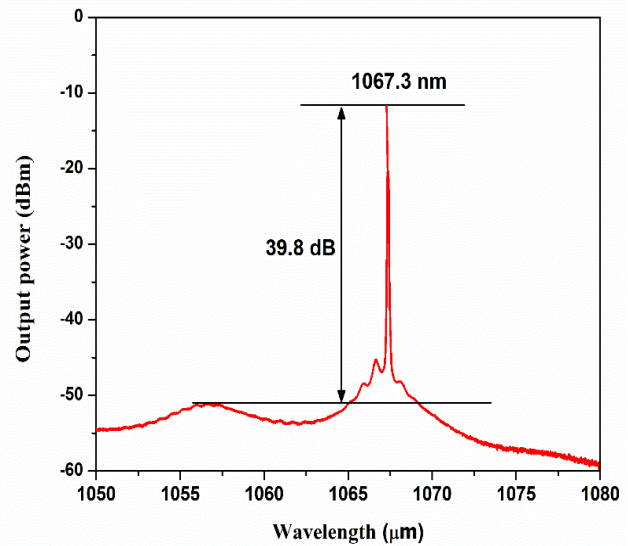
Fig. 3.2: YDFL output obtained before incorporating the proposed filter.

In the first step of the experiment, to carry out our experiments before incorporating the proposed filter, the laser diode was set at 93 mW, which was the threshold pump power of the currently constructed YDFL. The peak power of the YDFL was observed at 1067.3 nm with a maximal signal-to-noise ratio (SNR) of about 39.8 dB, as illustrated in Fig. 3.2.

Then, in order to achieve stable lasing performance, the YDFL cavity was pumped with a constant power of 115 mW. As the emission lasing wavelength is determined directly by the transmission peaks of the proposed comb filter, the single-wavelength lasing oscillation was observed at 1065.26 nm with a maximal SNR of about 38.8 dB at 40 mm bending diameter of SMF, as shown in Fig. 3.3. For the single-wavelength operation, only one lasing peak was resonating while others were alleviated. The following sections describe the influence of the balloon-like filter structure with different bending diameters.
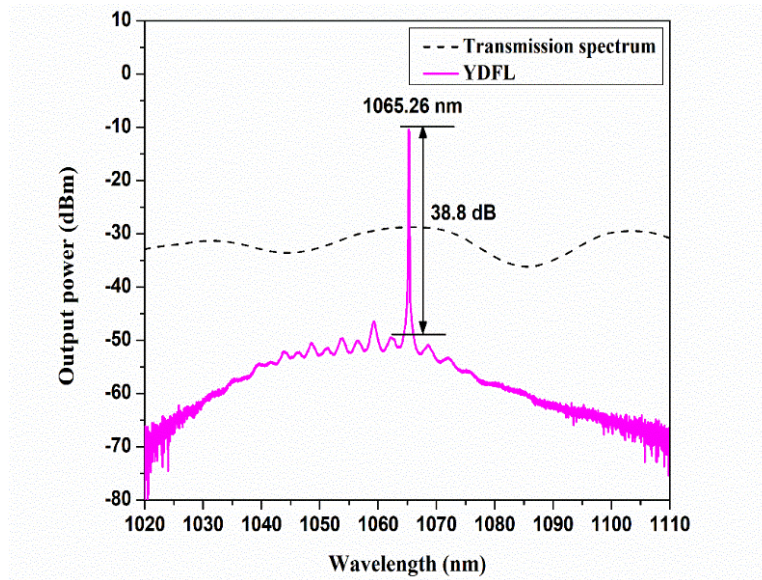
Fig. 3.3: Single-wavelength YDFL output obtained with 40mm bending diameter.

3.2.1 Characteristics of bending balloon-like MZI based Comb filter with YDFL

To achieve a tunable single-wavelength operation, the bending diameter of the SMF was adjusted by moving the capillary tube along the fiber. The curvature diameters of the bend SMF were changed from 40 to 5 mm with a decrement step of 5mm. As the bending diameter of the balloon-shaped based comb filter was varied from 40 to 20 mm, the lasing wavelength was tuned from 1065.26 nm to 1062 nm with stable channel spacing 0.8 nm. When the bending diameter decreased to a value slightly lower than 20 nm (in the interval from 15 to 5mm), an abrupt shift to a shorter wavelength occurs with channel spacing (2.5-4.6) nm.

The laser wavelength was shifted to 1059.5 nm at the bending diameter of 15 mm. With further bending the SMF to 5mm, the laser wavelength was tuned to 1048.6 nm with tuning shift 6.4 nm. Fig. 3.4 and Fig. 3.5 show the tuning of wavelength from 1065.26 to 1048.6 nm at different curvature diameters and with an almost linear tendency of R^2= 0.96. From Fig. 6, the decrement of the bending

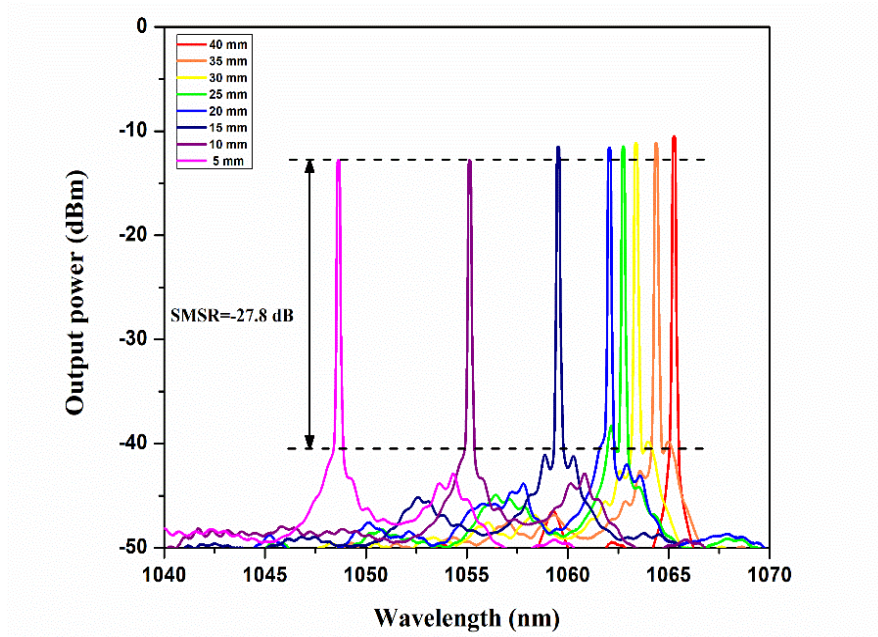diameter changed the effective refractive indices of the cladding modes and the laser cavity losses.

Fig. 3.4: Tunable YDFL based on balloon-like MZI based filter.
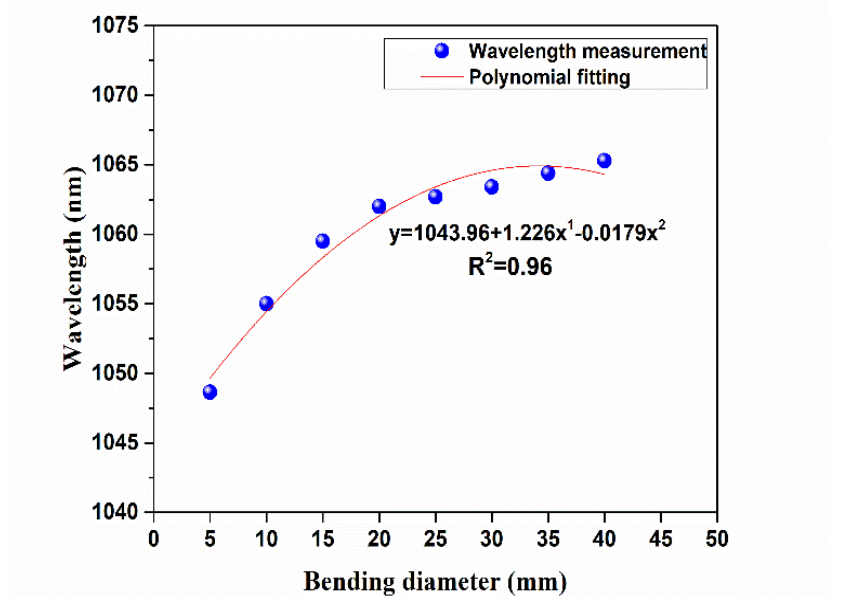

Fig. 3.5: Relationship between bending diameter variations with resonance wavelength shifts.

As it decreased, the central wavelength and the attenuation bands produced from the comb filter shifted towards the optical spectrum's blue side [87]. The resulting tunable single-wavelength exhibits a side mode suppression ratio (SMSR) of about 27.8 dB in the tuning range of 16.76 nm. "Mainly the shift in lasing wavelength depends on the selected length of the fiber formed the MZI" [98].

Also, due to the brittle nature of the bent fiber, which cannot go further in decreasing the radius of the bend, the obtained total tunability range is 16.76 nm ranging from 1048.6 to 1065.26 nm .The SMSR of the proposed method is very low at 27.8 dB. This is due to the macrobending fiber structure suffers high attenuation. When the core mode enters the bent section, the guided light power is split into two parts. Firstly, due to the SMF bending, the light power is partially leaked into the cladding modes is excited, and propagates along with the fiber.

Secondly, the light power which has not been coupled to the cladding will propagate as the core model. Light propagating parallel to the cladding-air interface will leak out. This results in a decrease in the magnitude of output power detected at the end of the SMF. Therefore, for any output lasing line, the SNR is low since the SNR is defined as the ratio of the signal power to the noise power. As a result, the overall SMSR for all has a moderate value.

In general, the operation principle of the tunable wavelength YDFL relies on the fact that the losses induced by bending the SMF interact with the gain at specific wavelengths within the emission bandwidth of the ytterbium ion. Also, by varying the bending diameter, the birefringence within the laser cavity can be adjusted, resulting in a balance between the gains and losses in the emission laser wavelengths. Moreover, the photoelastic effect resulted from the stress induced by controlling the applied curvature of the bend SMF section modifies the RI profile asymmetrically and causing the fundamental core mode and higher-order modes to propagate at

different phase delay, which adjusts the properties of the output comb-like spectral shape, like shifting the transmission spectrum output of the comb filter [99,100]. Thus a tunable fiber laser operation can be achieved.

3.2.2 Characteristics of the increasing power of balloon-like MZI based Comb filter with YDFL

In the fiber laser cavity, increasing the pump power can change the gain-and-loss distribution, resulting in shifting the peak wavelength of the spectral modulation to the other wavelength [100]. On the other hand, the controlled bending curvature diameter of the filter permits the selection between the single tunable wavelength or switchable multi-wavelength lasing performance [69].

Therefore, we concentrated on testing the lasing wavelength operation as a function of increasing pump power. Thus, the bending diameter applied to the proposed balloon-shaped interferometric filter was kept constant at 5 mm, and the injection pump power was increased to 127 mW and 170 mW, respectively. The refractive index of the YDFL decreases as the launched pump power increase, which causes the comb filter spectrum to shift with constant channel spacing.

The YDFL cavity is lased at a dual- and triple-wavelength. The dual-wavelength laser was achieved at 1048.6 nm and 1046.38 nm with a channel spacing of 2.3 nm, as shown in Fig. 3.6(a) and Fig. 3.6(b) represents the triple-wavelength laser at 1048.6 nm, 1046.38 nm, and 1043.8 nm with a channel space of 2.3 and 2.5 nm, respectively.

The dual and triple wavelength generation can be attributed to the pump power increases, more modes will acquire a sufficient gain to overcome the ring cavity losses [101,102].
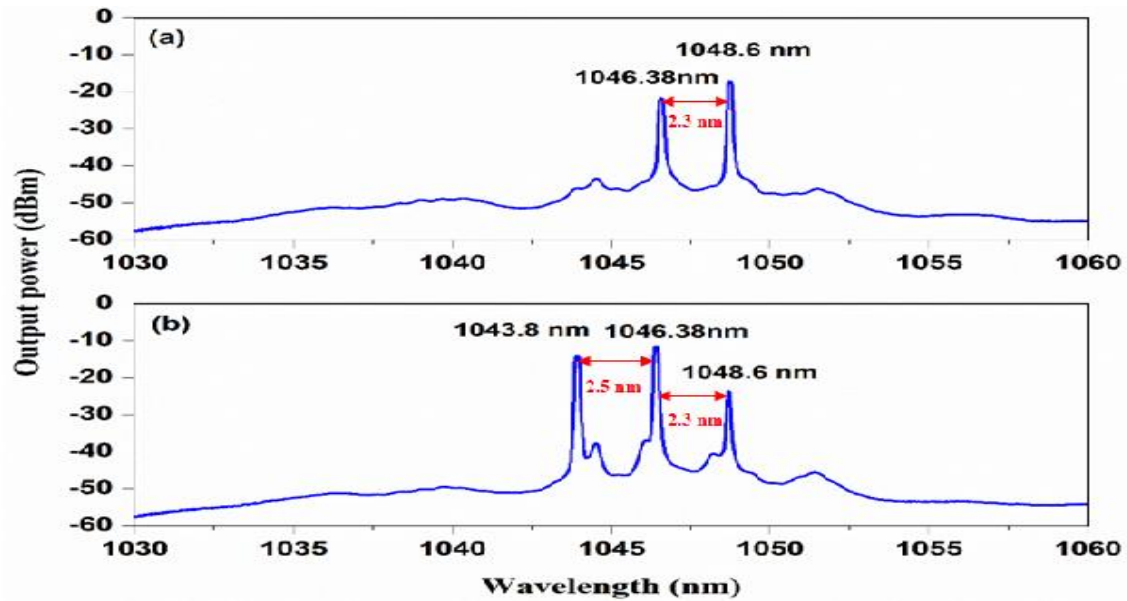
Fig. 3.6: Dual- and triple wavelength laser operations at pumping power of (a) 127 mW, (b) 170 mW.

3.2.3 Characteristics of adjusting PC of balloon-like MZI based Comb filter with YDFL

Owing to the ability to realize the almost constant channel spacing for multi-wavelength operation with increasing pump power, In this case, the switchable multi-wavelength operation and the channel number was investigated by continuously adjusting the cavity's polarization state. In this part of the experiment, the pump power was set to 210 mW to achieve better stability and lasing performance.

The filtering effect was formed by cascading the proposed MZI based comb filter with an in-line PC. By rotating the PC, the intracavity loss was varied. Accordingly, single-wavelength YDFL was achieved at 1042.18 nm with an SNR value of 39.5dB, as illustrated in Fig. 3.7. In this case, compared with Fig. 3.4, the single-wavelength lasing was switched from 1048.6 nm to 1042.18 nm at the same bending diameter of 5mm. Lasing lines generate at the interference peaks.

By appropriately controlling the polarization state of the laser cavity, the lasing wavelength can switch from one to the other one generating either single- or multi-wavelength oscillation.
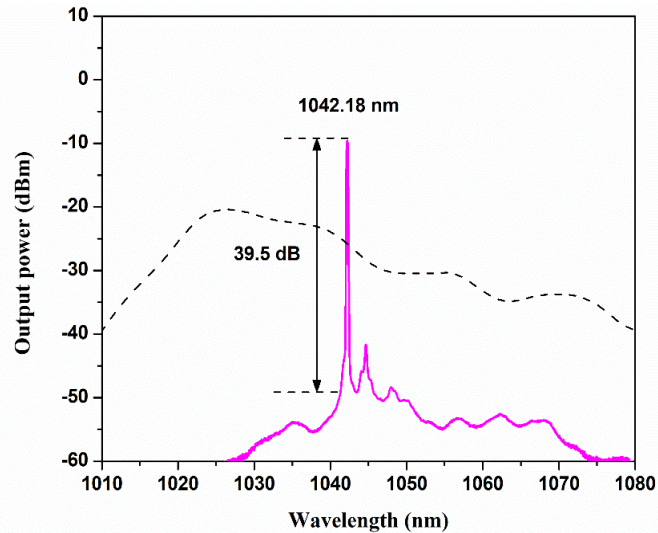
Fig. 3.7: Single-wavelength YDFL at a pump power of 210 mW.

The PC is employed to rotate the polarization state and permits to achieve a continuous adjustment of the birefringence within the ring cavity to balance the gain and loss and control the number of lasing wavelengths. The cavity birefringence is introduced into the laser cavity by bending the SMF into a balloon shape. Consequently, the effects of polarization hole burning (PHB) are achieved, which will reduce the homogeneous line-width of the gain medium [103].

By accurately squeezing and rotating the PC in the cavity, the generation of multi-wavelength YDFL was successfully obtained. It is well known that squeezing the fiber in the PC introduces polarization-dependent loss. The PC diversifies the polarization states of different wavelengths in the gain medium by controlling the wavelength-dependent polarization rotation and adjusting the birefringence in the laser cavity, thus inducing wavelength-dependent gain and loss. Therefore, the lasing wavelength will be suppressed if the polarization-dependent loss for one lasing wavelength is high enough [104].

Consequently, in this work, the lasing wavelength number can be regulated, and a single-, dual-, and triple wavelength and switchable YDFL can be achieved. The principle of the wavelength switchable YDFL relies on that at specific wavelengths, the losses induced by bending of the SMF interact with the gain within the ASE bandwidth of the gain medium. Stable multi-wavelength laser operation at room temperature was achieved, and the channel spacing was tuned smoothly through adjusting PC with the comb filter [2,17]. The evolution of the switchable multi-wavelength lasing operation is shown in Fig. 3.8.
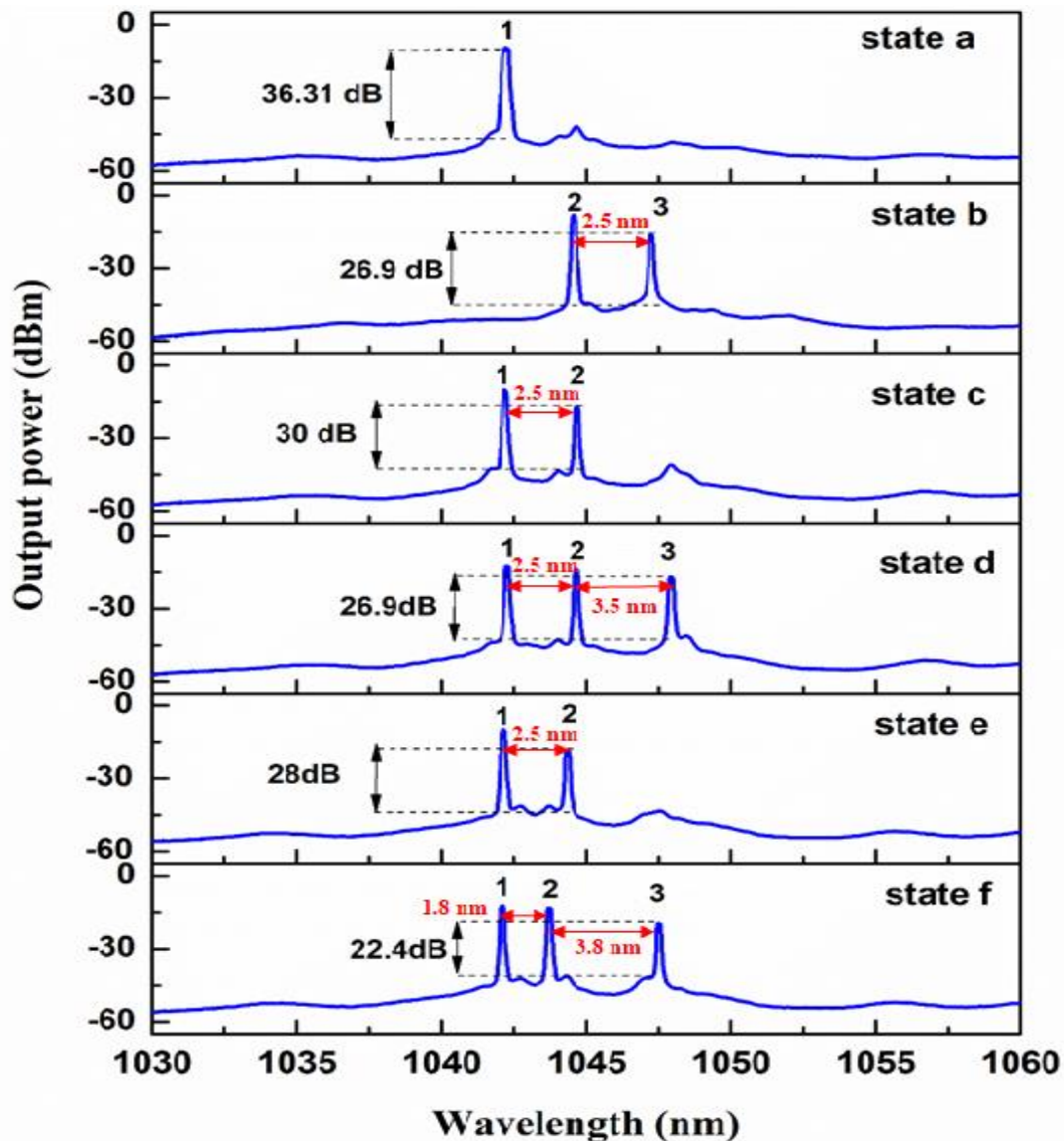

Fig. 3.8: Switchable multi-wavelength lasing for a different state of PC.

As it is observed, the output wavelengths may change from the oscillation as the polarization states vary from state a to f, and the dual wavelengths (at state b and c) are switched in the same set of wavelengths with constant channel spacing about 2.5 nm.

When the PC is adjusted to state a, the single-lasing line marked as "1" appears at 1042.2nm. Then, when the PC rotated to state b, a new two lasing lines marked as "2" and "3" show up. Turning PC to state c, the lasing line "3" disappears, and the lasing line marked as "1" shows up again.

If we were continuously rotating the PC to state d, the lasing line marked as "3" show up, and the lasing operation switched from dual to triple wavelength operation. Dual-wavelength will appear again when the PC rotated to state e with same channel spacing in state d between the lasing line "1" and "2" about 2.5 nm.

Lastly, rotating PC to state f, the laser oscillates up to triple wavelengths (1042.18, 1043.6, 1047.5) nm. Based on the above results, the reported method provides a simple and effective technique to achieve a single wavelength tunable lasing operating and switchable multi-wavelength oscillation in YDFL with channel spacing (1.8 – 3.8) nm.

From Fig. 3.8, it clear that the peak wavelength location is not precisely in conformity with the transmission peak of the proposed filter, and the channel spacing of the multi-wavelength operations is not uniform in some position. These might be attributed to the following: when the SMF is bent into a balloon shape, and the PC is rotated, the actual birefringence value of the bend SMF will be slightly higher from its effective birefringence value of 10^{-5}, and the transmission peak location will be continuously tuned [86].

Therefore, the experimentally obtained wavelength spacing wavelengths could not be accurately equal to the theoretical FSR. This phenomenon might be

attributed to the spectral hole burning (SHB) effect affected by the PC, which in turn affects the laser gain spectrum [92,105].

Also, SMF is not single-mode at 1μm region; consequently, the transverse mode mixing will probably be achieved between the LP_{01} and LP_{11} modes. The single-mode-multimode-single-mode (SMS) interference bandpass filters result from bending the SMF might also play a small role in this experiment[106].

Moreover, the experimentally obtained wavelength interval is not identical. This may be attributed to the interference pattern of the comb filter as polarization-dependent. Therefore, according to the PC rotation and setting, the interference pattern can be shifted, and the lasing line location can be switched. In our experiment, if a programmable PC were used to replace the mechanical PC, the characteristic of the output laser could be better adjusted. Generally, the controlling of the wavelength interval can be achieved by appropriately rotating the PC.

Finally, to examine the stability of the laser system at room temperature, the triple-wavelength YDFL was scanned every 10 minutes for 60 min, as shown in Fig. 3.9. It can be observed that there is no significant shift in the peak wavelength locations or fluctuation in the laser output power, as illustrated in Fig. 3.10 Furthermore, we checked the stability of YDFL for many days we found it very stable as shown in the following Fig. 3.11.
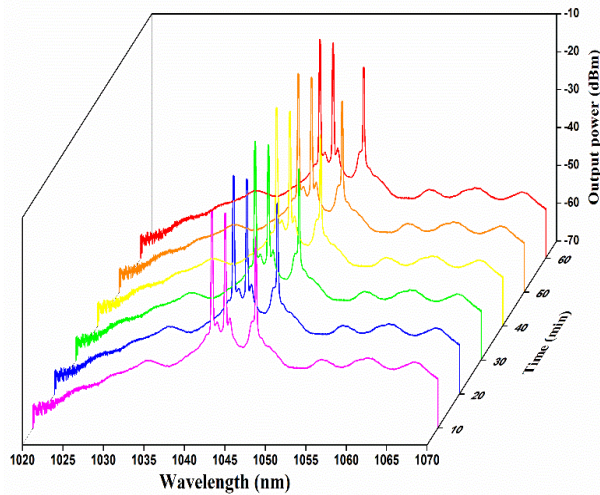
Fig. 3.9: The stability measurements of triple-wavelength lasing (state f).
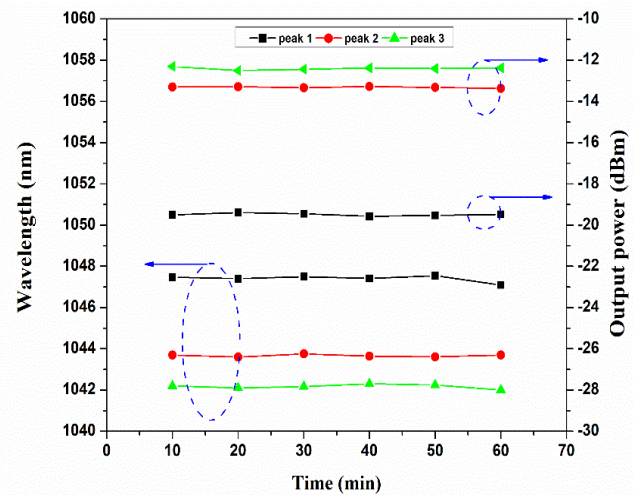
Fig. 3.10: Peak wavelength drift and the power fluctuation of triple-wavelength lasing (state f).
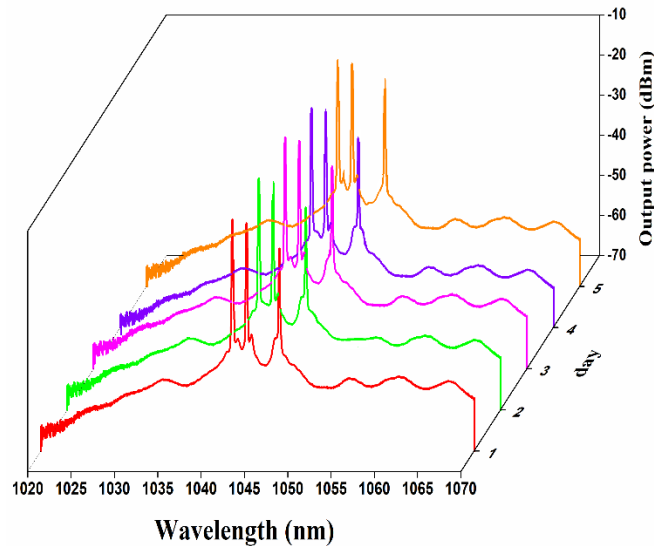
Fig. 3.11: The long-term stability measurements of triple-wavelength lasing.

3.3 Characteristics and Fabrication of balloon-like MZI based Comb filter with EDFL

In order to understand how the moving capillary tube corresponds to the bending diameter, as well as the resonance wavelength change of the transmitted spectrum, a broadband source (BBS, Thorlabs SLD1550S-A1) has been used to check the output spectrum with the bent diameter as shown in Fig. 3.12(a).

A clear interference dip was observed with the 15 mm bending diameter. While for bending diameter of 20 mm, interference fringes of a relatively low extinction ratio were observed. In contrast, no interference dip was detected in the transmission spectrum of the larger bending diameter. This might be attributed to most of the light modes was coupled into the cladding modes as the bending diameter decreases [39].

Then, to characterize the transmitting spectrum of the proposed balloon-like MZI-based filter at diverse bending diameters, ASE light of the EDF was launched through the constructed structure to examine the spectral response of the filter at different bending diameters, as shown in Fig. 3.12(b).

As shown in this figure, the transmitting spectrum of the proposed structure has a comb-like shape with a wide FSR, resulting from core and cladding mode interference and recoupling within the structure. It is also clear that the interferometer with a bending diameter of 15 mm has a better FSR. For this reason, in this work, a bending diameter of 15 mm was adopted for the construction of a comb filter for multi-wavelength fiber laser production. The bending radius induces an excess of losses into the cavity, as shown in Fig. 3.12. The value of the insertion and bending losses of the proposed balloon-like filter at the various bending diameter is illustrated in Table 3-1.

(a)   (b)
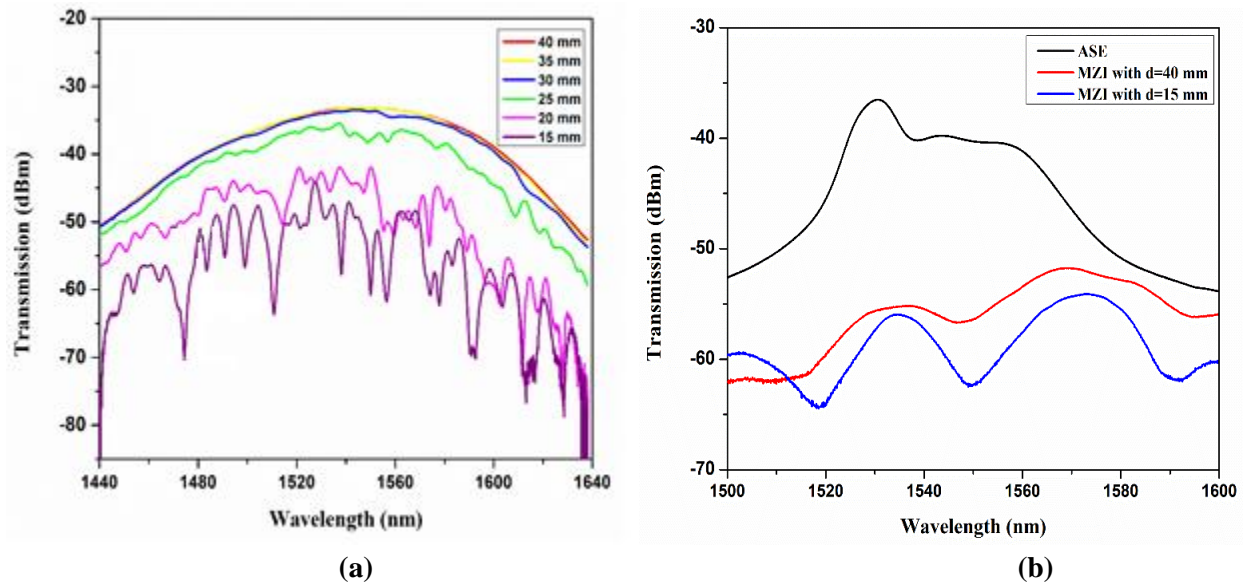
Fig. 3.12. Spectral response of the proposed filter at different bending diameters measured using: (a) a broadband light source, (b) measured using an ASE of the EDFL.

Table 3-1: The insertion losses of the proposed balloon-like filter at the various bending diameter.

Bending diameter (mm)	Insertion Loss (dB)
40	0.8275
35	0.8375
30	0.860
25	1.1366
20	1.7842
15	3.1353

At first, the transmission spectrum of the EDFL was investigated before incorporating the proposed filter into the laser ring cavity. Fig. 3.13(a) shows the single-wavelength spectrum obtained at the threshold pump power of 75 mW. The peak power of the single-wavelength EDFL is located at 1574 nm wavelength with

a SNR of about 46.1 dB. Then, the transmission spectrum of the EDFL was examined after incorporating the proposed filter of a 40 mm bending diameter, as shown in figure Fig. 3.13(b).

A stable single-wavelength EDFL located at 1571.9 nm with an SNR of about 44.3 dB was attained at the pump power threshold of 94 mW. As shown from this figure, the peak power of the single-wavelength is determined directly by the transmission peak of the proposed comb filter.
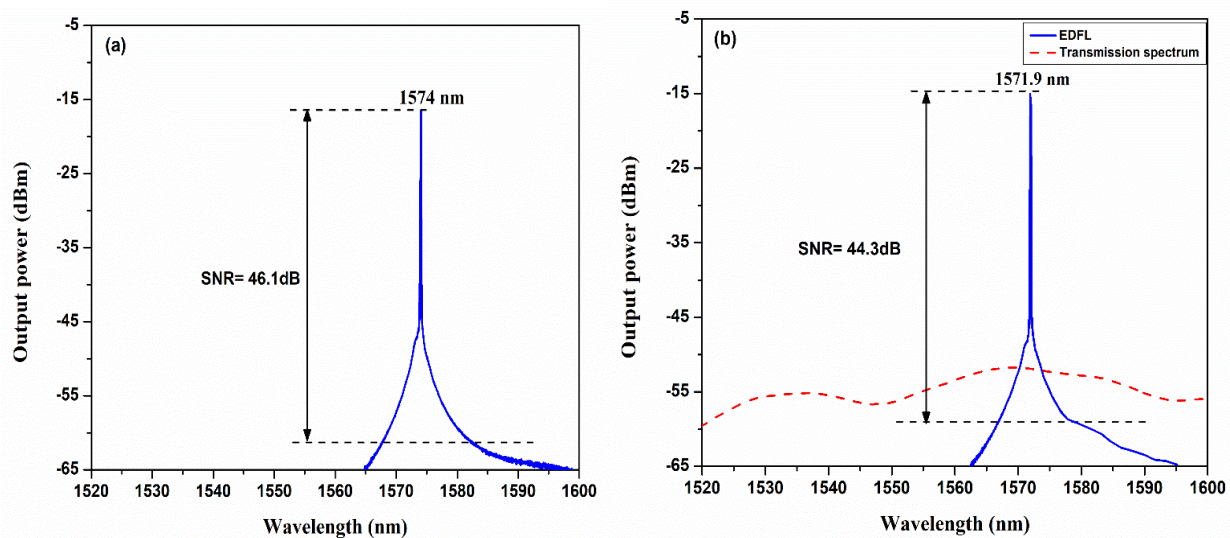
Fig. 3.13: Single-wavelength EDFL operation (a) without the proposed filter, and (b) with the proposed filter at bending diameter 40 mm.

3.3.1 Characteristics of bending balloon-like MZI based Comb filter with EDFL

After inserting the balloon-like MZI comb filter into the cavity setup, the laser's output characteristic was recorded based on the bending variation response of the balloon-like MZI. A tunable waveband lasing regime was obtained within the Conventional band (C- band), as shown in Fig. 3.13(a).

When the bending diameter was altered from 40 mm to 15 mm and the pump power is kept at 94 mW, the lasing wavelength moves towards the shorter wavelength direction from 1571.9 nm to 1560 nm. In this experiment, the bending diameter tuning steps was 5 mm, and the tuning range for the full waveband is 11.9 nm. The bending diameter is refered to the variable d as mentioned in the operating principle.

The appropriate bending diameter of the balloon-like MZI causes the non-symmetrical distribution of the refractive index along the SMF, and cavity loss is induced at particular wavelengths due to variation of phase constants between the propagation core and cladding modes [107]. As the diameter decreased, the proposed filter's attenuation bands shifted towards the shorter wavelength [104].

Moreover, fiber bending causes polarization variations and wavelength-dependent losses leading to transform the gain in the laser cavity and alter the dynamic range in the interference spectrum. As a result, the fringe peaks are mitigated due to the changes in the loss increment for higher-order cladding modes, and new laser emissions could be achieved due to polarization effects and the matching phase of lasing modes [108].

According to Fig. 3.14(a), we checked this point and the spectral region was enlarged where the laser lines occur as shown in Fig. 3.14(b). It is clear that this behavior was confirmed in this work. Initially, as the bending diameter of the balloon-shaped structure was adjusted to 40 mm and 35mm, dual lasing lines were achieved. Then, as the diameter was adjusted to 30 mm, 25 mm, 20 mm, and 15 mm, the dual lasing operation switch to a single-wavelength operation. This might be attributed to the two lasing modes' competition between each other for gain switching.

Therefore, the peak with higher power defeats the lower one. This is because of the MZI scheme for the coherent source where the lasing mode depends on the total fiber length difference for constructive interference [109].
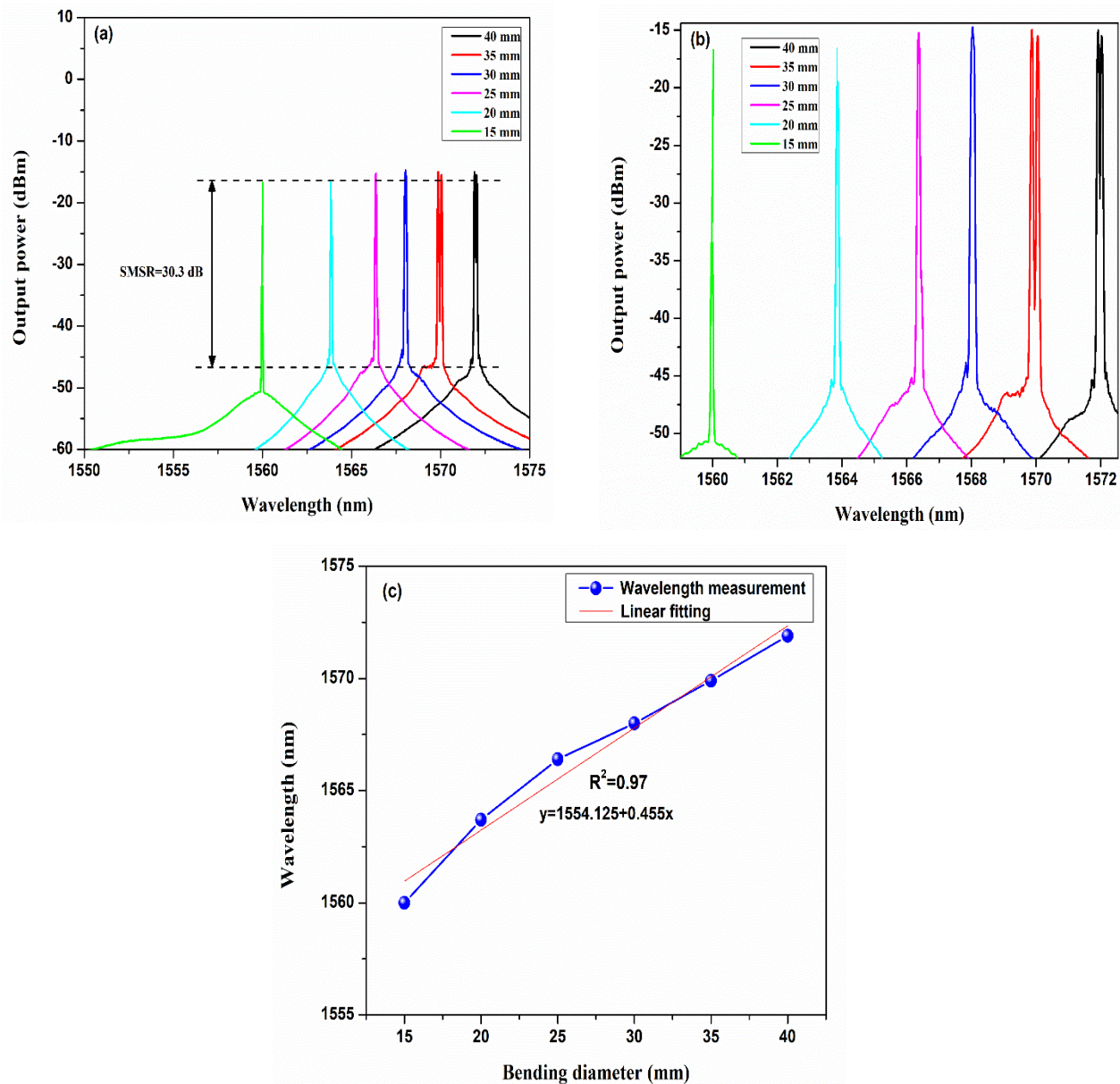
Fig. 3.14: EDFL output spectra as a function of on balloon-like MZI diameter (a) tunable operation, (b) zoom of the laser spectral region, and (c) linear fitting of bending diameter variation with the oscillation.

As a result, tunable waveband EDFL owns a SMSR of about 30.3 dB is achieved. The brittle nature of the bent fiber, which cannot go further in decreasing the diameter of the SMF bend section puts limitations on the achieved tunability range. In addition, the obtained SMSRs are of low values. This is attributed to the high attenuation induced in bending fiber structure.

To further investigate the bending response of the proposed tunable waveband EDFL, linear fittings between the bending diameter and oscillation peak with higher power of the EDFL were carried out as presented in Fig. 3.14(c). The fitting line of lasing wavelengths $R^2 = 0.97$ confirms good linear tunability.

3.3.2 Characteristics of the increasing power balloon-like MZI based Comb filter with EDFL

In this part of the experiment, the bending diameter was kept at 15 mm, and the pump power was set to 110 mW to realize better stability, SNR, and output lasing performance. As a result, the peak wavelength with the higher power of the EDFL was shifted from 1560.5 nm to 1557nm. It was pointed out in previously reported works, the refractive index of the EDFL decreases as the launched pump power increase, which causes the comb filter spectrum to shift [41].

Therefore, in this work, the effect of the increasing pump power at the fixed fitter bending diameter of 15 mm and at the absence of PC on the output characteristics of the proposed EDFL was investigated. Fig. 3.15 shows as the injected pump power were increased from 110 to 195 mW, the lasing wavelength tunes toward the shorter wavelength with a tuning range of 3.5 nm with a good linear tendency of $R^2 = 0.9\%$. The slight shift might be attributed to the small variation in the average refractive index.
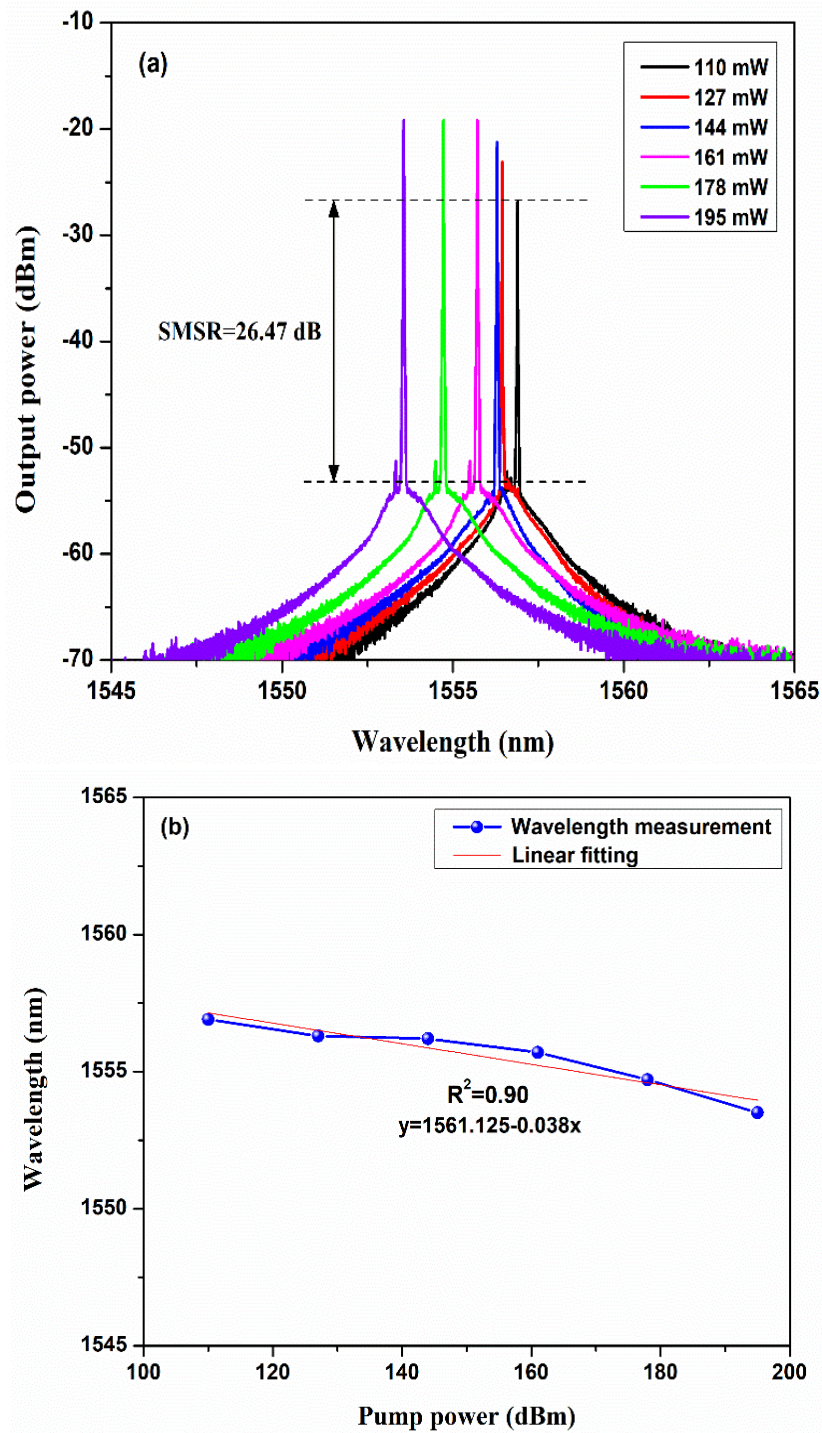
Fig. 3.15: Single-wavelength EDFL output spectra as a function of pump power (a) tunable operation and (b) linear fitting of power variation with the oscillation.

3.3.3 Characteristics of PC balloon-like MZI based Comb filter with EDFL

In this experiment, various multi-wavelength EDFL performances can be obtained by the appropriate cooperation between the proposed balloon-like MZI comb filter and PC. Fig. 3.16 illustrates the single wavelength operation of the proposed EDFL located at 1560.68 nm after incorporating the PC inside the laser cavity.

In this work, an in-line manual PC device (Thorlabs PLC-900) consists of a rotatable fiber squeezer and two fiber holding clamps was used. The center portion of the fiber strand is sandwiched in the fiber squeezer. It creates stress-induced birefringence within SMF by mechanically compressing the fiber. This acts like a variable, rotatable wave plate. Both the angle and retardance of the wave plate can be continuously, independently adjusted, which permits any arbitrary input polarization state to be converted to any required output polarization state.

The all-fiber design produces low intrinsic loss and back reflections, making this PC a good alternative to traditional free-space PCs, which consist of two quarter-wave plates and one half-wave plate. After inserting the PC into the cavity, the oscillating central wavelength was drifted to a short wavelength at 1560.68 nm. This is due to the variation of the cavity loss caused by the insertion loss of the PC component with the max output power during the lasing process, which suppresses the ASE bands for long wavelengths and allowing the laser lines to build up to shorter wavelengths [110].

When the 976 nm pump power was set to 127 mW with the assistant of adjusting the cavity's polarization state through the PC, the single-wavelength

operation of the EDFL switched to dual-, triple-quad-wavelength as shown in Fig. [(3.17), (3.18), (3.19)].
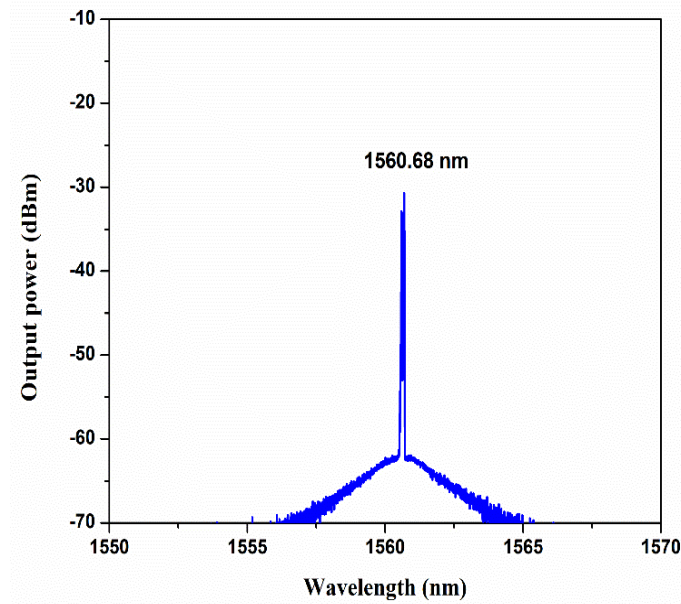
Fig. 3.16: Single-wavelength EDFL output spectra after with the proposed filter and PC.

The PC is an essential optical component to modulate the birefringence and produce multi-wavelength emissions. In this work, the PC was inserted in the cavity right after the proposed comb filter. Adjusting the PC causes a variation in the polarization state of the input light. Rotation of the polarization states arises due to the tuning of the PC. Thus the birefringence inside the EDFL cavity introduced by bending the SMF into a balloon shape might be modified continuously and balances the gain and loss of lasing wavelength [19].

On the other hand, squeezing the fiber in the PC introduces polarization-dependent loss. Therefore, the lasing wavelength will be mitigated when the polarization-dependent loss of one lasing wavelength is high enough [104].

Initially, by controlling the PC state (state a), the proposed cavity produced a set of dual-wavelength by altering the PC, as illustrated in Fig. 3.17. Dual-lasing lines were detected in which the first peak appeared at 1561.5 nm and the second

peak appeared at 1561.8 nm wavelength, and the two-lasing interval is 0.3 nm, as shown in Fig. 3.17 (state a).
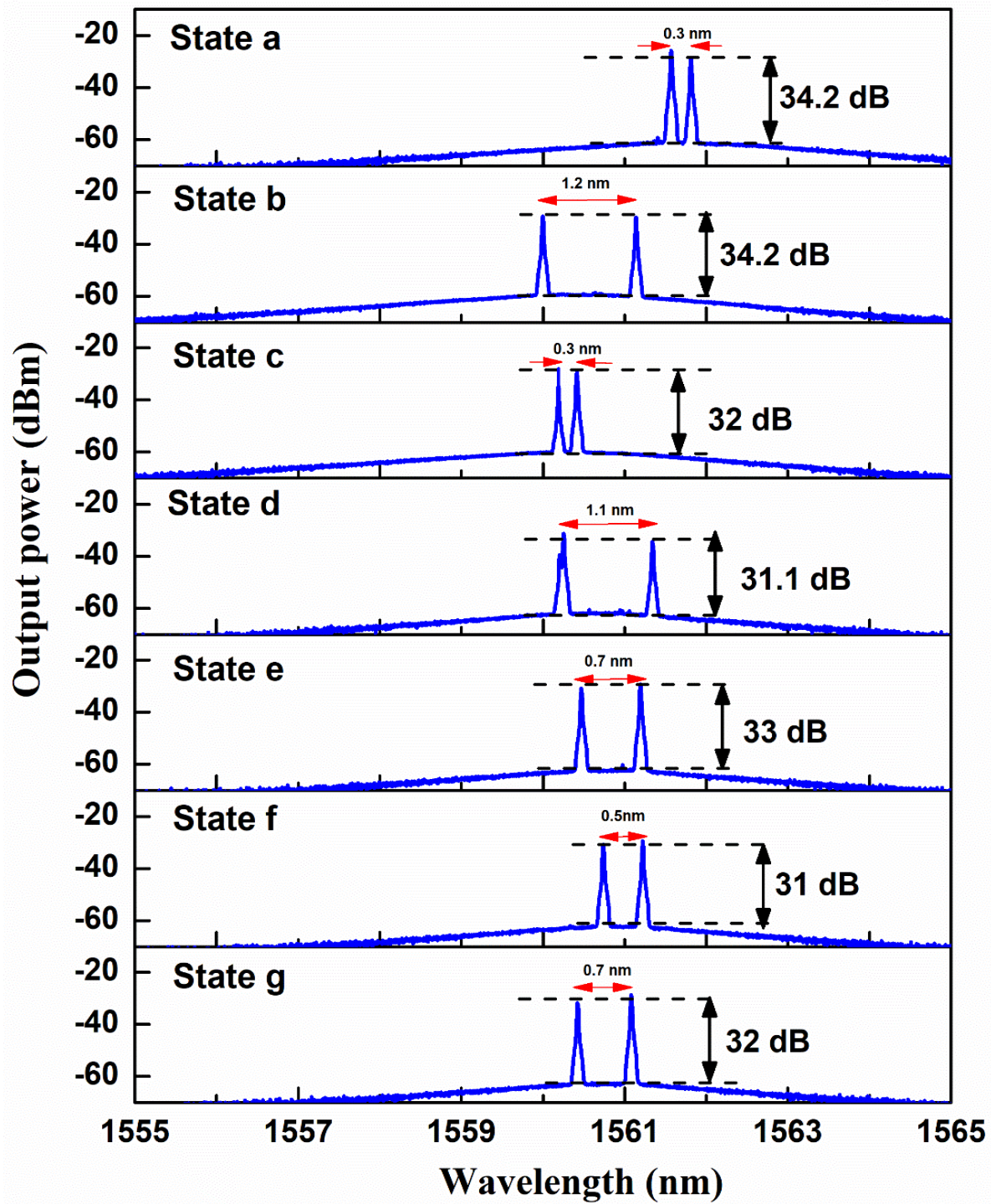
Fig.3.17: Output spectra of the dual-wavelength operation at different PC states.

Another set of dual-wavelength (second set) was detected by further rotating the PC to state b. The first peak and second peak are located at 1559.9 nm and 1561.1 nm, respectively, with a wavelength interval of 1.2 nm, as shown in Fig. 3.17. One more set of dual-wavelength EDFL (third set) has been obtained by changing the PC state (state c) at 1560.1 nm and 1560.4 nm, as shown in Fig. 3.17. The lasing wavelength interval for this set is 0.3 nm.

By varying the PC state, the c state to state d, e, f, and g, new sets of dual lasing peaks located at around 1560 nm with intervals of 1.1 nm,0.7nm,0.5nm, and 0.7nm were achieved, respectively. As can be seen from Fig.3.17, the combination of the proposed comb filter with PC helped the EDFL produce a set of dual-wavelength with tunable adjustment of wavelength interval. This phenomenon might be attributed to the polarization hole burning (PHB) effect induced by the PC, which alters the laser gain spectrum [105,106].

Generally, the modal interferometers cause a PHB effect that weakens the homogeneous gain broadening of the doped fiber and can help to generate multi-wavelength fiber lasers [111]. When the bending radius increases the introduced cavity losses increase too. Then by finely changing the orientation of the PC cascaded with the comb filter, the mode competition of EDF could be effectively alleviated, which makes new wavelengths appear. Therefore, three sets of triple-wavelength EDFL have been obtained by further squeezing and tuning the PC state (from state a to d), as shown in Fig. 3.18.
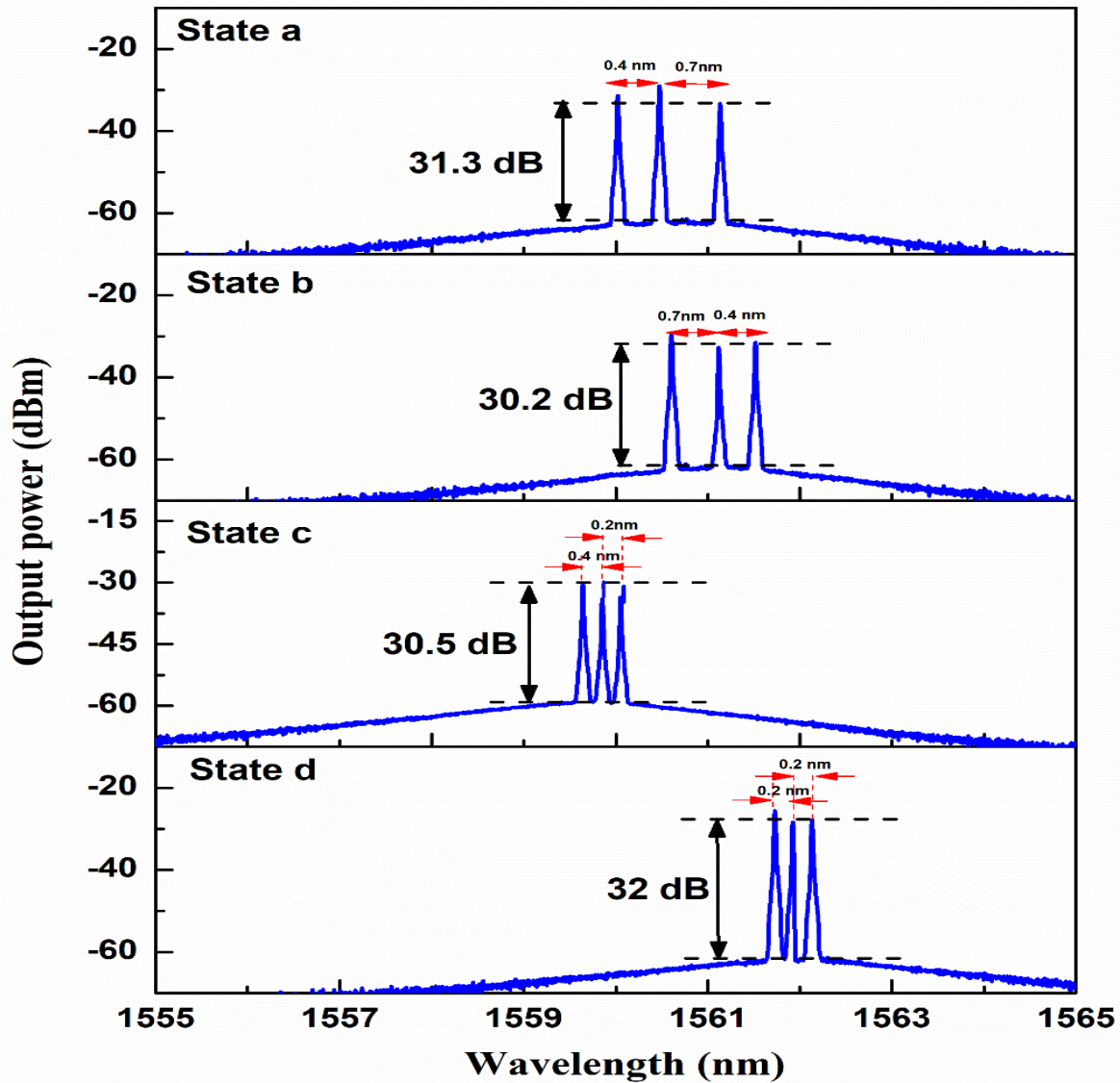
Fig. 3.18: Output spectra of the triple-wavelength operation at different PC states.

The first set in which the first peak, second, and third lasing peaks are located at 1560 nm, 1561.4 nm, and 1561.1 nm, respectively, with wavelength intervals of 0.4 nm and 0.7 nm.

While the second set has lasing peaks at 1560.6 nm, 1561.1 nm, and 1561.5 nm, respectively, with wavelength spacing of 0.7nm and 0.4nm. The third set has peaks lasing at 1559.6 nm, 1559.8 nm, and 1560 nm, with wavelength intervals of 0.2 nm and 0.4 nm.

The fourth set has peaks located at 1561.7 nm, 1561.9 nm, and 1562.1 nm with an equal wavelength interval of 0.2 nm. The output wavelength interval has randomness even in the peak locations, which might be attributed to the influence of cavity loss, characteristics of the gain medium, PHB, and filtering effect [40].

Similarly, quadruple-wavelength EDFL has been attained by further squeezing and finely rotating the PC. Two sets of quadruple-wavelength were detected, as shown in Fig.3.19. The first set in which the first peak, second at, third, and fourth lasing peaks were obtained at 1560.4 nm, 1561.7 nm, 1561nm, and 1561.3 nm, respectively.

The second set of four lasing outputs was observed at 1561.7 nm, 1561.9 nm, 1562.21nm, and 1562.6 nm. As shown from this figure, four lasing lines output with SMSR greater than 30 dB and almost an equal wavelength interval were generated.

As shown in Fig.3.12 the FSR experiences change as the bending diameter decreases. According to this figure, the transmission spectrum has a comb-like shape with a broad FSR. It is also obvious that the FSR of the transmission spectrum of the MZI filter was varied from 37.1 to 29.7 nm as the bending diameter of the balloon-like structure was varied from 40 mm to 15mm.

Moreover, as the SMF is bent into a balloon shape, and the PC is rotated, the actual birefringence value of the bend SMF will be slightly increased above its effective birefringence value of 10^{-5}, and the location transmission peak will be continuously tuned. Consequently, the experimentally obtained wavelength spacing wavelengths might not be accurately equal to the calculated FSR. This phenomenon could be attributed to the spectral hole burning (SHB) effect affected by the PC, which in turn affects the laser gain spectrum [13].

Finally, to test the quadruple-wavelength operation's stability after optimally setting the state of PC (state a) to generate a quadruple lasing line, the output transmission spectra were detected to 60 min by scanning repeated with an interval of 10 min, as illustrated in Fig. 3.20(a).

The output wavelength shows the maximum shift in the peak wavelength locations of 0.24 nm and maximum fluctuation in the laser output of 1.26 dB as illustrated in Fig. 3.20(b).

The stability measurement of quadruple-wavelength EDFL confirms the performance is demonstrated to be stable.
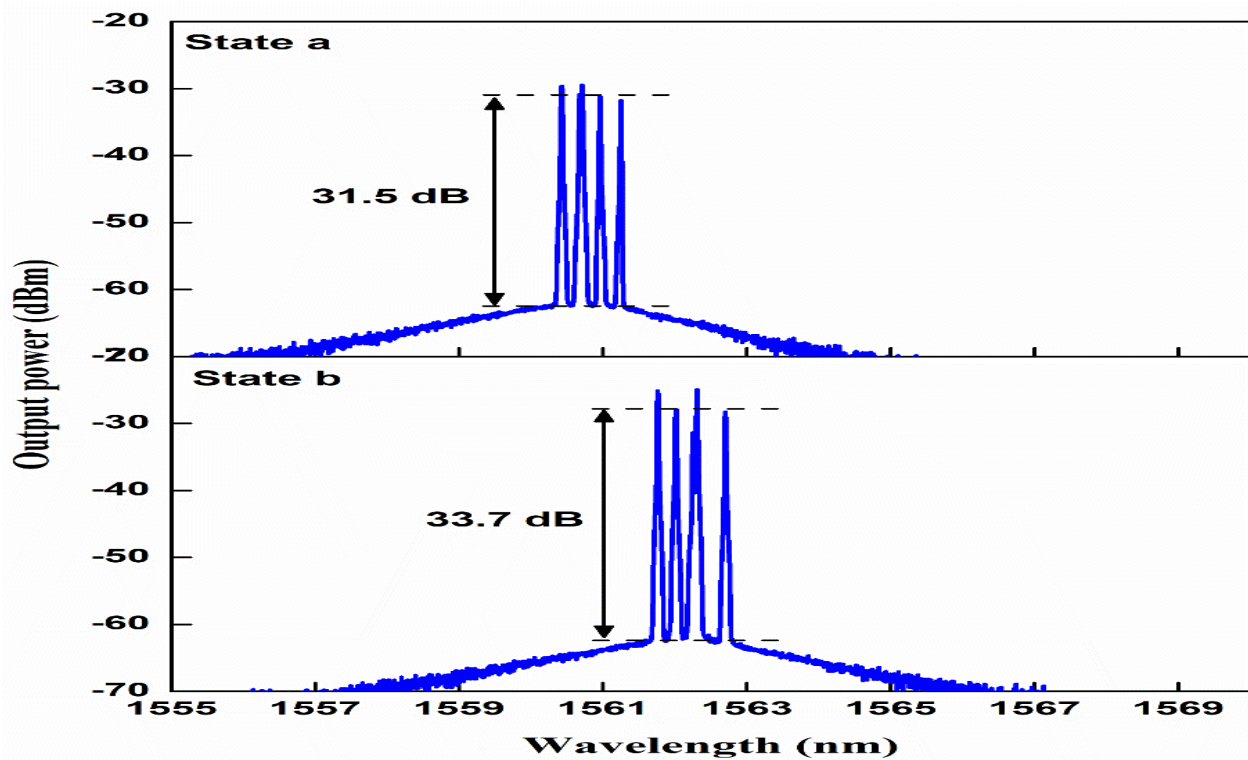
Fig.3.19: Output spectra of the quadruple-wavelength operation at different PC states.
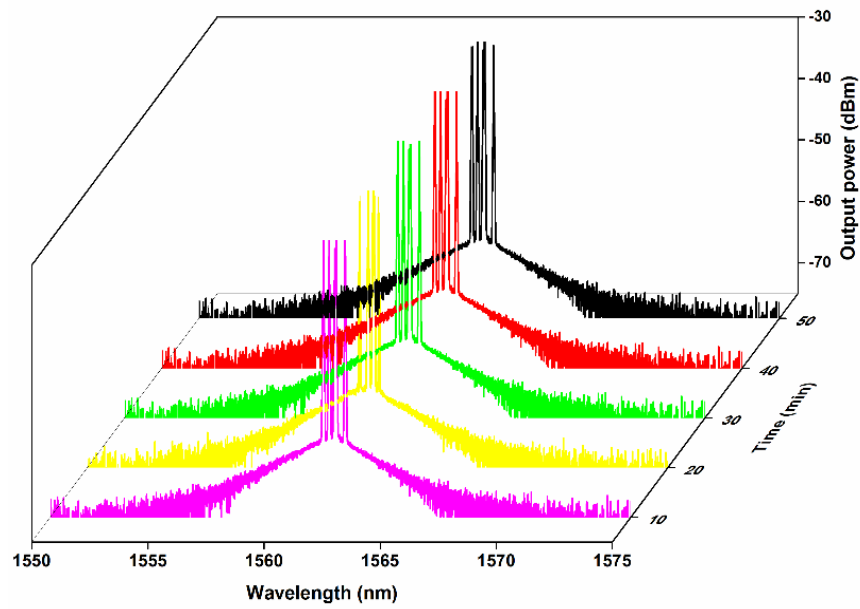
(a)
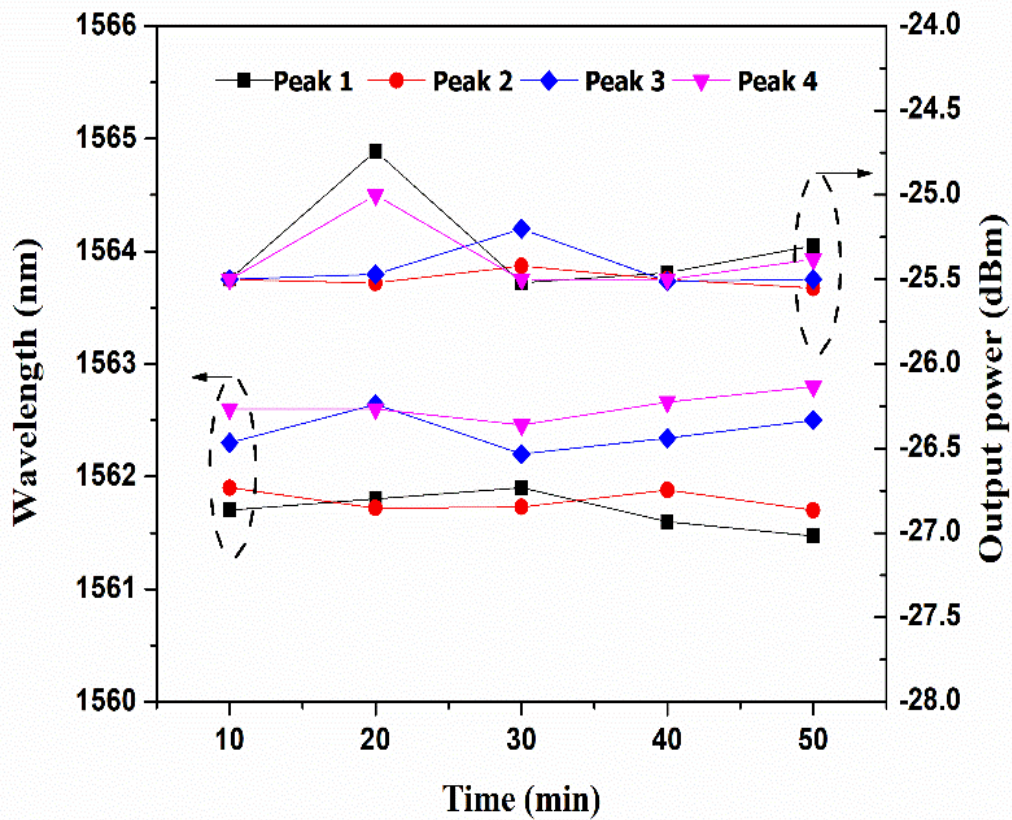
(b)

Fig.3.20: (a) Stability measurement for quad-wavelength output spectra, (b) Peak wavelength

drift and the power fluctuation of quadruple-wavelength lasing.

Furthermore, we checked the repeatability of the quadruple-multi-wavelength EDFL for many days we found it very repeatable and stable as shown in the following Fig. 3.21.

The proposed macro-bend structure-based comb filter offers simplicity and low-cost fabrication, where it was constructed just by bending a straight traditional SMF without any splicing or need to pre-or post-operation, such as tapering, as in the case of the non-adiabatic microfiber [19,112]. More ever in the sense of free spectral range (FSR), it owes as the others, but it has a simple structure
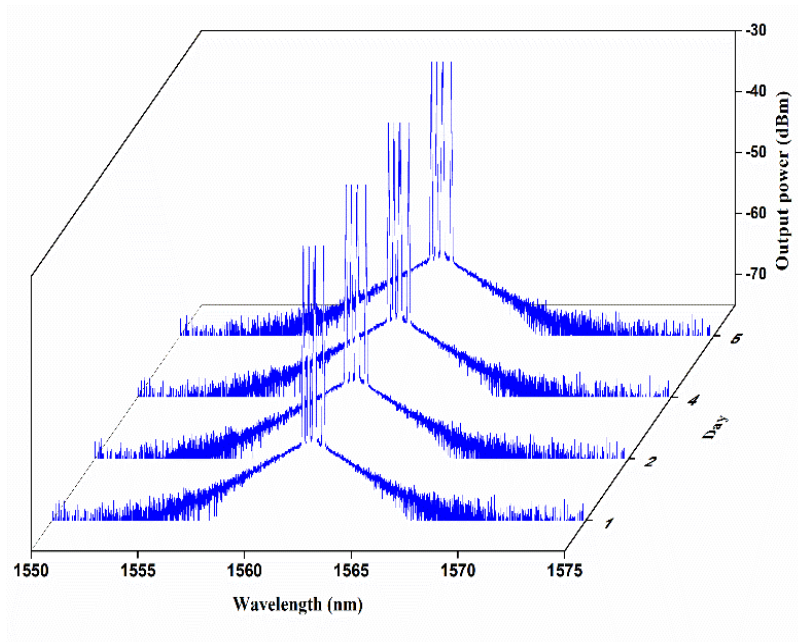
Fig. 3.21: The repeatability measurements of quadruple-wavelength lasing.

3.4 Conclusions

In this work, an all-fiber optic filter based on a Mach-Zehnder interferometer controlling spacing has been demonstrated experimentally. The proposed comb-filter allows the YDFL and EDFL to operate in two different regimes continuous tuning single- or generating switchable multi-wavelength laser operation.

For YDFL

1. Tuning the bending diameter of the SMF from 40 to 5 mm allowed to obtain a tunable single-wavelength.
2. Tuning range of 16.7 nm, operation over a range
3. From 1065.26 nm to 1048.5 nm.
4. An SMSR of 27.8 dB at the bending.
5. The number of lasing wavelengths was directly controlled by only altering the pump power, dual-and triple wavelength has been achieved as the pump power was increased to 127 mW and 170 mW, respectively.
6. The appropriate adjustment of the PC cascaded with the filter in the laser cavity allows to generate up to triple switchable wavelengths located between 1065.26 nm and 1047.5 nm.

For EDFL

1. By gradually changing the bending diameter of the SMF from (40 – 15) mm, the output tunable single-wavelength.
2. A tuning range of 11.9 nm.
3. An SMSR 30.3 dB at the bending.
4. Tunability for single-wavelengths was achieved when the launched pump power was increased from 110 mW to 195mW.

5. By adjusting the PC allowed switching from single- to multi-wavelength emission, dual-, triple-, quadruple -wavelength has been obtained.

3.5 Suggestions for future work

1. Studying a different construction of bending SMF as an interferometer.

2. Studying the effect of Figure of eight (8 shape) as MZI based comb filter

3. Using balloon-like MZI based gold coating with fiber laser system as a tunable filter.

3.6 Summary

Table 3-2: Summary the proposed balloon-like filter with various bending diameter.

	With bending diameter	**YDFL**	**EDFL**
1	Bending diameter for balloon filter like MZI	(40-5) mm step 5 mm	(40-15) mm step 5 mm
2	Filter performance	Tunable with blue shift	Tunable with blue shift
3	No. of wavelength	Single at all bending diameter	Single at d=(30 -15) mm Dual at d=(40, 35) mm
4	SMSR $_{max}$	27.8 dB	30.3 dB
5	Tuning range	16.76 nm	11.9 nm
6	Fitting line	0.96 polynomial fitting	0.97 linear fitting

Table 3-3: Summary of the proposed balloon-like filter with increasing power.

	Increasing power	YDFL	EDFL
1	Increasing power for balloon filter like MZI	From (110 -170) mW	From (110 -195) mW
2	Filter performance	Switchable	Tunable with blue shift
3	No. of wavelength	Single, dual, triple	Single
4	SMSR $_{max}$	39.5 dB	26.47 dB
5	Emission of wavelength	(1048.6, 1046.38, 1043.8)nm	From (1560.5- 1557)nm
6	Spacing	Dual =2.3 nm Triple =(2.3, 2.5)nm	Tune shift =3.5 nm

Table 3-4: Summary of the proposed balloon-like filter at rotate PC.

	Rotation PC	YDFL	EDFL
1	No. of state	6	14
2	Filter performance	Switchable multi-wavelength	Switchable multi-wavelength
3	No. of wavelength	Single, dual, triple	Single, dual, triple, quadruple
4	SMSR $_{max}$	36.31 dB	34.2 dB
5	Range of wavelength	From (1042.18- 1047.5) nm	From (1559.6- 1562.6) nm
6	Spacing channel for last state	1.8 nm, 3.8 nm	0.2 nm, 0.3 nm, 0.4 nm

References

[1]   R. E. Nuñez-Gomez, G. Anzueto-Sánchez, J. L. Camas-Anzueto, A. Martínez-Rios, M. A. Basurto-Pensado, and J. Castrellon-Uribe, "Switchable dual-wavelength erbium-doped fiber laser based on the broadband filtering performance of tapered long period fiber gratings," *Laser Phys.*, vol. 31, no. 1, p. 15101, 2020.

[2]   X. Dong, P. Shum, N. Q. Ngo, and C. C. Chan, "Multiwavelength Raman fiber laser with a continuously-tunable spacing," *Opt. Express*, vol. 14, no. 8, pp. 3288–3293, 2006.

[3]   M. A. M. Salim, H. Ahmad, S. R. Azzuhri, M. Z. A. Razak, and S. W. Harun, "Tunable wavelength generation in the 1 µm region incorporating a 16-channel arrayed waveguide grating (AWG)," *Laser Phys.*, vol. 27, no. 12, p. 125101, 2017.

[4]   M. S. Kang, M. S. Lee, J. C. Yong, and B. Y. Kim, "Characterization of wavelength-tunable single-frequency fiber laser employing acoustooptic tunable filter," *J. Light. Technol.*, vol. 24, no. 4, pp. 1812–1823, 2006.

[5]   G. Anzueto-Sánchez, A. Martínez-Rios, and J. Castrellon-Uribe, "Tuning and wavelength switching erbium-doped fiber ring lasers by controlled bending in arc-induced long-period fiber gratings," *Opt. Fiber Technol.*, vol. 18, no. 6, pp. 513–517, 2012.

[6]   A. D. Guzman-Chavez, E. Vargas-Rodriguez, L. Martinez-Jimenez, and B. L. Vargas-Rodriguez, "Switchable multi-wavelength and tunable waveband fiber laser based on a thermal sensitive filter," *Opt. Commun.*, vol. 482, p. 126613, 2021.

[7]   I. Torres-GóAmez, A. MartíAnez-Rios, G. Anzueto-SáAnchez, R. Selvas-

Aguilar, A. MartíAnez-Gáamez, and D. MonzóAn-HernáAndez, "Multi-Wavelength-Switchable Double Clad Yb 3+-Doped Fiber Laser Based on Reflectivity Control of Fiber Bragg Gratings by Induced Bend Loss," *Opt. Rev.*, vol. 12, no. 2, pp. 65–68, 2005.

[8] L. Gao and T. Zhu, "Wavelength Spacing Tunable, Multiwavelength Q-switched Fiber Laser Mode-locked by Graphene Oxide," *arXiv Prepr. arXiv1409.7417*, 2014.

[9] H. Zou, S. Lou, and G. Yin, "A wavelength-tunable fiber laser based on a twin-core fiber comb filter," *Opt. Laser Technol.*, vol. 45, pp. 629–633, 2013.

[10] H. Ahmad, S. N. Aidit, and M. Z. Samion, "Multi-and dual-wavelength Thulium-doped fluoride fiber laser assisted by four-wave mixing in S-band region," *Infrared Phys. Technol.*, vol. 111, p. 103485, 2020.

[11] D. A. Smith, M. W. Maeda, J. J. Johnson, J. S. Patel, M. A. Saifi, and A. Von Lehman, "Acoustically tuned erbium-doped fiber ring laser," *Opt. Lett.*, vol. 16, no. 6, pp. 387–389, 1991.

[12] M. Jiang, X. Q. Dinh, P. P. Shum, S. Molin, Z. F. Wu, and P. Nouchi, "Investigation of axial strain effects on microwave signals from a PM-EDF short cavity DBR laser for sensing applications," *IEEE Photonics J.*, vol. 4, no. 5, pp. 1530–1535, 2012.

[13] R. A. Faris, S. K. Al-Hayali, and A. H. Al-Janabi, "Au coated ZnO/MWCNTs nanocomposites film-induced four-wave-mixing effect for multi-wavelength generation in erbium-doped fiber laser," *Opt. Commun.*, vol. 485, p. 126746, 2021.

[14] X. He, X. Fang, C. Liao, D. N. Wang, and J. Sun, "A tunable and switchable single-longitudinal-mode dual-wavelength fiber laser with a simple linear

cavity," *Opt. Express*, vol. 17, no. 24, pp. 21773–21781, 2009.

[15] Y. Zhou, S. Lou, Z. Tang, T. Zhao, and W. Zhang, "Tunable and switchable C-band and L-band multi-wavelength erbium-doped fiber laser employing a large-core fiber filter," *Opt. Laser Technol.*, vol. 111, pp. 262–270, 2019.

[16] Z. Cao *et al.*, "Switchable dual-wavelength erbium-doped fiber ring laser with tunable wavelength spacing based on a compact fiber filter," *Opt. Laser Technol.*, vol. 56, pp. 137–141, 2014.

[17] Y.-G. Han, G. Kim, J. H. Lee, S. H. Kim, and S. B. Lee, "Lasing wavelength and spacing switchable multiwavelength fiber laser from 1510 to 1620 nm," *IEEE photonics Technol. Lett.*, vol. 17, no. 5, pp. 989–991, 2005.

[18] W. Wang, H. Meng, X. Wu, H. Xue, C. Tan, and X. Huang, "Three channel-spacing switchable multiwavelength fiber laser with two segments of polarization-maintaining fiber," *IEEE Photonics Technol. Lett.*, vol. 24, no. 6, pp. 470–472, 2011.

[19] M. A. M. Salim *et al.*, "Switchable erbium-doped fiber laser (EDFL) using non-adiabatic microfiber," *Opt. Fiber Technol.*, vol. 52, p. 101967, 2019.

[20] H. Wei, Z. Lianqing, and D. Mingli, "All-fiber Mach–Zehnder comb filter based on tapered fibers for wavelength switchable erbium-doped fiber lasers," *Int. J. Optomechatronics*, vol. 14, no. 1, pp. 18–28, 2020.

[21] Y. Zhou, X. Wang, Z. Tang, and S. Lou, "Switchable multi-wavelength erbium-doped fiber ring laser based on a tapered in-line Mach–Zehnder interferometer," *Laser Phys.*, vol. 28, no. 5, p. 55101, 2018.

[22] C.-C. Chiang and L. Tsai, "Perfectly notched long-period fiber grating filter based on ICP dry etching technique," *Opt. Lett.*, vol. 37, no. 2, pp. 193–195, 2012.

[23] D. Krčmařík, R. Slavík, Y. Park, and J. Azaña, "Nonlinear pulse compression of picosecond parabolic-like pulses synthesized with a long period fiber grating filter," *Opt. Express*, vol. 17, no. 9, pp. 7074–7087, 2009.

[24] Y. Wang, M. Wang, W. Xia, and X. Ni, "High-resolution fiber Bragg grating based transverse load sensor using microwave photonics filtering technique," *Opt. Express*, vol. 24, no. 16, pp. 17960–17967, 2016.

[25] H. He *et al.*, "Novel birefringence interrogation for Sagnac loop interferometer sensor with unlimited linear measurement range," *Opt. Express*, vol. 25, no. 6, pp. 6832–6839, 2017.

[26] H. Sun, J. Zhang, Z. Yang, L. Zhou, X. Qiao, and M. Hu, "An in-line quasi-Sagnac interferometer based comb filter used for tunable multi-wavelength fiber laser," *Opt. Laser Technol.*, vol. 72, pp. 65–69, 2015.

[27] Y. Lopez-Dieguez *et al.*, "Erbium ring fiber laser cavity based on tip modal interferometer and its tunable multi-wavelength response for refractive index and temperature," *Appl. Sci.*, vol. 8, no. 8, p. 1337, 2018.

[28] A. Camarillo-Avilés *et al.*, "Stable Multi-Wavelength Thulium-Doped All-Fiber Laser Incorporating a Multi-Cavity Fabry–Perot Filter," *IEEE Photonics J.*, vol. 11, no. 6, pp. 1–7, 2019.

[29] J. N. Sikta, M. S. Islam, O. F. Rasel, and N. N. Ripa, "Wavelength spacing tenable capability of optical comb filter using Polarization Maintaining Fiber," *IOSR J. Appl. Phys*, vol. 6, no. 3, pp. 57–62, 2014.

[30] G. Zhou *et al.*, "A simple all-fiber comb filter based on the combined effect of multimode interference and Mach-Zehnder interferometer," *Sci. Rep.*, vol. 8, no. 1, pp. 1–8, 2018.

[31] M. Han, X. Li, S. Zhang, H. Han, J. Liu, and Z. Yang, "Tunable and channel

spacing precisely controlled comb filters based on the fused taper technology," *Opt. Express*, vol. 26, no. 1, pp. 265–272, 2018.

[32] A. A. Jasim and H. Ahmad, "A highly stable and switchable dual-wavelength laser using coupled microfiber Mach-Zehnder interferometer as an optical filter," *Opt. Laser Technol.*, vol. 97, pp. 12–19, 2017.

[33] W. A. Khaleel and A. H. Al-Janabi, "Erbium-doped fiber ring laser with wavelength selective filter based on non-linear photonic crystal fiber Mach–Zehnder interferometer," *Laser Phys.*, vol. 27, no. 10, p. 105104, 2017.

[34] Y.-W. Zhou, G.-Y. Sun, and A.-P. Luo, "Optically tunable multiwavelength fiber laser based on a Mach–Zehnder comb filter incorporating ytterbium-doped fibers," *Laser Phys.*, vol. 28, no. 1, p. 15105, 2017.

[35] Q. Zhang, X. Zeng, F. Pang, M. Wang, and T. Wang, "Switchable multiwavelength fiber laser by using a compact in-fiber Mach–Zehnder interferometer," *J. Opt.*, vol. 14, no. 4, p. 45403, 2012.

[36] D. I. Al-Janabi, A. M. Salman, and A. H. M. Al-Janabi, "All fiber, highly sensitive sensor based on gold nanoparticle-coated macrobent single mode fiber for human temperature monitoring," *J. Nanophotonics*, vol. 14, no. 4, p. 46013, 2020.

[37] D. I. Al-Janabi, A. M. Salman, and A. Al-Janabi, "High-sensitivity balloon-like thermometric sensor based on bent single-mode fiber," *Meas. Sci. Technol.*, vol. 31, no. 11, p. 115106, 2020.

[38] S. K. Al-Hayali, A. M. Salman, and A. H. Al-Janabi, "High sensitivity balloon-like interferometric optical fiber humidity sensor based on tuning gold nanoparticles coating thickness," *Measurement*, vol. 170, p. 108703, 2021.

[39] S. K. Al-Hayali, A. M. Salman, and A. H. Al-Janabi, "Effect of hygroscopic

polymer-coatings on the performance of relative humidity sensor based on macro-bend single-mode fiber," *Opt. Fiber Technol.*, vol. 62, p. 102460, 2021.

[40] Q. Zhao *et al.*, "Tunable and interval-adjustable multi-wavelength erbium-doped fiber laser based on cascaded filters with the assistance of NPR," *Opt. Laser Technol.*, vol. 131, p. 106387, 2020.

[41] G. Sun, D. S. Moon, A. Lin, W.-T. Han, and Y. Chung, "Tunable multiwavelength fiber laser using a comb filter based on erbium-ytterbium co-doped polarization maintaining fiber loop mirror," *Opt. Express*, vol. 16, no. 6, pp. 3652–3658, 2008.

[42] K. L. Lee, M. P. Fok, S. M. Wan, and C. Shu, "Optically controlled Sagnac loop comb filter," *Opt. Express*, vol. 12, no. 25, pp. 6335–6340, 2004.

[43] R. Mary, D. Choudhury, and A. K. Kar, "Applications of fiber lasers for the development of compact photonic devices," *IEEE J. Sel. Top. Quantum Electron.*, vol. 20, no. 5, pp. 72–84, 2014.

[44] H. Pang *et al.*, "Design of an erbium-doped fiber laser based on ring cavity," in *4th International Symposium on Advanced Optical Manufacturing and Testing Technologies: Advanced Optical Manufacturing Technologies*, 2009, vol. 7282, p. 72822P.

[45] R. Paschotta, "Field guide to optical fiber technology," 2010.

[46] K. Thyagarajan and A. Ghatak, *Lasers: fundamentals and applications*. Springer Science & Business Media, 2010.

[47] D. DiGiovanni, R. Shubochkin, T. F. Morse, and B. Lenardic, "Rare earth–doped fibers," *Spec. Opt. Fibers Handb.*, pp. 195–242, 2007.

[48] G. E. Villanueva Ibáñez, "Continuous wave and pulsed erbium-doped fiber

lasers for microwave photonics applications." Universitat Politècnica de València, 2012.

[49]   J. J. Le Roux, J. Meyer, and R. M. Manuel, "Principles of Increasing the Output Power of a Fiber Laser."

[50]   M. H. M. Ahmed *et al.*, "Q-switched erbium doped fiber laser based on single and multiple walled carbon nanotubes embedded in polyethylene oxide film as saturable absorber," *Opt. Laser Technol.*, vol. 65, pp. 25–28, 2015.

[51]   Z. C. Tiu, F. Ahmad, S. J. Tan, H. Ahmad, and S. W. Harun, "Multi-wavelength Q-switched Erbium-doped fiber laser with photonic crystal fiber and graphene–Polyethylene oxide saturable absorber," *Optik (Stuttg).*, vol. 126, no. 17, pp. 1495–1498, 2015.

[52]   A. Babazadeh *et al.*, "Simulating Q-switched ytterbium-doped double clad fiber laser," in *Laser Optics 2010*, 2011, vol. 7822, p. 782205.

[53]   V. Ter-Mikirtychev, "Fundamentals of fiber lasers and fiber amplifiers," 2014.

[54]   D. D. Michel, "Linear-cavity tunable fibre lasers employing an Opto-VLSI processor and a MEMS-based device," 2012.

[55]   M. J. F. Digonnet, *Rare-earth-doped fiber lasers and amplifiers, revised and expanded*. CRC press, 2001.

[56]   R. A. Pérez-Herrera, M. A. Quintela, M. Fernández-Vallejo, A. Quintela, M. López-Amo, and J. M. López-Higuera, "Stability comparison of two ring resonator structures for multiwavelength fiber lasers using highly doped Er-fibers," *J. Light. Technol.*, vol. 27, no. 14, pp. 2563–2569, 2009.

[57]   M. Azadeh, *Fiber optics engineering*. Springer, 2009.

[58]   A. Al-Azzawi, *Fiber optics: principles and practices*. CRC Press, 2017.

[59] T. Plc-, "PLC-900 Fiber Polarization Controller."

[60] R. Menzel, *Photonics: linear and nonlinear interactions of laser light and matter*. Springer Science & Business Media, 2013.

[61] G. P. Agrawal and N. K. Dutta, *Semiconductor lasers*. Springer Science & Business Media, 2013.

[62] A. R. Gizatulin and A. K. Sultanov, "Application of whispering gallery modes (WGM) in optical communications," in *Optical Technologies in Telecommunications 2017*, 2018, vol. 10774, p. 107741S.

[63] P. Feron, "Whispering gallery mode lasers in erbium doped fluoride glasses," in *Annales de la Fondation Louis de Broglie*, 2004, vol. 29, no. 1–2, pp. 317–329.

[64] L. Dong and B. Samson, *Fiber Lasers: Basics, Technology, and Applications*. CRC press, 2016.

[65] G. P. Agrawal, *Fiber-optic communication systems*, vol. 222. John Wiley & Sons, 2012.

[66] W. Zhu, L. Qian, and A. S. Helmy, "Implementation of three functional devices using erbium-doped fibers: An advanced photonics lab," *Laser*, vol. 1520, p. 1570nm, 2007.

[67] Z.-C. Luo, A.-P. Luo, and W.-C. Xu, "Tunable and switchable all-fiber comb filter using a PBS-based two-stage cascaded Mach–Zehnder interferometer," *Opt. Commun.*, vol. 284, no. 18, pp. 4167–4170, 2011.

[68] J. Jung and Y. W. Lee, "Continuously wavelength-tunable passband-flattened fiber comb filter based on polarization-diversified loop structure," *Sci. Rep.*, vol. 7, no. 1, pp. 1–10, 2017.

[69] R. E. Nuñez-Gomez, G. Anzueto-Sanchez, A. Martinez-Rios, M. A. Basurto-

Pensado, J. Castrellon-Uribe, and J. Camas-Anzueto, "Combining comb-filters based on tapered fibers for selective lasing performance in erbium-doped fiber lasers," *Laser Phys.*, vol. 26, no. 12, p. 125101, 2016.

[70] J. Lumeau, C. Koc, O. Mokhun, V. Smirnov, M. Lequime, and L. B. Glebov, "Single resonance monolithic Fabry–Perot filters formed by volume Bragg gratings and multilayer dielectric mirrors," *Opt. Lett.*, vol. 36, no. 10, pp. 1773–1775, 2011.

[71] A. A. Salman and A. H. Al-Janabi, "Multiwavelength Q-switched erbium-doped fibre laser-based aluminum nanoparticles saturable absorber and sagnac loop filter," *Laser Phys.*, vol. 29, no. 6, p. 65103, 2019.

[72] S. K. M. Al-Hayali, S. Selleri, and A. H. Al-Janabi, "Dual-wavelength passively Q-switched ytterbium-doped fiber laser based on aluminum oxide nanoparticle saturable absorbers," *Chinese Phys. Lett.*, vol. 34, no. 11, p. 114201, 2017.

[73] A. Urrutia, I. Del Villar, P. Zubiate, and C. R. Zamarreño, "A comprehensive review of optical fiber refractometers: Toward a standard comparative criterion," *Laser Photon. Rev.*, vol. 13, no. 11, p. 1900094, 2019.

[74] G. Hernández, *Fabry-perot interferometers*, no. 3. Cambridge University Press, 1988.

[75] B.-H. Lee, J.-B. Eom, K.-S. Park, S.-J. Park, and M.-J. Ju, "Specialty fiber coupler: fabrications and applications," *J. Opt. Soc. Korea*, vol. 14, no. 4, pp. 326–332, 2010.

[76] L. S. Grattan and B. T. Meggitt, *Optical fiber sensor technology: advanced applications-Bragg gratings and distributed sensors*. Springer Science & Business Media, 2013.

[77] G. P. Agrawal, *Applications of nonlinear fiber optics*. Elsevier, 2001.

[78] A. R. Bahrampour, S. Tofighi, M. Bathaee, and F. Farman, "Optical fiber interferometers and their applications," *Interferom. Appl. Sci. Technol.*, vol. 1, pp. 3–30, 2012.

[79] Q. Wang *et al.*, "High sensitivity refractive index sensor based on splicing points tapered SMF-PCF-SMF structure Mach-Zehnder mode interferometer," *Sensors Actuators B Chem.*, vol. 225, pp. 213–220, 2016.

[80] B. H. Lee *et al.*, "Interferometric fiber optic sensors," *sensors*, vol. 12, no. 3, pp. 2467–2486, 2012.

[81] E. Huerta-Mascotte *et al.*, "A core-offset Mach Zehnder interferometer based on a non-zero dispersion-shifted fiber and its torsion sensing application," *Sensors*, vol. 16, no. 6, p. 856, 2016.

[82] G. Keiser, "Optical fiber communications," *Wiley Encycl. Telecommun.*, 2003.

[83] X. Zhang and W. Peng, "Bent-fiber intermodal interference based dual-channel fiber optic refractometer," *Opt. Express*, vol. 23, no. 6, pp. 7602–7610, 2015.

[84] L. Zhao, B. Liu, Y. Wu, T. Sun, Y. Mao, and T. Nan, "Measurement of refractive index and temperature using balloon-shaped Mach-Zehnder interferometer," *Optik (Stuttg).*, vol. 188, pp. 115–119, 2019.

[85] T. Liu, Y. Chen, Q. Han, F. Liu, and Y. Yao, "Sensor based on macrobent fiber Bragg grating structure for simultaneous measurement of refractive index and temperature," *Appl. Opt.*, vol. 55, no. 4, pp. 791–795, 2016.

[86] K. Tian, G. Farrell, W. Yang, X. Wang, E. Lewis, and P. Wang, "Simultaneous measurement of displacement and temperature based on a balloon-shaped bent SMF structure incorporating an LPG," *J. Light. Technol.*, vol. 36, no. 20, pp. 4960–4966, 2018.

[87] Z. Liu, X. Zhang, Z. Gong, Y. Zhang, and W. Peng, "Fiber ring laser-based displacement sensor," *IEEE Photonics Technol. Lett.*, vol. 28, no. 16, pp. 1723–1726, 2016.

[88] R. T. Schermer and J. H. Cole, "Improved bend loss formula verified for optical fiber by simulation and experiment," *IEEE J. Quantum Electron.*, vol. 43, no. 10, pp. 899–909, 2007.

[89] M. Han *et al.*, "Wavelength switchable, free spectral range accurately control single-pass Mach-Zehnder interferometer comb filter," in *2017 16th International Conference on Optical Communications and Networks (ICOCN)*, 2017, pp. 1–3.

[90] A. Khattak, G. Tatel, and L. Wei, "Tunable and switchable erbium-doped fiber laser using a multimode-fiber based filter," *Appl. Sci.*, vol. 8, no. 7, p. 1135, 2018.

[91] L. Wei and G. Tatel, "Wavelength Continuously Tunable All-Fiber Flat-Top Comb Filter Based on a Dual-Pass Mach–Zehnder Interferometer," *J. Light. Technol.*, vol. 37, no. 15, pp. 3740–3749, 2019.

[92] Y. Chang, L. Pei, T. Ning, and J. Zheng, "Switchable multi-wavelength fiber laser based on hybrid structure optical fiber filter," *Opt. Laser Technol.*, vol. 124, p. 105985, 2020.

[93] J. D. Filoteo-Razo *et al.*, "Numerical analysis of DP-MZI–SI comb filter improvement using polarisation-maintaining fibre," *Results Phys.*, vol. 19, p. 103363, 2020.

[94] H. You, J. He, Q. Zhang, X. Xin, and J. Zhang, "A mathematical research on flattop all-fiber MZI interleaver based on double-deviations models and uniform design method," in *AOPC 2020: Optical Information and Network*, 2020, vol.

11569, p. 115690H.

[95] P. Zheng, X. Xu, G. Hu, R. Zhang, B. Yun, and Y. Cui, "Integrated multi-functional optical filter based on a self-coupled microring resonator assisted mzi structure," *J. Light. Technol.*, vol. 39, no. 5, pp. 1429–1437, 2021.

[96] F. F. Ridha, A. M. Salman, and A. Al-Janabi, "Stable evanescent wave mode-locked laser based on a photonic-crystal-fiber-induced Mach–Zehnder filter as a gain-tilt equalizer," *Appl. Opt.*, vol. 60, no. 12, pp. 3290–3301, 2021.

[97] R. Parvizi, H. Arof, N. M. Ali, H. Ahmad, and S. W. Harun, "0.16 nm spaced multi-wavelength Brillouin fiber laser in a figure-of-eight configuration," *Opt. Laser Technol.*, vol. 43, no. 4, pp. 866–869, 2011.

[98] W. A. Khaleel and A. H. M. Al-Janabi, "High-sensitivity sucrose erbium-doped fiber ring laser sensor," *Opt. Eng.*, vol. 56, no. 2, p. 26116, 2017.

[99] U. L. Block, M. J. F. Digonnet, M. M. Fejer, and V. Dangui, "Bending-induced birefringence of optical fiber cladding modes," *J. Light. Technol.*, vol. 24, no. 6, pp. 2336–2339, 2006.

[100] Y. Wu, F. Meng, H. Li, G. Yan, and L. Zhu, "Simultaneous measurement of micro-displacement and temperature based on balloon-like interferometer and fiber Bragg grating," *Optik (Stuttg).*, vol. 183, pp. 875–880, 2019.

[101] X.-H. Li *et al.*, "Wavelength-switchable and wavelength-tunable all-normal-dispersion mode-locked Yb-doped fiber laser based on single-walled carbon nanotube wall paper absorber," *IEEE Photonics J.*, vol. 4, no. 1, pp. 234–241, 2012.

[102] Y. Tang and J. Xu, "A random Q-switched fiber laser," *Sci. Rep.*, vol. 5, no. 1, pp. 1–5, 2015.

[103] Q. Zhao *et al.*, "Switchable multi-wavelength erbium-doped fiber laser based on core-offset structure and four-wave-mixing effect," *Opt. Fiber Technol.*, vol. 54, p. 102111, 2020.

[104] W. Chen, S. Lou, L. Wang, H. Zou, W. Lu, and S. Jian, "Switchable multi-wavelength fiber ring laser using a side-leakage photonic crystal fiber based filter," *Opt. Laser Technol.*, vol. 44, no. 3, pp. 611–616, 2012.

[105] M. Lin, J. Sun, Q. Yan-Hui, K. Ze-Xin, and J. Shui-Sheng, "Switchable multi-wavelength fiber laser based on modal interference," *Chinese Phys. B*, vol. 24, no. 8, p. 84201, 2015.

[106] S. Huang, Y. Wang, P. Yan, J. Zhao, H. Li, and R. Lin, "Tunable and switchable multi-wavelength dissipative soliton generation in a graphene oxide mode-locked Yb-doped fiber laser," *Opt. Express*, vol. 22, no. 10, pp. 11417–11426, 2014.

[107] A. Z. Zulkifli *et al.*, "Dual-wavelength fiber laser with a bent single-mode multimode single-mode fiber structure," *J. Optoelectron. Adv. Mater.*, vol. 19, no. 3–4, pp. 127–131, 2017.

[108] J.-H. Han, "SINGLE-CAVITY WAVELENGTH-SWITCHED FIBER RING LASER BASED ON FIBER BENDING EFFECT IN MACH–ZEHNDER INTERFEROMETER," *Mod. Phys. Lett. B*, vol. 22, no. 14, pp. 1367–1373, 2008.

[109] C. R. Biazoli, S. Silva, M. A. R. Franco, O. Frazão, and C. M. B. Cordeiro, "Multimode interference tapered fiber refractive index sensors," *Appl. Opt.*, vol. 51, no. 24, pp. 5941–5945, 2012.

[110] Y. Chen *et al.*, "Large energy, wavelength widely tunable, topological insulator Q-switched erbium-doped fiber laser," *IEEE J. Sel. Top. Quantum Electron.*,

vol. 20, no. 5, pp. 315–322, 2013.

[111] G. Yin, X. Wang, S. Lou, and Y. Wang, "Tunable Single-, Dual-and Multi-wavelength Fibre Lasers by Using Twin Core Fibre-based Filters," *Fiber Laser*, p. 125, 2016.

[112] A. S. Zulkhairi *et al.*, "Switchable multiwavelength ytterbium-doped fiber laser using a non-adiabatic microfiber interferometer," *Laser Phys.*, vol. 27, no. 5, p. 55104, 2017.

PUBLICATIONS

The following publications prior to this thesis:

1. **All-fiber Mach–Zehnder interferometric comb filter based on macrobend single-mode optical fiber for selecting lasing performance in 1-micron region**, Optics Communications, 15 August 2021, 127017, published. https://doi.org/10.1016/j.optcom.2021.127017.

2. **Tunable full waveband- and adjustable spacing multi-wavelength erbium-doped fiber laser based on controlling cavity losses through bending sensitive interferometric filter**, Infrared Physics and Technology, August 2021, 103791, published. https://doi.org/10.1016/j.infrared.2021.103791

All-fiber Mach–Zehnder interferometric comb filter based on macrobend single-mode optical fiber for selecting lasing performance in 1-micron region

Haneen Qassim Merza [a,*], Sarah Kadhim Al-Hayali [b], Abdul Hadi Al-Janabi [a]

[a] *Institute of Laser for Postgraduate Studies, University of Baghdad, Baghdad, Iraq*
[b] *Al-Turath University College, Baghdad, Iraq*

ARTICLE INFO

ABSTRACT

We report on a new method to select between tunable single- and multi-wavelength switchable lasing performances in continuous-wave (CW) ytterbium-doped fiber laser (YDFL). The wavelength selection and switching techniques are based on the whispering gallery mode (WGM) effect in a Mach–Zehnder interferometric comb-filter formed by bending a standard single-mode fiber (SMF) into a balloon-like shape. By incorporating the proposed comb-filter into the laser ring cavity and adjusting the SMF's bending diameter to control the spectral cavity losses, the single-wavelength lasing was tuned from 1065.26 to 1048.6 nm. Furthermore, by appropriately rotating the polarization controller (PC) cascaded with the filter, the laser can be switched between the dual and triple-wavelength lasing operations. Two sets of switchable triple-wavelength lasing operations around 1045 nm were obtained with a side-mode suppression ratio (SMSR) of 26.9 dB and 22.4 dB, respectively. To the best of our knowledge, this is the first demonstration of a balloon-like interferometer based comb-filter using a bare bending SMF. The experimental results indicate that the proposed filter provides a promising method to achieve tunable single- or switchable multi-wavelength YDFL.

1. Introduction

Due to the increasing demand for an effective technology for high-speed information transmission medium in both the long haul systems and the local networks, optical fiber communication systems components have been developed extensively. A great deal of attention has been drawn to find novel devices for dense wavelength-division-multiplexing (DWDM) optical networks [1–3]. Optical comb filters as essential components play a significant role in optical signal processing, isolating the unwanted neighboring channels causing cross-talks in DWDM. This is due to their simple design, low insertion loss, low cost, ease of use, and good fiber compatibility with the communication system. [2–4]. Beside, comb filters find potential applications to be used as selective elements in multi-wavelength lasers generation, and it is possible to modulate their transmission spectra by the external physical perturbations, such as torsion, strain, and curvature. Furthermore, it can be implemented with various fiber structures and configurations [5].

In recent years, tunable wavelength fiber lasers have been widely investigated due to their increasing applications in optical spectroscopy, optical sensors, and fiber communication systems such as in wavelength division multiplexed (WDM) [6,7]. On the other hand, in some practical applications, it is desirable to switch the fiber laser operation from one single lasing line to another. For example, a switchable fiber laser may be employed as a light source for the wavelength routers of WDM networks and to characterize photonics systems [8]. The basic idea behind switchable and tunable wavelength operation requires a selective element to alleviate the mode competition of the gain medium. One of the essential limiting factors in obtaining stable tunable wavelength and switchable multi-wavelength fiber laser emission is the severe mode competition caused by the homogeneous gain broadening effect of the doped fiber. One possible method to overcome this limitation is by introducing wavelength-dependent losses in the laser cavity [9–18]. Incorporating optical filters with a comb-like spectrum in the ring cavity can be a good solution to alleviate mode competition and accomplish stable multi-wavelength fiber lasers [11]. In this sense, various types of optical filters have been proposed and realized, such as Lyot birefringent filters [12], Sagnac loop interferometers [13,14], birefringent material with polarization-dependent loss [15], and Mach–Zehnder filter (MZI) [5]. Among the types mentioned above, MZI based comb-filter has been considered as the better choice due to its advantages of high reliability and environmental change insensitivity [1]. Thus to this end, several approaches have been investigated to construct

* Corresponding author.
E-mail address: haneen.qassim@ilps.uobaghdad.edu.iq (H.Q. Merza).

Regular article

Tunable full waveband- and adjustable spacing multi-wavelength erbium-doped fiber laser based on controlling cavity losses through bending sensitive interferometric filter

Haneen Qassim Merza [a,*], Sarah Kadhim Al-Hayali [b], Abdul Hadi Al-Janabi [a]

[a] Institute of Laser for Postgraduate Studies, University of Baghdad, Baghdad, Iraq
[b] Al Turath University College, Baghdad, Iraq

ABSTRACT

In this work, tunable full waveband and adjustable spacing multi-wavelength erbium-doped fiber laser (EDFL) based on the interferometric filtering performance of a bent single-mode fiber (SMF) is experimentally demonstrated. The tunable full waveband EDFL operation with a wide-wavelength-tunable range of 11.9 nm was realized by gradually varying the bent diameter of the interferometric filter structure, formed by bending a standard SMF into a balloon shape. Also, when the launched diode pump power was enhanced from 110 to 195 mW, the central wavelength of the EDFL was shifted from 1562.9 nm to 1559.5 nm. Moreover, by adjusting the polarization state inside the cavity, the wavelength operation was switched from a single to multi-wavelength operation. Dual-, triple-, and quadruple- wavelength emission were achieved. To the best of our knowledge, this is the first time that a bending SMF into a balloon-like MZI has been employed as an all-fiber filter to manipulate the spectral output characteristic of EDFL. The proposed EDFL output characteristics of tunability and switchability can provide great potential in diverse photonics applications.

1. Introduction

In recent years, spectral manipulation of erbium-doped fiber lasers (EDFL) is an important issue, and efforts have been devoted on achieving a versatile performance such as tunability, switching, or multi-wavelength emission due to their wide broad range of applications such as in fiber communication systems, fiber optic sensors, etc. [1]. Tunable wavelength fiber lasers have been under intensive study in recent years due to their growing optical spectroscopy applications, optical sensors, and wavelength division multiplexing (WDM) [2,3]. In certain applications, such as fabrication of light source for the wavelength routers of WDM network and photonics systems' characterization, switching the fiber laser's operation from one single lasing line to another is preferable [4]. On the other hand, in some applications, such as dense wavelength-division-multiplexing (DWDM) optical networks, signal processing, generation of soliton pulses, and multi-parameter measurement, a multi-wavelength operation is ideal [5,6]. Moreover, in a practical view, a multi-wavelength fiber laser has more potential than a fixed wavelength fiber laser since the variable wavelength output with adjustable spacing may satisfy various applications such as in high-

resolution spectroscopy, optical frequency metrology, microwave/Terahertz generation, optical sensing, and in fiber communications where the current WDM systems require various channels spacing depend on their specific applications [7,8]. In addition, their advantages, like low operating costs, compactness, long operational lifetimes, and a high signal-to-noise ratio, are all benefits from these multi-wavelength fiber lasers [4,9,10].

The basic principle behind a tunable and multi-line output characteristic of EDFL at room temperature requires an optical filter to reduce the gain medium's mode competition [11–13]. However, two main concerns need to be carefully handled to achieve a stable operation of tunable and multi-wavelength EDFL operation: The strong homogeneous line broadening and the cross-gain saturation induced in the erbium-doped fiber (EDF) gain medium [14]. These limitations are still challenging to obtain stably tunable-, and multi-wavelength fiber lasers outputs [15,16]. Therefore, high-performance optical filters with low cost, ease of handling, and fabrication to implement these types of EDFL output characteristics are of great interest [14]. Optical fiber comb filters are one form of these optical filters [17]. Various techniques to realize all-fiber comb filters have been reported, including the usage of

APPENDIX 1

Pumping LD Specifications

1-a

THORLABS

975 nm Pigtailed Laser Diode, Butterfly Package

PL980P330J

Description

The PL980P330J consists of a field-proven, 975 nm quantum-well laser chip in a 14-pin butterfly package. The compact design includes an integrated thermoelectric cooler, a monitor photodiode, and a wavelength-stabilizing fiber Bragg grating (FBG), which ensures very little drift in the output wavelength as the temperature and current are varied. The laser is coupled into a single mode fiber pigtail (SMF: HI1060 fiber) with a Ø1.5 mm PTFE loose tube jacket and an FC/APC connector. This laser diode's patented device structure (F000038US01) is Telecordia GR-468-CORE qualified.

Specifications

Absolute Maximum Ratings

	Symbol	Min	Max
Storage Temperature	T_S	-40°C	85°C
Operating Temperature	T_{CASE}	-20°C	75°C
Soldering Temperature*	-	-	250°C
LD Forward Current	I_F	-	800 mA
LD Reverse Current	V_R	-	2 V
TEC Current	I_{TEC}	-	2.5 A
TEC Voltage	V_{TEC}	-	3.2 V
Monitor Reverse Voltage	V_{PD}	-	10 V
ESD Damage	V_{ESD}	-	500 V
Fiber Pigtail Bend Radius	-	25 mm	-

*Max 10 Seconds

Characteristics (T_C = 25°C, P = 330 mW)

	Symbol	Min	Typical	Max
Center Wavelength	λ_C	974 nm	975 nm	976 nm
Operating Current	I_{OP}	-	600 mA	720 mA
Output Power	P_{OUT}	330 mW	-	-
Spectral Bandwidth (FWHM)	$\Delta\lambda$	-	0.5 nm	1.0 nm
Spectral Bandwidth (at 95% Power)	$\Delta\lambda$	-	-	2.0 nm
Threshold Current	I_{TH}	-	75 mA	90 mA
Forward Voltage at I_{OP}	V_F	-	1.7 V	1.9 V
Kink-Free Power	P_{Kink}	363 mW	-	-
Spectral Shift with Temperature	$\Delta\lambda/\Delta T$	-	-	0.02 nm/°C
Side Mode Suppression	-	-13 dB	-	-
Monitor Responsivity	R_{PD}	1 µA/mW	-	10 µA/mW

1-b

Specifications (Cont.)

Characteristics (T_c = 25 °C, P = 220 mW), TEC Operation

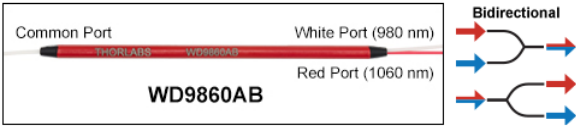|	Symbol	Min	Typical	Max
TEC Current	I_{TEC}	-	1.2 A	1.8 A
TEC Voltage	V_{TEC}	-	2.0 V	3.0 V
Thermistor Resistance	R_{TH}	9.5 kΩ	10 kΩ	10.5 kΩ
Thermistor Constant	B	3600 K	3920 K	4200 K

Drawings
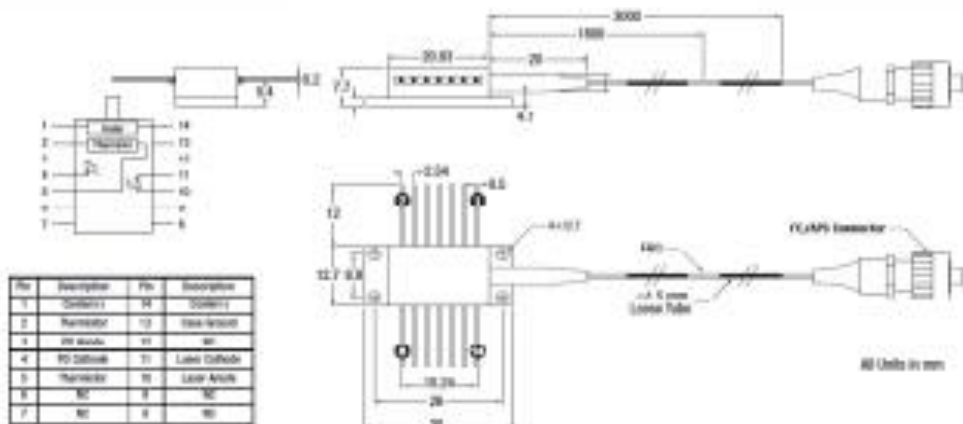
APPENDIX 2

WDM 980/1060 nm for YDFL

Wavelength Division Multiplexers: 980 nm / 1060 nm

- ▶ Combine or Split 980 nm and 1060 nm Signals
- ▶ ±5 nm Bandwidth
- ▶ Includes a Product-Specific Data Sheet (Click Here for a Sample)
- ▶ HI1060 or HI1060 FLEX Fiber Options
- ▶ Available with Unterminated Fiber Leads or with 2.0 mm Narrow Key FC/PC or FC/APC Connectors

WD9860FA

Zoom

Common Port — White Port (980 nm)
THORLABS WD9860AB — Red Port (1060 nm)

WD9860AB

Bidirectional

Click for Details
The housings of these WDMs are engraved with the Item # and port wavelengths. The common port is located on the single fiber side and has a white jacket.

These WDMs are designed for combining or splitting two signals at 980 nm and 1060 nm and feature a ±5 nm bandwidth around the center wavelength of each channel. They can handle a maximum power of 1 W with connectors or bare fiber and a maximum power of 5 W when spliced (see the *Damage Threshold* tab for more details). As seen in the image to the right, the red housing of these multiplexers is engraved with the Item # and the port wavelengths. A detailed test report is included with each WDM; click here for a sample data sheet. They are available with no connectors or with 2.0 mm narrow key FC/PC or FC/APC connectors.

These WDMs are available with HI1060 or HI1060 FLEX fiber. HI1060 fiber offers a Ø5.3 μm core size and a 0.14 NA, while HI1060 FLEX fiber offers a Ø3.4 μm core size, a 0.22 NA, and reduced bending loss relative to HI1060.

Item #	Info[a]	Operating Wavelengths	Bandwidth	Insertion Loss[b]	Isolation[b]	Polarization-Dependent Loss[b]	Directivity[b]	Fiber Type	Termination
WD9860BA	ⓘ	980 nm / 1060 nm	±5 nm	≤0.3 dB (Click for Plot)	≥15 dB	≤0.2 dB	≥60 dB	HI1060 (0.14 NA)	No Connectors, Scissor Cut
WD9860FA	ⓘ								FC/PC
WD9860AA	ⓘ								FC/APC
WD9860BB	ⓘ	980 nm / 1060 nm	±5 nm	≤0.3 dB (Click for Plot)	≥15 dB	≤0.2 dB	≥60 dB	HI1060 FLEX (0.22 NA)	No Connectors, Scissor Cut
WD9860FB	ⓘ								FC/PC
WD9860AB	ⓘ								FC/APC

a. Please click on the blue icon for complete specifications.
b. These specifications were measured without connectors.

Based on your currency / country selection, your order will ship from Newton, New Jersey
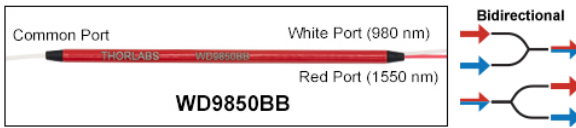
APPENDIX 3

WDM 980/1550 nm for EDFL

Wavelength Division Multiplexers: 980 nm / 1550 nm

- ▶ Combine or Split 980 nm and 1550 nm Signals
- ▶ ±10.0 nm Bandwidth
- ▶ Includes a Product-Specific Data Sheet (Click Here for a Sample)
- ▶ HI1060 or HI1060 FLEX Fiber Options
- ▶ Available with Unterminated Fiber Leads or with 2.0 mm Narrow Key FC/PC or FC/APC Connectors

WD9850BB

Zoom

Common Port — White Port (980 nm)
THORLABS WD9850BB — Red Port (1550 nm)

WD9850BB

Bidirectional

Click for Details
The housings of these WDMs are engraved with the Item # and port wavelengths. The common port is located on the single fiber side and has a white jacket.

These WDMs are designed for combining or splitting two signals at 980 nm and 1550 nm and feature a ±10.0 nm bandwidth around the center wavelength of each channel. Each WDM can handle a maximum power of 1 W with connectors or unterminated (bare) fiber and a maximum power of 5 W when spliced (see the *Damage Threshold* tab for details). They are available without connectors or with 2.0 mm narrow key FC/PC or FC/APC connectors. A detailed test report is included with each WDM; click here for a sample data sheet.

These WDMs are available with HI1060 or HI1060 FLEX fiber. HI1060 fiber offers a Ø5.3 μm core size and a 0.14 NA, while HI1060 FLEX fiber offers a Ø3.4 μm core size, a 0.22 NA, and reduced bending loss relative to HI1060.

Item #	Info[a]	Operating Wavelengths	Bandwidth	Insertion Loss[b]	Isolation[b]	Polarization-Dependent Loss[b]	Directivity[b]	Fiber Type	Termination
WD9850BA	ⓘ	980 nm / 1550 nm	±10.0 nm	≤0.3 dB (Click for Plot)	≥19 dB	≤0.2 dB	≥60.0 dB	HI1060 (0.14 NA)	No Connectors, Scissor Cut
WD9850FA	ⓘ								FC/PC
WD9850AA	ⓘ								FC/APC
WD9850BB	ⓘ	980 nm / 1550 nm	±10.0 nm	≤0.3 dB (Click for Plot)	≥19 dB	≤0.2 dB	≥60.0 dB	HI1060 FLEX (0.22 NA)	No Connectors, Scissor Cut
WD9850FB	ⓘ								FC/PC
WD9850AB	ⓘ								FC/APC

a. Please click on the blue icon for complete specifications.
b. These specifications were measured without connectors.

Based on your currency / country selection, your order will ship from Newton, New Jersey

APPENDIX 4

YDF Specification sheet

Ytterbium-Doped Single-Mode Single Clad Fiber

Nufern single-mode Yb-doped fibers are designed to support low power fiber lasers and amplifiers based on single-mode diode pump technology, rather than the multimode pumps used in high-power applications. For applications where high efficiency and very short device lengths are critical, these single-mode fibers are compatible with standard "telecom" fiber technology ensuring low splice loss to numerous fiber pigtailed components. The PM variety is designed with the PANDA-style stress structure which delivers linearly polarized light suitable for frequency conversion. These fibers make the ideal gain medium for low average power femtosecond fiber lasers and pre-amplifiers for higher power double-clad amplifiers. These High Performance (-HP) versions provide tighter optical and geometric tolerances, improving device performance, system compatibility and manufacturing process control.

Typical Applications

- Low power CW and pulsed fiber lasers
- Femtosecond fiber lasers
- Pre-amps for high-power, double-clad devices

Features & Benefits

- Single-mode output — Compatiable with standard telecom 980/1060 nm fiber-based components with low splice loss
- PANDA-style stress structure — Linearly polarized output for frequency conversion
- High Ytterbium concentration — Short fiber lengths to reduce detrimental non-linear effects
- High slope efficiency (typically 75%) — Efficient utilization of pump power
- Higher Prooftest Yields — Critical for long-term reliability in tight bend applications

Optical Specifications	PM-YSF-HI-HP	SM-YSF-HI-HP	PM-YSF-LO-HP	SM-YSF-LO-HP
Operating Wavelength	1015 – 1115 nm	1015 – 1115 nm	1015 – 1115 nm	1015 – 1115 nm
Core NA	0.110	0.110	0.130	0.130
Mode Field Diameter	7.5 ± 0.7 µm @ 1060 nm	7.5 ± 0.7 µm @ 1060 nm	6.5 ± 0.7 µm @ 1060 nm	6.5 ± 0.7 µm @ 1060 nm
Cutoff	860 ± 50 nm	860 ± 50 nm	860 ± 50 nm	860 ± 50 nm
Core Attenuation	≤ 10.0 dB/km @ 1200 nm	≤ 10.0 dB/km @ 1200 nm	≤ 10.0 dB/km @ 1200 nm	≤ 10.0 dB/km @ 1200 nm
Core Absorption	85.0 ± 10.0 dB/m at 915 nm 250.0 dB/m at 975 nm	85.0 ± 10.0 dB/m at 915 nm 250.0 dB/m at 975 nm	26.0 ± 4.0 dB/m at 915 nm 80.0 dB/m at 975 nm	26.0 ± 4.0 dB/m at 915 nm 80.0 dB/m at 975 nm
Birefringence	> 2.8 × 10^{-4}	N/A	> 2.8 × 10^{-4}	N/A
Geometrical & Mechanical Specifications				
Cladding Diameter	125.0 ± 1.0 µm	125.0 ± 1.0 µm	125.0 ± 1.0 µm	125.0 ± 1.0 µm
Core Diameter	6.0 µm	6.0 µm	5.0 µm	5.0 µm
Coating Diameter	245.0 ± 10.0 µm	245.0 ± 10.0 µm	245.0 ± 10.0 µm	245.0 ± 10.0 µm
Coating Concentricity	< 5.0 µm	< 5.0 µm	< 5.0 µm	< 5.0 µm
Core/Clad Offset	≤ 0.50 µm	≤ 0.50 µm	≤ 0.50 µm	≤ 0.50 µm
Coating Material	Acrylate	Acrylate	Acrylate	Acrylate
Operating Temperature Range	-55 to 85 °C	-55 to 85 °C	-55 to 85 °C	-55 to 85 °C
Prooftest Level	≥ 200 kpsi (1.4 GN/m²)	≥ 200 kpsi (1.4 GN/m²)	≥ 200 kpsi (1.4 GN/m²)	≥ 200 kpsi (1.4 GN/m²)

APPENDIX 5

EDF Specification sheet

nLIGHT

HIGH-POWER SEMICONDUCTOR LASERS AND FIBERS

LIEKKI™ Er80-4/125

Erbium Doped Fiber

LIEKKI™ Er80-4/125 fibers are very highly doped erbium fibers for fiber lasers and amplifiers.

High erbium concentration reduces required application fiber length considerably while providing strong gain and reduced non-linear effects.

Applications

- Short pulse amplifiers
- Low non-linearity applications

Features

- Excellent batch consistency of erbium peak absorption and spectral shape
- Very short fiber lengths reduces non-linear effects like FWM, SRS and SBS
- Very good temperature behavior
- Low splice loss, LIEKKI™ EasySplice software for splicing parameters
- Suitable for both 980 nm and 1480 nm pumping
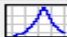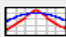- Dual layer UV-cured acrylate coating

Typical device specification

		LIEKKI™ Er80-4/125
Optical		
Mode field diameter at 1550 nm	µm	6.5 ± 0.5
Peak core absorption at 1530 nm	dB/m	80 ± 8
Core numerical aperture (nominal)		(0.2)
Cut-off wavelength	nm	800 - 980
Geometrical and mechanical		
Core concentricity error	µm	< 0.7
Cladding diameter	µm	125 ± 2
Cladding geometry		round
Coating diameter	µm	245 ± 15
Coating material		high index acrylate
Proof test	%	> 1

APPENDIX 6

ISO 1064 nm for YDFL

1064 nm Polarization-Independent Isolator with SM Fiber

Click Image to Enlarge		
Item #	IO-H-1064B IO-H-1064B-APC	IO-F-1064 IO-F-1064APC
Polarization	Independent	Independent
Fiber Type	SM	SM
Center Wavelength	1064 nm	1064 nm
Operating Range	1059 - 1069 nm	1054 - 1074 nm
Max Power[b]	300 mW (CW)[c]	3 W (CW)[c]
Isolation[e]	30 dB (Min)	35 dB (Min) 36 dB (Typ.)
Performance Graph (Click for Plot)		
Insertion Loss	1.8 dB (Max) (IO-H-1064B) 2.1 dB (Max) (IO-H-1064B-APC)	1.0 dB (Typ.) 1.2 dB (Max)
Polarization Dependent Loss (PDL)	≤0.15 dB	≤0.15 dB
Return Loss (Input/Output)	≥55/50 dB (IO-H-1064B) ≥50/45 dB (IO-H-1064B-APC)	≥50 dB
Fiber	HI1060	HI1060

APPENDIX 7

ISO 1550 nm for EDFL

1550 nm Polarization-Independent Isolators with SM Fiber

Click Image to Enlarge		
Item #[a]	IO-H-1550 IO-H-1550APC IO-H-1550FC	IOT-H-1550A
Polarization	Independent	Independent
Fiber Type	SM	SM
Isolator Design	Single Stage	Dual Stage
Center Wavelength	1550 nm	1550 nm
Operating Range	1530 - 1570 nm	1535 - 1565 nm
Max Power[b]	300 mW (CW)[c,d]	300 mW (CW)[d]
Isolation[f]	29 dB (Min)	45 dB (Min) 55 dB (Peak)
Performance Graph (Click for Plot)		
Insertion Loss (Without Connectors)	0.7 dB (Max)	≤0.85 dB
Polarization Dependent Loss (PDL)	≤0.15 dB	<0.10 dB
Return Loss	≥55/50 dB (Input/Output)	>55/50 dB (Input/Output)
Fiber	SMF-28e+	SMF-28 Ultra

APPENDIX 8

OC 1060 nm for YDFL

PMC1060-50B-APC - September 2. 2016

Item # PMC1060-50B-APC was discontinued on September 2, 2016. For informational purposes, this is a copy of the website content at that time and is valid only for the stated product.

1064 NM 1X2 POLARIZATION-MAINTAINING FIBER OPTIC COUPLERS / TAPS

► Narrowband PM Couplers for 1064 nm
► Available with 50:50, 75:25, 90:10, or 99:1 Coupling Ratio
► Standard and Premium Versions Available

Use for Splitting Signals

PMC1060-90B-APC
90:10 PM Coupler with FC/APC Connectors

PN1064R5F1
50:50 PM Coupler with FC/PC Connectors

FC/APC   FC/PC

Hide Overview

OVERVIEW

Features

- Polarization-Maintaining Fiber Optic Couplers for Use at 1064 nm
- Two Versions Available
  - Standard: 1060 nm ± 15 nm and ≥18 dB PER Excluding Connectors
  - Premium: 1064 nm ± 15 nm and ≥20 dB PER Including Connectors
- 50:50, 75:25, 90:10, or 99:1 Split Ratios
- 2.0 mm Narrow Key FC/PC or FC/APC Connectors
- Individual Test Report Included with Each Premium Coupler (See the *PER Measurement* Tab; Click Here for a Sample Data Sheet)
- Contact Us for Custom Wavelength, Coupling Ratio and Connector Options

1x2 PM Coupler Selection Guide	
Center Wavelength	Bandwidth
630 nm	±15 nm
780 nm	±15 nm
1064 nm	±15 nm
1310 nm	±15 nm
1550 nm	±15 nm

PN1064R1A1

Click for Details
Each premium coupler is engraved with the Item #, serial number, and key specifications for easy identification. When the white port on the left is used as the input, the coupling ratios listed below correspond to the ratio of the measured output power from the white (signal output) port to the red (tap output) port.

Panda PM Fiber Cross Section

These 1x2 Polarization-Maintaining (PM) Fiber Couplers are designed for operation at 1064 nm and are available with 50:50, 75:25, 90:10, or 99:1 coupling ratios. 1x2 couplers have only one input port for simplified use and cable management. These couplers are ideal for applications where light is split from the input port into two output ports at the

90:10 Fiber Couplers

Premium Item #	Info	Center Wavelength	Bandwidth[a]	Coupling Ratio[a] (%)	Extinction Ratio[b]	Insertion Loss[a]	Excess Loss[a]	Fiber Type[c]	Termination[d]
PN1064R2F1	ℹ	1064 nm	±15 nm	90:10	≥20.0 dB / ≥20.0 dB (Including Connectors)	≤0.8 dB / ≤10.5 dB	≤0.3 dB (Typ.)	PM 98-U25D	FC/PC
PN1064R2A1	ℹ								FC/APC

- Values are specified with a slow axis launch at room temperature without connectors and measured at the center wavelength through the white input port, as indicated in the diagram above.
- Extinction ratio is specified with a slow axis launch at room temperature with connectors and measured at the center wavelength through the white input port, as indicated in the diagram above. See the *PER Measurement* tab for more information on how extinction ratio is measured.
- The fiber used in this coupler is compatible with PM980-XP fiber. Other fiber types may be available upon request. Please contact Tech Support with inquiries.
- The connector key is aligned to the slow axis of the fiber.

Standard Item #[a]	Info	Center Wavelength	Bandwidth	Coupling Ratio (%)	Extinction Ratio	Insertion Loss	Excess Loss	Fiber Type[b]	Termination[c]
PMC1060-90B-FC	ℹ	1060 nm	±15 nm	90:10	≥18.0 dB / ≥18.0 dB (Excluding Connectors)	≤1.2 dB / ≤11.6 dB	≤0.4 dB (Typ.)	SM98-PR-U25D-H	FC/PC
PMC1060-90B-APC	ℹ								FC/APC

- All specifications are measured without connectors during the manufacturing process.
- The fiber used in this coupler is compatible with PM980-XP fiber.
- The connector key is aligned to the slow axis of the fiber.

APPENDIX 9

OC 1550 nm for EDFL

1550 nm 1x2 Single Mode Fused Fiber Optic Couplers / Taps

► 1550 nm Wideband or Narrowband 1x2 Couplers
► Available with 50:50, 75:25, 90:10, 99:1, or 99.9:0.1 Coupling Ratio
► Terminated with 2.0 mm Narrow Key FC/PC or FC/APC Connectors

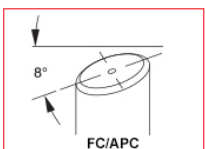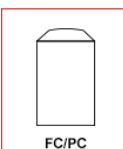Use for Splitting Signals

TW1550R5A1
50:50 Wideband Coupler
with FC/APC Connectors

TN1550R2F1
90:10 Narrowband Coupler with
FC/PC Connectors

8°

FC/APC

FC/PC

Related Items
Other Fiber Couplers
Fiber Patch Cables
Fiber Component Tray
1550 nm 2x2 SM Couplers

90:10 Fiber Optic Couplers

Thorlabs offers both narrowband and wideband fiber optic couplers. All specifications are measured without connectors during the manufacturing process. Additional information on the testing process for our wideband couplers can be found on the *Coupler Verification* tab above. Our wideband couplers are highlighted green in the table below.

Item #	Info	Center Wavelength	Bandwidth	Coupling Ratio[a,b] (%)	Coupling Ratio Tolerance	Insertion Loss[a,b]	Excess Loss[a,b]	Uniformity[a,b]	Fiber Type[c]	Termination
TW1550R2F1	ⓘ	1550 nm	±100 nm	90:10 (Click for Plot)	±2.5%	≤0.7 dB / ≤11.4 dB	≤0.15 dB	≤0.6 dB (Click for Plot)	SMF-28	FC/PC
TW1550R2A1	ⓘ									FC/APC
TN1550R2F1	ⓘ	1550 nm	±15 nm	90:10 (Click for Plot)	±2.0%	≤0.7 dB / ≤11.1 dB	≤0.15 dB	-	SMF-28	FC/PC
TN1550R2A1	ⓘ									FC/APC

a. All values are specified at room temperature over the bandwidth and measured without connectors using the white port as the input, as indicated in the diagram above.
b. Please see the *1x2 Coupler Tutorial* tab for more information on these terms.
c. Corning SMF-28 fiber type will be specified on the documentation that ships with the coupler. Other fiber types may be available upon request. Please contact Tech Support with inquiries.

Based on your currency / country selection, your order will ship from Newton, New Jersey

APPENDIX 10

Corning SMF-28

10-a

Corning® SMF-28® Ultra Optical Fiber
Product Information

Corning® SMF-28® Ultra optical fiber is an ITU-T Recommendation G.652.D compliant optical fiber with Corning's enhanced low-loss and bend fiber technologies. This full-spectrum fiber has bend performance that exceeds the ITU-T Recommendation G.657.A1 standard and still splices the same as the installed base of standard single-mode fibers such as SMF-28e+ fiber. SMF-28 Ultra fiber offers industry-leading specifications for attenuation, macrobend loss, and polarization mode dispersion values, which provide a solid foundation for new network deployments as well as upgrades to existing networks. Since Corning brought the first fiber to market more than 40 years ago, Corning's leadership in single-mode fiber innovation has been unparalleled.

Optical Specifications

Maximum Attenuation

Wavelength (nm)	Maximum Value* (dB/km)
1310	≤ 0.32
1383**	≤ 0.32
1490	≤ 0.21
1550	≤ 0.18
1625	≤ 0.20

* Alternate attenuation offerings available upon request.
** Attenuation values at this wavelength represent post-hydrogen aging performance.

Attenuation vs. Wavelength

Range (nm)	Ref. λ (nm)	Max. α Difference (dB/km)
1285 – 1330	1310	0.03
1525 – 1575	1550	0.02

The attenuation in a given wavelength range does not exceed the attenuation of the reference wavelength (λ) by more than the value α.

Macrobend Loss

Mandrel Radius (mm)	Number of Turns	Wavelength (nm)	Induced Attenuation* (dB)
10	1	1550	≤ 0.50
10	1	1625	≤ 1.5
15	10	1550	≤ 0.05
15	10	1625	≤ 0.30
25	100	1310, 1550, 1625	≤ 0.01

*The induced attenuation due to fiber wrapped around a mandrel of a specified radius.

Point Discontinuity

Wavelength (nm)	Point Discontinuity (dB)
1310	≤ 0.05
1550	≤ 0.05

Cable Cutoff Wavelength (λ_{cc})

λ_{cc} ≤ 1260 nm

Mode-Field Diameter

Wavelength (nm)	MFD (μm)
1310	9.2 ± 0.4
1550	10.4 ± 0.5

Dispersion

Wavelength (nm)	Dispersion Value [ps/(nm·km)]
1550	≤ 18.0
1625	≤ 22.0

Zero Dispersion Wavelength (λ_o): 1304 nm ≤ λ_o ≤ 1324 nm
Zero Dispersion Slope (S_o): S_o ≤ 0.092 ps/(nm²·km)

Polarization Mode Dispersion (PMD)

	Value (ps/√km)
PMD Link Design Value	≤ 0.04*
Maximum Individual Fiber PMD	≤ 0.1

*Complies with IEC 60794-3: 2001, Section 5.5, Method 1, (m = 20, Q = 0.01%), September 2001.

The PMD link design value is a term used to describe the PMD of concatenated lengths of fiber (also known as PMD$_Q$). This value represents a statistical upper limit for total link PMD. Individual PMD values may change when fiber is cabled.

How to Order

Contact your sales representative, or call the Optical Fiber Customer Service Department:
Ph: 1-607-248-2000 (U.S. and Canada)
+44-1244-525-320 (Europe)
Email: cofic@corning.com
Please specify the fiber type, attenuation, and quantity when ordering.

10-b

Dimensional Specifications

Glass Geometry

Fiber Curl	≥ 4.0 m radius of curvature
Cladding Diameter	125.0 ± 0.7 μm
Core-Clad Concentricity	≤ 0.5 μm
Cladding Non-Circularity	≤ 0.7%

Coating Geometry

Coating Diameter	242 ± 5 μm
Coating-Cladding Concentricity	< 12 μm

Environmental Specifications

Environmental Test	Test Condition	Induced Attenuation 1310 nm, 1550 nm, and 1625 nm (dB/km)
Temperature Dependence	-60°C to +85°C*	≤ 0.05
Temperature Humidity Cycling	-10°C to +85°C up to 98% RH	≤ 0.05
Water Immersion	23°C ± 2°C	≤ 0.05
Heat Aging	85°C ± 2°C	≤ 0.05
Damp Heat	85°C at 85% RH	≤ 0.05

*Reference temperature = +23°C
Operating Temperature Range: -60°C to +85°C

Mechanical Specifications

Proof Test

The entire fiber length is subjected to a tensile stress ≥ 100 kpsi (0.69 GPa).*
*Higher proof test levels available.

Length

Fiber lengths available up to 63.0 km/spool.

Performance Characterizations

Characterized parameters are typical values.

Core Diameter	8.2 μm
Numerical Aperture	0.14 NA is measured at the one percent power level of a one-dimensional far-field scan at 1310 nm.
Effective Group Index of Refraction (N_{eff})	1310 nm: 1.4676 1550 nm: 1.4682
Fatigue Resistance Parameter (N_d)	20
Coating Strip Force	Dry: 0.6 lbs. (3N) Wet, 14-day room temperature: 0.6 lbs. (3N)
Rayleigh Backscatter Coefficient (for 1 ns Pulse Width)	1310 nm: -77 dB 1550 nm: -82 dB

APPENDIX 11

PC (PLC-900)

THORLABS

In-Line Optical Fiber Polarization Controller
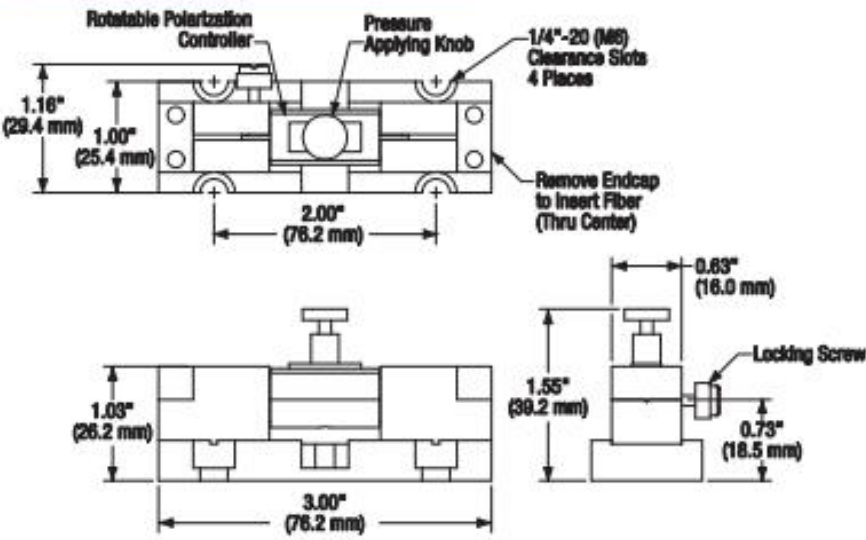
PLC-900

Description

The PLC-900 is a compact, in-line polarization controller that can be conveniently dropped into a fiber optic system. Simply insert a length of fiber into the slot located on the top of the device and you are ready to control the polarization state of light without having to disconnect your set-up.

Specifications

PLC-900*	
Operating wavelength range	780 – 1550 nm
Insertion Loss	< 0.05 dB
Return Loss	> 65 dB
Extinction Ratio	> 40 dB
Operating Temperature	- 40 to 85 °C
Storage Temperature	- 40 to 85 °C
Fiber Jacket	900 μm
Dimensions	0.05" x 0.84" x 3.00" (W x H x L)

*Note: Values referenced without connectors

Drawings

الخلاصة

مرشح الألياف الضوئية هو طريقة رائعة محتملة لنطاق موجة كامل قابل للضبط وتباعد متعدد الطول الموجي قابل للتعديل في موجة مستمرة (CW) لليزر ألياف إربيوم (EDFL) وليزر ألياف ايتربيوم (YDFL)، نظرًا لفوائدها الوفيرة ، البساطة ، خفة الوزن ، قلة تكلفة التصنيع ، الموثوقية ، النطاق الواسع ، والتكرار من الميزات المرغوبة للغاية في مرشحات الألياف البصرية. في الوقت الحاضر ، تم التخطيط لمرشح الألياف المبتكر القائم على مقياس التداخل (MZI) وإثباته تجريبياً. يعتمد اختيار الطول الموجي، تباعد القنوات وتقنيات التبديل على تأثير إعادة تداخل الموجات (WGM) في مرشح مشط قياس التداخل Mach-Zehnder الذي تم تشكيله عن طريق ثني الألياف أحادية الوضع القياسية (SMF) إلى شكل يشبه البالون. من خلال دمج مرشح المشط المقترح في تجويف حلقة الليزر وضبط قطر ثني SMF للتحكم في خسائر تجويف الليزر ، تم ضبط الليزر أحادي الموجة من 1065.26 إلى 1048.6 نانومتر مع نطاق ضبط يبلغ 16.76 نانومتر لـ YDFL. علاوة على ذلك ، من خلال التدوير المناسب لوحدة التحكم في الاستقطاب (PC) متوالية الربط مع المرشح ، يمكن تبديل الليزر بين عمليات الليزر ذات الطول الموجي المزدوج والثلاثي. تم الحصول على مجموعتين من عمليات الليزر ذات الأطوال الموجية الثلاثية القابلة للتحويل حوالي 1045 نانومتر مع نسبة قمع للأسلوب الجانبي (SMSR) تبلغ 26.9 ديسيبل و 22.4 ديسيبل على التوالي. أيضًا ، عندما تم تحسين طاقة مضخة الصمام الثنائي التي تم إطلاقها في إعداد ليزر الألياف من 110 إلى أكثر من 210 ملي واط ، فإن تجويف YDFL يعمل بالليزر بطول موجي مزدوج وثلاثي. تم تحقيق الليزر ثنائي الموجة عند 1048.6 نانومتر و 1046.38 نانومتر مع تباعد قناة 2.3 نانومتر.

تم تحقيق عملية EDFL ذات النطاق الموجي الكامل القابل للضبط مع نطاق ضبط الطول الموجي العريض البالغ 11.9 نانومتر من خلال التغيير التدريجي للقطر المنحني لهيكل مرشح قياس التداخل. أيضًا ، عندما تم تحسين طاقة مضخة الصمام الثنائي من 110 إلى 195 ملي واط ، تم تحويل الطول الموجي المركزي لـ EDFL من 1562.9 نانومتر إلى 1559.5 نانومتر مع تباعد القناة 2.5 نانومتر. علاوة على ذلك ، من خلال ضبط حالة الاستقطاب داخل التجويف ، تم تحويل عملية الطول الموجي من عملية واحدة إلى عملية متعددة الأطوال الموجية. تم تحقيق انبعاثات أطوال موجية مزدوجة وثلاثية ورباعية.

على حد علمنا ، هذه هي المرة الأولى التي يتم فيها استخدام SMF المنحني إلى MZI الشبيه بالبالون كمرشح كامل الألياف لمعالجة خاصية الإخراج الطيفي لـ EDFL / YDFL. إن خصائصُ إخراج YDFL / EDFL المقترحة لقابلية التوليف والتحويل مع التحكم في تباعد القنوات يمكن أن توفر إمكانات كبيرة في تطبيقات الضوئيات المتنوعة.

وزارة التعليم العالي والبحث العلمي

جامعة بغداد

معهد الليزر للدراسات العليا

توليد ليزر ليفي منغّم أحادي / متعدد الطول الموجي المعتمد
شكل البالون على مقياس تداخل Mach-Zehnder

رسالة مقدمة الى

معهد الليزر للدراسات العليا /جامعة بغداد /لاستكمال متطلبات نيل شهادة ماجستير علوم في الليزر/ الهندسة الالكترونية والاتصالات

من قبل

حنين قاسم مرزة

بكالوريوس هندسة الليزر والالكترونيات البصرية - 2009

بإشراف

الأستاذ الدكتور عبد الهادي مطشر الجنابي

1443 هـ   **2021 م**